Ing. Franz Zitzenbacher, BSc

Design of a low specific speed diffusor pump and construction of the experimental setup

MASTER'S THESIS

to achieve the university degree of

Diplom-Ingenieur

Master's degree programme: Mechanical Engineering and Business Economics

submitted to

Graz University of Technology

Supervisor

Assoc. Prof. Dipl. Ing. Dr. techn. Helmut Benigni

Institute of Hydraulic Fluid Machinery

O. Univ.-Prof. Dipl.-Ing. Dr.techn. Helmut Jaberg

Graz, May 2015

Abstract

Design of a low specific speed diffusor pump and construction of the experimental setup.

The aim of this Master Thesis is a test rig for validation of the centrifugal pump designed at the Institute of Hydraulic Machinery, which is used for final acceptance measurements.

Subject-matter of this Master Thesis is the one-dimensional design of a centrifugal pump with a specific speed of 36 rpm and with a diffusor for multi-stage use, the concept-finding, the detailed single part construction and the manufacturing support as well as final hydraulic measurements. As of a very tight schedule, it was necessary to realise the hydraulic optimisation regarding the development of the final geometry of the impeller and of the diffusor in parallel to the design and construction of the test rig. Most of the manufacturing work was done at the labor-workshop of the institute. However, some single parts have been outsourced for manufacturing as of deadlines and production-oriented reasons. The development work began in May 2014 and ended in February 2015 with final acceptance measurements for and with the purchaser on the test rig of the institute.

Kurzfassung

Auslegung und Konstruktion einer Kreiselpumpe mit Diffusor geringer spezifischer Drehzahl und Konstruktion eines Pumpenprüfstandes.

Das Ziel dieser Arbeit ist ein Pumpenprüfstand zur Validierung der am Institut entworfenen Kreiselpumpe mit dem abschließende Abnahmemessungen durchgeführt werden.

Inhalt dieser Masterarbeit ist die eindimensionale Auslegung einer Kreiselpumpe mit einer spezifischen Drehzahl von 36 min^{-1} mit nachgeschaltetem Diffusor für den Einsatz in mehrstufigen Pumpen sowie die Konzeption, die Detailkonstruktion und der Bau eines Pumpenprüfstandes mit abschließenden hydraulischen Messungen. Aufgrund eines sehr engen Zeitplans wurden die hydraulische Optimierung und schlussendlich die Entwicklung der hydraulischen Geometrie von Laufrad und Diffusor zeitgleich mit der Entwicklung des Pumpenprüfstandes am Institut für Hydraulische Maschinen durchgeführt. Der Bau des Prüfstandes erfolgte zum größten Teil in der institutseigenen Laborwerkstätte, wobei aus zeitlichen und fertigungstechnischen Gründen die Produktion einiger Einzelteile an Dritte vergeben wurde. Die Entwicklungstätigkeiten begannen im Mai 2014 und endeten im Februar 2015 mit den hydraulischen Abnahmemessungen, welche mit dem Auftraggeber am Prüfstand des Instituts durchgeführt wurden.

Deutsche Fassung:

Beschluss der Curricula-Kommission für Bachelor-, Master- und Diplomstudien vom 10.11.2008 Genehmigung des Senates am 1.12.2008

Eidesstattliche Erklärung

Ich erkläre an Eides statt, dass ich die vorliegende Arbeit selbstständig verfasst, andere als die angegebenen Quellen/Hilfsmittel nicht benutzt, und die den benutzten Quellen wörtlich und inhaltlich entnommene Stellen als solche kenntlich gemacht habe. Das in TUGRA-Zonline hochgeladene Textdokument ist mit der vorliegenden Masterarbeit identisch.

Graz, am …….. …….

Unterschrift

English version:

Affidavit

I declare that I have authored this thesis independently, that I have not used other than the declared sources/resources, and that I have explicitly indicated all material which has been quoted either literally or by content from the sources used. The text document uploaded to TUGRAZonline is identical to the present master thesis.

Graz, at …….. …….

Signature

Preface

For the final Master Thesis of the Master programme “Mechanical Engineering and Business Economics” at the Graz Technical University, I wanted to gain experiences in the design, construction and manufacturing of hydraulic machinery as well as in hydraulic measurements of centrifugal pumps. The reason for this is, that I specialised my education in the Master programme in “Technology of Energy” as well as hydraulic fluid machinery, because I was interested in the background of the design and calculation of three-dimensional curved surfaces in pumps and turbines to achieve the hydraulic design characteristics with a high efficiency. Since 2007, I am working for a pump manufacture, who produces sewage pumps and mixers, and want to improve my knowledge in the development process of hydraulic fluid machinery. With this Master Thesis I got a general overview of the development process and how to do acceptance measurements in this product sector.

This Master Thesis is used to document the approach of this development, the statements of construction details and the stress analysis. In this case the documentation should constitute a basis for further design concepts and developments for pumps with similar requirements.

It was a great experience for me to work on this project and I have learned a lot about design methods of centrifugal pumps, acceptance measurements and also about manufacturing engineering.

For the opportunity to write this Master Thesis at the Institute of Hydraulic Fluid Machinery, I would like to thank Mr. O.Univ.Prof. Dipl.Ing. Dr.techn. Helmut Jaberg and Mr. Assoc.Prof. Dipl.Ing. Dr.techn. Helmut Benigni for the supervision and their support during this project. At least, I would also like to thank all the others who helped me to finish this Master Thesis.

May 2015 Franz Zitzenbacher

Table of Contents

List of abbreviations

A

A_2	cross-section area at impeller outlet without blades	[mm^2]
A_{ref}	reference area	[mm^2]
A_{2_as}	assumption of cross-section area at impeller outlet without blades	[mm^2]
A_1	cross-section area at impeller inlet without blades	[mm^2]
A_{1_v}	variable of cross-section area at impeller inlet without blades	[mm^2]
α_1	flow angle between absolute und circumf. velocity at impeller inlet	[°]
α_2	flow angle between absolute und circumf. velocity at impeller outlet	[°]
a_{el}	width factor for elliptic inlet profile	[-]
A_{1_r}	realized cross-section area at impeller inlet without blades	[mm^2]
A_{2_r}	realized cross-section area at impeller outlet without blades	[mm^2]
A_{ne}	net area used for calculation of axial load	[mm^2]
A_{repl_X}	replacement area for compliance calculation of each part X	[mm^2]
α_{ob}	surface factor for bending load	[-]
α_{ot}	surface factor for trosion load	[-]
α_{gb}	size factor for bending load	[-]
α_{gt}	size factor for torsion load	[-]

B

BEP	operating point at best efficiency	[-]
b_1	width of the impeller inlet	[mm]
b_{2_as}	assumption of the width of the impeller outlet	[mm]
b_{2_total}	assumption of the width of the impeller outlet	[mm]
$\beta_{1\_A/B/C}$	relative flow angle between “u”-“w” at plane A/B/C, impeller inlet	[°]
$\beta`_{1\_A/B/C}$	rel. flow angle at plane A/B/C with blades, impeller inlet	[°]
$\beta_{1B\_A/B/C}$	blade angle plane A/B/C, impeller inlet	[°]
β_2	relative flow angle between “u”-“w”, impeller outlet	[°]

$\beta`_2$	rel. flow angle at plane A/B/C with blades, impeller outlet	[°]
β_{2B_v}	blade angle, assumption, impeller outlet	[°]
β_{2B}	blade angle, impeller outlet	[°]
β_{2B_as}	blade angle, impeller outlet, assumption	[°]
b_{el}	length-factor for elliptic inlet profile	[-]
b_{1_r}	realized width of the impeller inlet	[mm]
b_{2_r}	realized width of the impeller outlet	[mm]
β_{kb}	notch factor for bending load	[-]
β_{kt}	notch factor for torsion load	[-]

C

c_{ax}	axial velocity through the gap seal	[m/s]
c_{1m}	meridional velocity without blades at the impeller inlet	[m/s]
c_{1m_v}	variable of meridional velocity without blades	[m/s]
$c_{1\_A/B/C}$	absolute velocity at impeller inlet on plane A/B/C	[m/s]
$c_{1m\_A/B/C}$	meridional velocity at impeller inlet on plane A/B/C	[m/s]
$c_{1u\_A/B/C}$	circumferential component of absolute velocity at impeller inlet	[m/s]
c_{2u}	circumferential component of absolute velocity at impeller outlet	[m/s]
$c_{p\_min\_SF}$	factor pressure drop at impeller blades at inlet	[-]
c_{1m_v}	variable meridional velocity without blades at the impeller inlet	[m/s]
c_{2m_v}	variable meridional velocity without blades at the impeller outlet	[m/s]
c_{1_v}	variable absolute velocity at impeller inlet	[m/s]
c_{2_v}	variable absolute velocity at impeller outlet	[m/s]
C_a	basic dynamic load rating, axial	[N]
C_r	basic dynamic load rating, radial	[N]
C_{0a}	basic static load rating, axial	[N]
$C_{1\text{-}16}$	coefficients for bending equations	[N]

D

d	diameter	[mm]
d_{2o_as}	assumption of outer diameter of the impeller outlet	[mm]
d_{1o_v}	variable of outer diameter at impeller inlet	[mm]
d_{1o}	outer diameter at impeller inlet	[mm]
d_{gr}	diameter of the gap ring	[mm]
d_{Ref}	diameter of reference	[mm]
ΔH_{gap}	difference in head at the gap seal	[m]
d_{1i}	inner diameter at impeller inlet	[mm]
$d_{1\_A/B/C}$	diameter at impeller inlet on plane A/B/C	[mm]
$d_{1\_A/B/C\_r}$	realised diameter at impeller inlet on plane A/B/C	[mm]
$d_{2\_A/B/C}$	diameter at impeller outlet on plane A/B/C	[mm]
$d_{2\_A/B/C\_r}$	realised diameter at impeller outlet on plane A/B/C	[mm]
d_{1m}	middle diameter at impeller inlet	[mm]
d_{1m_r}	realized middle diameter at impeller inlet	[mm]
d_{2m}	middle diameter at impeller outlet	[mm]
d_{1m_r}	realised middle diameter at impeller outlet	[mm]
d_{shaft}	shaft diameter	[mm]
d_{seal_r}	diameter of the seal at the bearing unit	[mm]
$d_{gap\_c\_r}$	diameter of the gap ring at the suction side (cover disk)	[mm]
$d_{gap\_w\_r}$	diameter of the gap ring at the suction side (wear disk)	[mm]
$d°_{1m}$	middle inner diameter dimensionless (referred to d_2)	[-]
d_{2o}	outer diameter at impeller outlet	[mm]
δ	deviation angle at impeller outlet	[°]
ΔH_{gap}	difference of pressure at the gap sealing	[m]
$\Delta p_{A/B/C}$	reduction of pressure at blade at impeller inlet, plane A/B/C	[Pa]
Δp_{run_v}	increase of pressure in the impeller	[Pa]
δ_X	compliance of part X	[mm/N]

E

e_1	diameter of blade profile at impeller inlet	[mm]
e_2	diameter of blade profile at impeller outlet	[mm]
ε_{lim}	parameter for calculation of disperse	[-]
E	coefficient of elasticity	[N/mm²]
η_{BEP}	overall efficiency at the point of operating with best efficiency	[-]
η_{total}	total efficiency	[-]
η_{th_reach}	theoretically reachable efficiency	[-]
η_{h_v}	hydraulic efficiency variable	[-]
η_h	hydraulic efficiency	[-]
η_{h_BEP}	hydraulic efficiency at BEP	[-]
η_v	volumetric efficiency	[-]
η_{v_BEP}	volumetric efficiency at BEP	[-]
$\eta_{bearing}$	mechanical efficiency of the bearing unit	[-]
η_m	mechanical efficiency of the bearing and the sealing unit	[-]
η_{total_calc}	overall efficiency calcualted	[-]

F

f_q	number of venting	[-]
f_1	parameter for calculation of disperse	[-]
F_{cd}	load on the cover disk due to the difference of pressure	[N]
F_{wd}	load on the wear disk due to the difference of pressure	[N]
F_I	incentive load due to the hydraulic flow passing the impeller	[N]
F_{shaft}	axial force as of unbalanced pressure load at the pump-shaft	[N]
F_C	axial force induced from coupling between test rig and electr. m.	[N]
F_{ax}	resulting axial force as a function of Q	[N]
F_{ax1_min}	minimum axial load, calculation model 01 for check	[N]
F_{ax1_max}	maximum axial load, calculation model 01 for check	[N]

F_{ax2}	axial load, calculation model 02 for check	[N]
F_{rad}	radial load as a function of Q	[N]
F_{rad_equ}	equivalent radial load due to the load spectrum	[N]
F_{axial}	axial load for further calculations, including application factor	[N]
F_{radial}	radial load for further calculations, including application factor	[N]
F_{ax_equ}	equivalent axial load due to the load spectrum	[N]
F_m	weight	[N]
F_{m_ts}	weight of the torque sensor	[N]
F_{m_run}	weight of the impeller	[N]
$F_{a\_A/B}$	axial force at bearing A or B	[N]
$F_{r\_A/B}$	radial force at bearing A or B	[N]
$f_{0\_A/B}$	factor for friction losses of bearing A or B	[-]
$f_{1\_A/B}$	factor for friction losses of bearing A or B	[-]
F_{key}	transmitted force per fitting key	[N]
F_B	operating axial force for screws dimensioning	[N]
ΔF_{add}	additional screw load in consequence of the axial force	[N]
F_z	loss of preload force in order of intrusion	[N]
F_{cl}	clamping force	[N]
F_{pre_nec}	preload force necessary	[N]
F_{sc_max}	maximum screw force	

G

γ_{BEP}	disperse parameter at BEP	[-]

H

H_{BEP}	delivery head at operating point with best efficiency	[m]
h_{kop}	sea level at Kopernikusgasse, Graz	[m]
H	delivery head	[m]

H_{th}	theoretical delivery head	[m]
H_p	static head at impeller outlet	[m]

I

$i_{1\_A/B/C}$	incident angle at impeller inlet at plane A/B/C	[°]
I_y	geometrical moment of inertia	[mm^4]

K

k	factor of rotation (gap seal)	[-]
k_w	parameter for calculation of disperse	[-]
k_m	factor of rotation (calculation of the axial force)	[-]
k_{R0}	coefficient for radial load, closed valve	[-]
$k_{R0.5}$	coefficient for radial load, part load 50% of Q_{BEP}	[-]
k_{R1}	coefficient for radial load, at BEP	[-]
k_A	factor for application according to DIN 3990	[-]
k_{RR}	friction loss coefficient	[-]

L

λ	power coefficient	[-]
λ_{BEP}	power coefficient at BEP	[-]
L_{gap_min}	maximum length of the gap seal calculated	[mm]
L_{gap}	length of the gap seal performed	[mm]
λ_l	friction loss factor at laminar flow	[-]
λ_t	friction loss factor at turbulent flow	[-]
λ_{gap}	friction loss factor at gap clearance	[-]
λ_c	factor at impeller inlet including losses and accelerations	[-]
λ_w	factor including pressure drop at impeller blades	[-]
$\lambda_{1run\_A/B/C}$	angle of blade profile at impeller inlet at plane A/B/C	[°]
λ_{2run}	angle of blade profile at impeller outlet	[°]

L_p	length of profiling at impeller inlet	[mm]
$L_{B\_A/B/C}$	length of the blade at plane A/B/C	[mm]
$L°_{B\_A/B/C}$	dimensionless length of the blade at plane A/B/C	[-]
l	distance, length	[mm]
L_h	lifetime	[h]
$L_{h.mod}$	lifetime modified	[h]

M

m_x	exponent	[-]
m_h	exponent	[-]
m_{ij}	parameter for pressure pulsation	[-]
m	mass	[kg]
M_0	friction moment of bearings non load depending part	[Nmm]
M_1	friction moment of bearings load depending part	[Nmm]
M_m	moment of mechanical friction (bearings and seals)	[Nm]
M_t	torque	[Nm]
M_{x_y}	internal moment at section x (1; 2; 3; 4) and position y (0,A,B,run)	[Nm]

N

n_{shaft}	rotating speed	[min^{-1}]
$N_{ssX\%}$	specific suction number at the operating point at X% of Q_{BEP}	[min^{-1}]
n_q	specific speed	[min^{-1}]
n_{q_Ref}	specific speed reference	[min^{-1}]
NPSH	net positive suction head	[m]
$NPSH_3$	net positive suction head at 3% reduction of delivery head	[m]
$NPSH_{3\_\lambda w}$	$NPSH_3$ at a particular λ_w	[m]
n_p	number of fitting keys	[-]
n_{crit}	critical rotating speed of the pump shaft	[Hz]

O

ω	angular velocity	[rad^{-1}]
ω_{c0-2}	critical bending speed of each case (0; 1; 2)	[Hz]
ω_{crit}	critical bending of the pump shaft	[Hz]

P

p_{amb}	air pressure at sea level	[Pa]
P_h	hydraulic power of the pump	[W]
P_P	power consumption of the pump	[W]
P_{gap}	power loss in case of leakage flow through the gap sealing	[W]
ψ	pressure number	[-]
ψ_{BEP}	pressure number at BEP	[-]
ψ_{BEP_as}	pressure number at BEP assumption	[-]
ψ_{0_as}	pressure number at 0% flow rate assumption	[-]
φ	delivery coefficient	[-]
Φ_{BEP}	delivery coefficient at BEP	[-]
P_{gap}	power loss as a result of the leakage flow	[W]
ρ_{H2O}	density of water	[kg/m^3]
p_{1_stat}	absolute static pressure at the suction pipe	[Pa]
$p_{2\_run\_0}$	absolute pressure at impeller outlet	[Pa]
P	equivalent load	[N]
P_r	friction loss of the bearing unit	[W]
p_0	pressure at impeller backside	[Pa]
p_{diff_seal}	difference of pressure at the radial shaft seal ring	[Pa]
P_{RR}	power loss in reference to friction losses at impeller side room	[W]
p_{perm}	permissible pressure	[N/mm^2]
p_p	wearing number for fitting keys	[-]
Φ	load rate for screw dimensioning	[-]

Q

Q_{BEP}	volumetric flow at the operating point with best efficiency	[m^3/s]
Q_{ref}	volumetric flow as reference	[m^3/s]
Q	variable for volumetric flow	[m^3/s]
Q_L	leakage flow rate through relief hole	[m^3/s]
Q_h	leakage flow rate for other use	[m^3/s]
Q_{gap}	leakage flow rate through the gap ring	[m^3/s]
Q_{run}	volumetric flow through the impeller	[m^3/s]
$q_{x\%}$	percentage of operating time at X% of Q_{BEP} referring to total lifetime	[%]
q_{total}	sum of all q_x has to be 100%	[%]
q	equivalent line load	[N/m]

R

r_H	shut-off head ratio	[%]
R_{HR}	matrix of coefficients Herbst-Roegner	[m³/kg]
Re	Reynolds number	[-]
$R_{p0.2\_1.1191}$	yield strength at 0.2% plastic deformation of Ck45_normalised	[N/mm²]
$R_{m\_1.1191}$	minimum specified tensile strength of Ck45_normalised	[N/mm²]
R_{e_AW7075}	yield strength of AlZn5,5MgCu	[N/mm²]
R_{m_AW7075}	minimum specified tensile strength of AlZn5,5MgCu	[N/mm²]
$R_{e\_1.0037}$	yield strength of S235JR	[N/mm²]
$R_{m\_1.0037}$	minimum specified tensile strength of S235JR	[N/mm²]

S

s_{gap}	gap of the gap seal in radial direction calculated	[mm]
s_{gap_API}	gap of the gap seal in radial direction according to API 610	[mm]
$\sigma_{tcS/Sch/W}$	tension and compressive stress, static load/cycling load/alternating load	[N/mm²]
$\sigma_{bS/Sch/W}$	bending stress, static load/cycling load/alternating load	[N/mm²]

$\tau_{tS/Sch/W}$	torsion stress, static load/cycling load/alternating load	[N/mm²]
S	reliability factor	[-]
σ_{max}	maximum normal stress	[N/mm²]
σ_m	mean normal stress	[N/mm²]
σ_a	deflection normal stress	[N/mm²]
σ_A	permissible deflection normal stress	[N/mm²]
σ_{NA}	adapted permissible deflection normal stress (notch influence)	[N/mm²]
σ_{va}	equivalent deflection normal stress	[N/mm²]

T

t_{BEP}	tolerance of the efficiency at the operating point	[%]
$t_{nqu/nqo}$	acceptable tolerance of n_q	[min^{-1}]
$t_{rh\_low/high}$	acceptable tolerance of shut-off head	[%]
$\tau_{1\_A/B/C}$	blade obstruction at impeller inlet at plane A/B/C	[-]
t_2	width from blade to blade in angular direction	[mm]
a_{2_min}	minimum width from blade to blade in direct direction	[mm]
a_{2_max}	maximum width from blade to blade in direct direction	[mm]
$T_{x°C}$	temperature at x°C	[K]
t	temperature	[°C]
$t_{1/2\_run}$	deep of the fitting key	[mm]
τ_{perm}	permissible shear stress	[N/mm²]
T_{m_nec}	mounting torque necessary	[Nm]
T_{m_avail}	mounting torque available	[Nm]
τ_{max}	maximum shear stress	[N/mm²]
τ_m	mean shear stress	[N/mm²]
τ_a	deflection shear stress	[N/mm²]
τ_A	permissible deflection shear stress	[N/mm²]
τ_{NA}	adapted permissible deflection shear stress (notch influence)	[N/mm²]

U

u_{2o_as}	circumferential velocity at the outer diameter of the impeller outlet	[m/s]
u_{gap}	circumferential velocity at the gap seal	[m/s]
u_1	circumferential velocity at impeller inlet	[m/s]
$u_{1\_A/B/C}$	circumferential velocity at impeller inlet on plane A/B/C	[m/s]
u_2	circumferential velocity at impeller outlet (90° outlet)	[m/s]
$u_{2\_A/B/C}$	circumferential velocity at impeller outlet at plane A/B/C	[m/s]
u_{1_v}	variable circumferential velocity at impeller inlet	[m/s]
u_{2_v}	variable circumferential velocity at impeller outlet	[m/s]

W

w_1	relative velocity at impeller inlet	[m/s]
w_2	relative velocity at impeller outlet	[m/s]
w_{1_v}	variable of relative velocity at impeller inlet	[m/s]
w_{2_v}	variable relative velocity at impeller outlet	[m/s]
$w_{1\_A/B/C}$	relative velocity at impeller inlet on plane A/B/C	[m/s]
w_{1u}	relative velocity in circumferential direction at impeller inlet	[m/s]
w_{2u}	relative velocity in circumferential direction at impeller outlet	[m/s]
$w°_{1\_A/B/C}$	dimensionless relative velocity at impeller inlet at plane A/B/C	[-]
w_{1_m}	relative velocity at the middle diameter at the impeller inlet	[m/s]
$w_{1\_m\_up}$	upper limit of the relative velocity at the impeller inlet	[m/s]
$w_{1\_m\_lo}$	lower limit of the relative velocity at the impeller inlet	[m/s]
$w_{1\text{-}4}$	defection of the pump shaft	[mm]
W_y	section modulus	[mm³]
W_p	polar section modulus	[mm³]

X

$x_{gap\_s\_}$	ratio of the gap ring diameter to the outer diameter of the impeller	[-]
$\xi_{eff\_A/B/C}$	effective blade load at plane A/B/C	[-]
$\xi_{acep\_A/B/C}$	accepted blade load at plane A/B/C	[-]

Y

y_{gap}	factor for gap seal	[-]

Z

ζ_{EA}	factor for losses at in- and outlet of the gap seal	[-]
z_{run}	number of blades at the impeller	[-]
z_{dif}	number of blades at the diffusor	[-]
z_{run_r}	realised number of blades at the impeller	[-]
z_{dif_r}	realised number of blades at the diffusor	[-]
z	control variable	[mm]

1 Introduction

The subject-matter of this Master Thesis is the design of a low specific speed diffusor pump and the construction of the experimental setup.

The impulse for the hydraulic development of this semi-axial pump was given by a pump manufacturer from South Korea, Hyosung Goodsprings Inc. (473 Gongdeok-Dong, Mapo-Gu, Seoul, 121-805, Republic of Kroea), who placed an order for the "Hydraulic Development and Engineering Services Agreement for semi-axial pumps". The development work for this project was divided into two parts: on the one hand the hydraulic one-dimensional design of the main dimensions, the construction and the manufacturing of the test rig, which is the content of this Master Thesis, and on the other hand, the hydraulic optimisation with Ansys CFX®, which was done by Dipl. Ing. Stefan Höller-Litzlhammer. The concept of the test rig is based on the experiences of the Institute of Hydraulic Fluid Machinery and is based on the existing design concept of Dipl.Ing. Handl [1] and Dipl.Ing. Hopfgardner [2]. The main data for the developed pump were defined in detail in [3], and provides the basic data for construction and design. The start of the project was in May 2014 and the end was in February 2015. Due to the very tight schedule, the work on the concept-finding, the detailed construction and manufacturing of the test rig was realised in parallel to the hydraulic optimisation with Ansys CFX®. The final geometry of the detailed design of the impeller and the diffusor was finished just in time with the beginning of the production of the last parts for the test rig.

A large range of adjustments during the production of the test rig had to be done in order to get good results.

1.1 Scope of this Master thesis

1. Hydraulic dimensioning of impeller and diffuser
2. Concept design and layout finding
3. Stress analysis of all relevant parts
4. 3D construction and drawings (single parts and assembly)
5. Support manufacturing
6. Measurements and analysis of data

The steps have to be passed in the same chronological order as these chapters above.

1.2 Requirements

The requirements are scheduled in an agreement between the customer and the Institute of Hydraulic Fluid Machinery. The condition framework is shown in detail in Table 1.1.

Table 1.1: Requirements [3]

Specification	Target Value	Unit	Acceptance Tolerance
Specific Speed (@ BEP)	280	(m^3/min, m)	± 10
Q_{Design}	430	(m^3/h)	ISO 9906 grade 1B
H (@ Q_{Design})	34.5	(m)	ISO 9906 grade 1B
Speed	1.490	(rpm)	N/A
Specific Speed (@ Q_{Design})	280	(m^3/min, m)	N/A
Overall Pump Efficiency (@ Q_{BEP})	87	(%)	- 1.5
Wear Ring Seal Clearance	API 610 11^{th}	-	API 610 11^{th}
Shut-off Head Ratio H_0/H_{Design}	124	(%)	± 4
Minimum Continuous Stable Flow Rate (Recommendation)	120	(m^3/h)	Second Party shall do the best to make the minimum flow lower than 30%. Minimum flow measurement method shall be proposed by Second Party as an Option.
Stage Length	1,3 * d2	(mm)	If exceeds agreement shall be made between two parties.
Maximum Diffuser Outer Diameter	1,3 * d2	(mm)	If exceeds agreement shall be made between two parties.
Shaft Diameter (@ hub cap)	75	(mm)	N/A
Hub Diameter (@ hub cap)	90	(mm)	N/A
Nss (@ 70% Q_{Design})	1.400	(m^3/min, m)	- 0.0 (Zero negative tolerance)
Nss (@ Q_{Design})	1.600	(m^3/min, m)	- 0.0 (Zero negative tolerance)
Nss (@ 130% Q_{Design})	1.400	(m^3/min, m)	- 0.0 (Zero negative tolerance)
multistage use			constructional consideration

1.3 Preface on centrifugal pumps

In this chapter, the fundamental information on centrifugal pumps, their structure, data of performance and use will be explained in general.

1.3.1 Functionality

A centrifugal pump is a type of a turbo machine, which is used for hauling fluids. A particular volumetric flow rate has to be brought from a lower pressure level to a higher pressure level. The energy exchange in turbo machines is done by hydrodynamic processes, which are characterised by the proportionality of the difference of pressure and energy to the square of velocity.[4, p. 39]

1.3.2 Setup of centrifugal pumps

The main parts of a centrifugal pump are the spiral casing, the bearing unit with the shaft and the impeller (Figure 1.1). At the inlet of the pump, the fluid directly flows to the impeller, which is moved across a connector by an engine. The impeller accelerates the fluid in radial direction and transfers the necessary energy so that the static pressure rises as the fluid is moving on a curved path. In the leading unit, a part of the kinetic energy of the fluid, which comes from the outlet of the impeller, is transferred to the static pressure like it is done in a diffuser. The leading unit in Figure 1.1 consists of a spiral casing, which is connected with a diffuser and the discharge nozzle. On the right side of the impeller, a sealing unit prevents the fluid of leaking into the environment or into the bearing unit. This can be done by means of a packing box or a rotating mechanical seal. On the left side of the impeller, a short gap between the rotating impeller and the stationary housing reduces the leakage flow from the impeller outlet to the impeller inlet. The same gap can be used at the backside of the impeller to reduce the axial force and to minimize the axial load on the bearing unit. [4, p. 39]

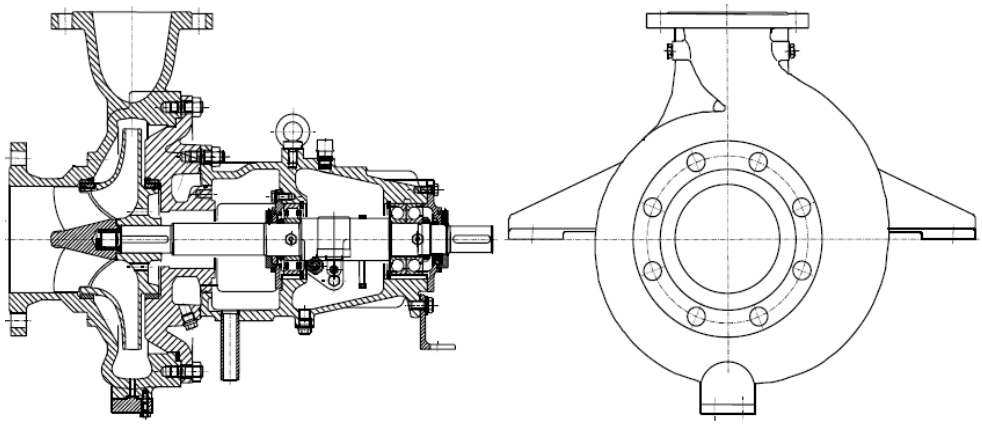

Figure 1.1: Single stage spiral casing pump with bearing unit, Sulzer Pumpen AG [4, p. 39]

1.3.3 The impeller of a centrifugal pump

In general, the impeller of a centrifugal pump consists of three parts, namely the hub, which is the connection to the pump shaft, the blades, which are used to transfer energy to the fluid, and the shroud. Not every impeller is necessarily equipped with a shroud as such an equipment is depending on the type of application of the pump. An impeller without a shroud is called “half-open impeller” (Figure 1.2), and without a shroud and an extensive opened hub are called “open impeller”. [4, p. 40]

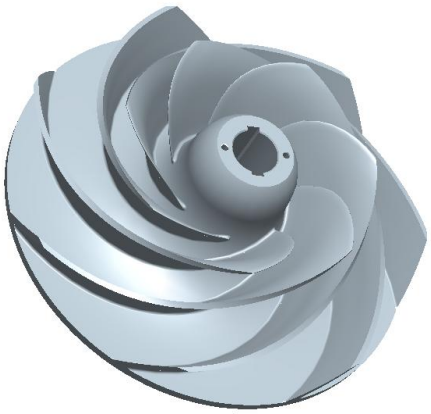

Figure 1.2: Half open impeller of a centrifugal pump

Depending on the application, there are a lot of different types of pumps and components which are used to manage different tasks of conveying. There are different aspects to distinguish these different types of centrifugal pumps.

1. Flow direction in the impeller:
    a. radial flow
    b. mixed flow
    c. axial flow
2. Impeller-design:
    a. closed
    b. semi-open
    c. open
3. Leading unit: flow direction at the inlet:
    a. radial
    b. semi-radial
4. Design of the housing:
    a. single or double spiral housing
    b. concentric annular space
    c. no concentric annular space (like a spiral housing)
    d. diffusor

5. Inlet housing:
    a. annular space housing
    b. symmetric inlet
    c. asymmetric inlet
6. Serial arrangement (multistage):
    a. return blades instead of guide blades
    b. diffusor (spiral housing with special designed channels) instead of guide blades
7. Parallel arrangement:
    a. single stage
    b. multistage

A combination of different arrangements allows for the creation of a variety of different pump types for different applications. [4, p. 41]

1.3.4 Performance Data

For the specification of a centrifugal pump, various information is necessary. [4, p. 43]

1. Volumetric flow rate Q (at the outlet of the pump)
2. Delivery head H (at the outlet of the pump)
3. Required power (at the pump shaft coupling)
4. Overall efficiency (at the pump shaft coupling)
5. NPSH (Net positive suction head at the impeller inlet)

1.3.5 Applications of centrifugal pump

Centrifugal pumps are used to deliver a wide range of various fluids in different applications. The typical volumetric flow begins at 0.001m³/s and goes to 60m³/s, the delivery head reaches from 1 to 5.000 metres and the rotating speed can go up to 30.000rpm, however there are also pumps with parameters which are out of these ranges. These three parameters are used to characterise the delivery performance and the meridional design of centrifugal pump. [4, p. 47]

The corresponding equation called “specific speed”, is shown in equation 1.1 and provides values for radial pumps between 7 and 100rpm, for half axial pumps between 35 and 160rpm and for axial pumps between 160 and 400rpm. The borderline between these different types of pumps is not very strict, because the type of the pump also depends on the type of construction.[4, p. 49]

$$n_q = n \cdot \frac{\sqrt{Q}}{H_{tot}^{0.75}} \tag{1.1}$$

Equation 1.1 refers to the volumetric flow and the delivery head of only one impeller. If there is a parallel arrangement, the volumetric flow has to be divided by the number of

entries, and in case of a multi-stage pump, the delivery head has to be divided by the number of stages.

If the specific speed is very low, the efficiency of the pump decreases very fast, hence an economic use is not possible. In this case, the type of the pump has to be changed or a second stage has to be used instead. For a high discharge and low differential head, the economic limit of n_q is between 350 and 400rpm, as the effort of construction and the hydraulic losses are too high. In order to develop pumps with high n_q, a parallel installation may be useful. [4, p. 48]

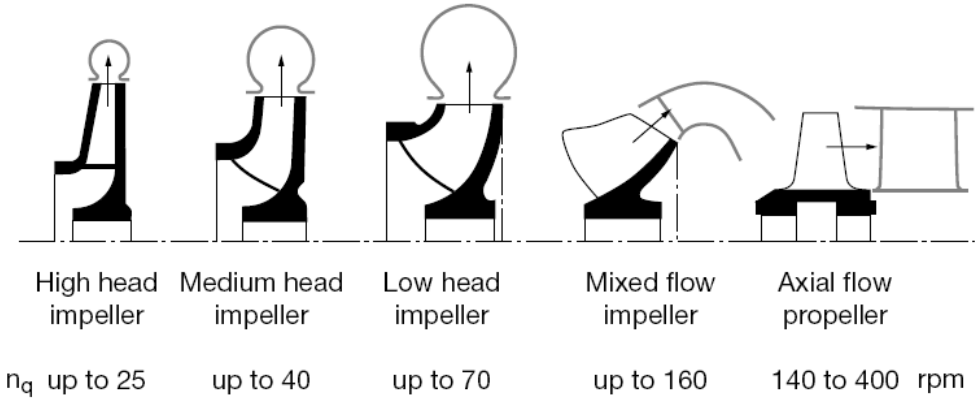

Figure 1.3: Design of centrifugal pump impellers depending on n_q [5, p. 12]

1.4 Cavitation and NPSH

1.4.1 Cavitation

A fluid will evaporate, if the static pressure is lower than the steam pressure, which depends on the temperature. This may happen when the velocity of a flowing fluid is partially accelerated in case of a constriction and when the static pressure decreases in reference with the Bernoulli's equation. Cavities are built up, which are filled with steam and transported downstream with the flowing fluid. If these cavities get to a region of higher static pressure, the steam at the inside of these cavities condensates and the cavitation bubbles implode immediately. If this implosion happens very close to a wall (e.g pipe wall, blades of an impeller), extremely high pressure peaks may lead to a damage of the material and will lead to cavitation erosion.

In centrifugal pumps, cavitation can lead to a damage of the impeller because of cavitation erosion, a destruction of the sealing in case of vibrations and at last to a failure of the pump. Furthermore, an increase of the intensity of cavitation leads to a decrease of the efficiency and the delivery head.

These are the reasons for limitation and minimisation of the acceptable intensity of cavitation in pumps which is done based on the NPSH-value, as mentioned in chapter 1.4.2.

1.4.2 Net positive suction head - NPSH

The intensity of cavitation depends on the size of the region in which the static pressure is lower than the steam pressure of the fluid. If this region is small, cavitation starts, however is not detectable from the outside of the pump. If this region is large, the cavitation intensity increases which leads to full cavitation of the impeller. Full cavitation at the impeller leads to a collapse of the fluid flow.

Due to the fact that the local pressure at the impeller inlet is not measurable, a more convenient method to characterise the cavitation behaviour of the pump has to be defined. Hence, a NPSH value has to be defined, which is equal to the difference of the total head and the steam head at the inlet of the pump (equation 1.2).

$$NPSH = \frac{p_s - p_V}{\rho_{H2O} \cdot g} - \frac{c_s^2}{2 \cdot g} \qquad 1.2$$

On the one hand NPSH value depends on the vapour pressure of the fluid, and on the other hand of the flow conditions at the pump inlet, whereas all are measurement data. If the flow rate is the same, and the static pressure at the inlet of the pump is getting lower, the NPSH value will also decrease. The static pressure which causes the first cavitation bubbles than leads to the $NPSH_i$-value. It is the maximum value for the pump running without cavitation. However, the NPSH value defines the difference between the total head and vapour head in reference to cavitation criteria. Different $NPSH_R$-values are used to characterise the cavitation behaviour of a pump, shown in the list below.

- $NPSH_i$: beginning cavitation, first cavitation bubbles are visible
- $NPSH_0$: 0% loss of delivery head
- $NPSH_1$: 1% loss of delivery head
- $NPSH_3$: 3% loss of delivery head
- $NPSH_x$: x% loss of delivery head
- $NPSH_{fc}$: collapse of the delivery head, the impeller is running in full cavitation
- Defined loss of efficiency
- Defined erosion of material
- Defined lifetime of the impeller

The most widespread NPSH criterion is $NPSH_3$, as its measurement is easier than for other criteria. Figure 1.4 schematically shows the typical curves of different NPSH values for radial impellers.

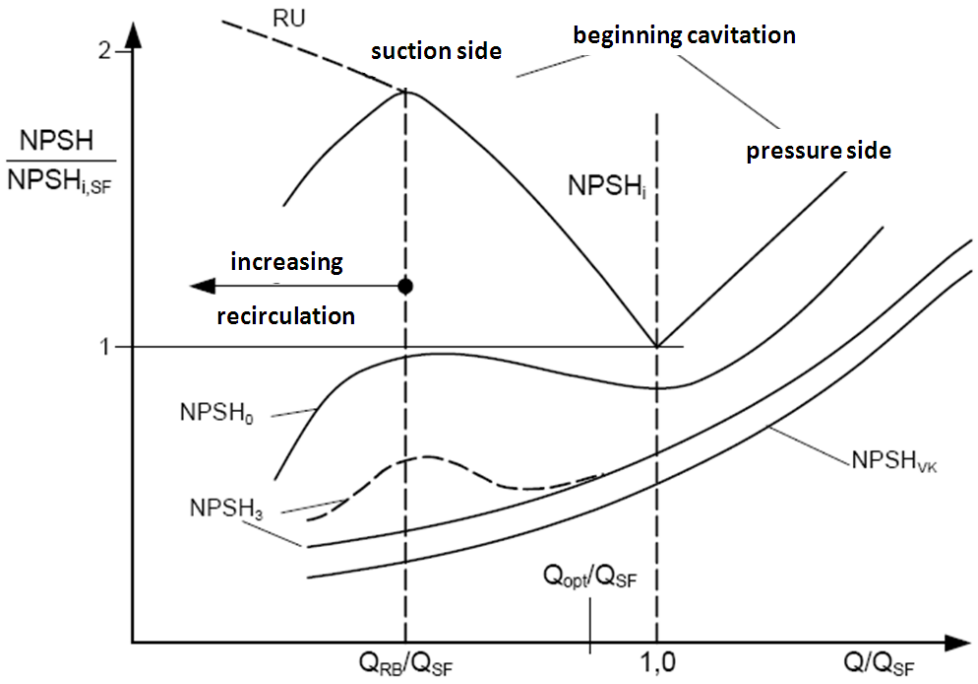

Figure 1.4: Typical NPSH curves of radial impeller (schematically) [4, p. 276]

1.4.3 Suction specific speed n_{ss}

The suction specific speed is used to compare the cavitation behaviour of different pumps, which are not geometrically similar. This is done at the best efficiency point (correctly it would be the point of operation without swirl) in a similar way as it is realised for the specific speed n_q, seee equation 1.3.

$$n_{ss} = n \cdot \frac{\sqrt{Q_{BEP}}}{NPSH^{0.75}} \qquad 1.3$$

The units used for n_{ss} are for the rotating speed rpm, for the volumetric flow m³/h and for the NPSH meter. It has to be mentioned that the customer has used the same definition for the suction specific speed but a different unit for the volumetric flow (m³/min). The link between n_{ss} and N_{ss} defined by the customer is shown in equation 1.4.

$$N_{ss} = n_{ss} \cdot \sqrt{60} \qquad 1.4$$

2 Dimensioning of the test rig

First of all, a one-dimensional design of the centrifugal pump is used to get the main dimensions of the test rig. With this information, initial layouts can be designed to check the feasibility and the fulfillment of the requirements. The most important information used for the design of the test rig is shown in the following list:

- meridional design, radial- mixed- ore axial-flow
- inner, outer diameter of the impeller
- inner diameter of the suction pipe
- power consumption of the test rig (rotating speed, torque)
- axial and radial load of the impeller
- pressure distribution inside the pump
- pressure inside the suction and pressure pipe

The hydraulically dimensioning of the centrifugal pump is the first step before the first concept will be realised.

2.1 Fundamental information

The parameters given by the customer are shown in Table 1.1. These are used for the one-dimensional design of the test rig. The specific speed, the volumetric flow rate, the delivery head and the rotating speed of the pump shaft are indicated as follows.

$$n_{q\_BEP\_requ} := 280$$

$$Q_{BEP} := 430 \cdot \frac{m^3}{hr}$$

$$H_{BEP} := 34.5 \cdot m$$

$$n_{shaft} := 1490 \cdot min^{-1}$$

The overall pump efficiency η_{BEP} is specified as 87%, including the hydraulic and the mechanical efficiency with an acceptable variance of -1,5%.

The shut-off head ratio is defined as r_H=1,24, which leads to a shut-off head of 42,78m with an accepted variation of +/- 4%.

$$H_0 := H_{BEP} \cdot r_H = 42.78\,m \tag{2.1}$$

To define the cavitation behaviour of this centrifugal pump, the customer uses the suction specific speed N_{ss} at 70%, 100% and 130% of the flow rate best efficiency point (Q_{BEP}).

$$Nss_{70\%} := 1400\ rpm$$

$$Nss_{100\%} := 1600\ rpm$$

$$Nss_{130\%} := 1400\ rpm$$

The design of the gap ring, especially the dimension of the wear ring seal clearance, has to be according to API 610 version 11 [6, p. 39].

The following geometrical requirements are also given:

- the stage length must be not longer than 130% of the outer diameter of the impeller;
- the maximum diameter of the diffusor must be not longer than 130% of the outer diameter of the impeller;
- the shaft diameter of 75mm must be realisable;
- the diameter of the hub of the impeller must be at least 90mm;

Each of the above mentioned requirements was given by the customer and are used for the one-dimensional design of the impeller and the diffusor.

The density of water is calculated by the method of Herbst-Roegner, which is corresponding to [7, p. 169]. This method of calculation is applied to a temperature of 18°C as follows and is used for the evaluation of the measurements results later on.

The air pressure is defined with p_{abs} and is 1,013 bar.

$$\rho_{H2O} = 10^2 \cdot \left[\sum_i \left[\sum_j \left[R_{ij} \cdot \alpha^j \cdot \beta^{(i-1)} \right] \right] \right]^{-1} \tag{2.2}$$

$$\rho_{H2O} = 998.59\,\frac{kg}{m^3}$$

The exact approach according to this method is shown in Appendix A.

2.2 Power consumption

The power consumption of the pump is depending on the hydraulic power and the overall efficiency, which were defined by the customer.

$$P_h := \rho_{H2O} \cdot g \cdot H_{BEP} \cdot Q_{BEP} = 40.35 \cdot kW \tag{2.3}$$

$$P_P := \frac{P_h}{\eta_{BEP}} = 46.38 \cdot kW \tag{2.4}$$

Another way to write the power consumption is, to divide it up into the hydraulic power and the energy losses in resulting of the friction, as shown in equation 2.5.[4, p. 135]

$$P_P = \sum_{st} \frac{\left(\rho_{H2O} \cdot g \cdot H_{BEP} \cdot Q_{BEP}\right)}{\eta_h \cdot \eta_v} + \sum_{st} P_{RR} + \sum_{st} P_{S3} + P_m + P_{er} + P_{Rec} \tag{2.5}$$

In equation 2.5, the following losses are combined and are shown in Figure 2.1 [4, p. 85]:

1) Mechanical losses P_m
2) Volumetric losses η_v
3) Losses of rotating disks of the impeller P_{RR}
4) Losses of rotating disks of other components P_{er}
5) Losses of power in reference to leakage flow in multistage pumps P_{S3}
6) Hydraulic losses η_h
7) Losses in reference to recirculation P_{Rec}

For the actual pump in a single arrangement, the losses 4 and 5 do not exist and in the point of best efficiency no recirculation is assumed. The final equation for the balancing of power is defined as follows.

$$P_P = \frac{\rho_{H2O} \cdot g \cdot H_{BEP} \cdot Q_{BEP}}{\eta_h \cdot \eta_v} + P_{RR} + P_m \tag{2.6}$$

In order to reach the required N_{ss} values, the hydraulic efficiency may be lower than expected in case of geometrical differences to the recommended hydraulic design. The required overall efficiency is rather high with reference to the expected values referred to the literature. The volumetric leakage is defined by the maximum gap clearance, and the optimisation of the friction losses at the impeller side chamber is limited. In any case, the mechanical friction losses have to be as low as possible to reach the required overall efficiency. Furthermore, a highly efficient power train has to be designed (see chapter 2.4.5).

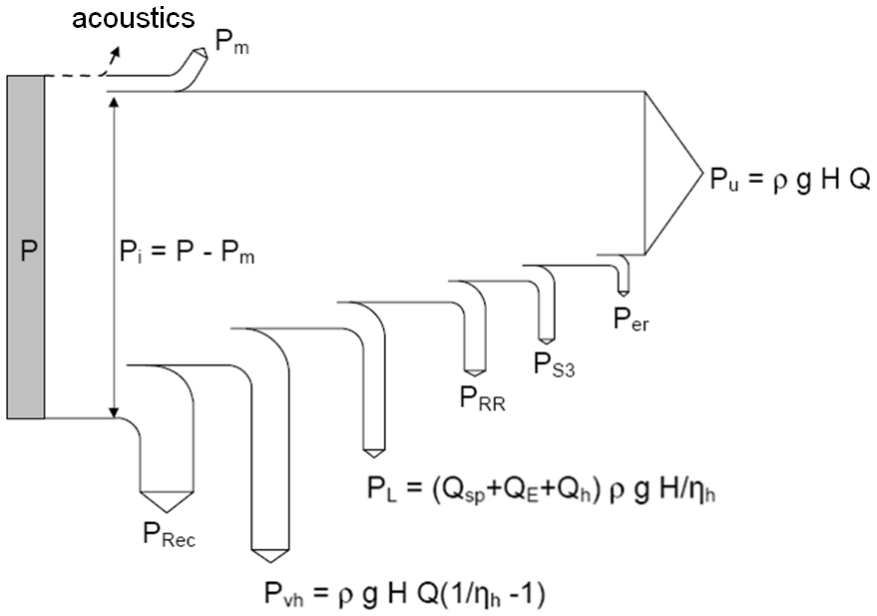

Figure 2.1: power balance of a pump [4, p. 85]

2.3 Characteristic numbers

2.3.1 The specific speed

The specific speed is used do define the meridional design as it is mentioned in 1.3.5, and in this case is calculated as follows. The rotating speed has the unit [rpm], Q_{BEP} has the unit [m³/s] and H has the unit [m].

$$n_q = n_{shaft} \cdot \frac{\sqrt{Q_{BEP}}}{H_{BEP}^{\frac{3}{4}}} = 36.17 \qquad 2.7$$

The customer defines the specific speed in the agreement in the same way as shown in equation 2.7, but the units used for this definition are selected in the following way: the rotating speed has the unit [rpm], the flow rate Q_{BEP} has the unit [m³/min] and the delivery head has the unit [m]. Thus, the connection between equation 2.7 and the specific speed defined by the customer is shown in equation 2.8.

$$n_{q\_customer} := n_q \cdot \sqrt{60} = 280.21 \qquad 2.8$$

The tolerance of $n_{q\_customer}$ is established as +/- 10.

Another dimensionless number to show the meridional layout has already been used in Germany for water use, as shown in equation 2.9. The connection between these two characteristic numbers (equation 2.7 and 2.9) can be looked up in [8, p. 84].

$$n_s = n_q \cdot 3.652 = 132.1 \qquad 2.9$$

2.3.2 Head coefficient

For further calculations, the dimensionless head coefficient is needed to get the main dimensions of the impeller. The head coefficient is defined as shown in equation 2.10 and is a dimensionless number to characterise the operating behaviour of a pump.

$$\psi = \frac{2 \cdot g \cdot H}{u_2^{\,2}} \qquad 2.10$$

There are statistical values for centrifugal pumps published in [4, p. 112], which are used to estimate the outer diameter of the impeller. Figure 2.2 shows the head coefficient with reference to the specific speed, the mean value can be calculated with equation 2.11 which is the result of the .

$$n_{q.Ref} := 100$$

$$\psi_{BEP\_as} := 1.21 \cdot e^{-0.77 \cdot \frac{n_q}{n_{q.Ref}}} = 0.92 \qquad 2.11$$

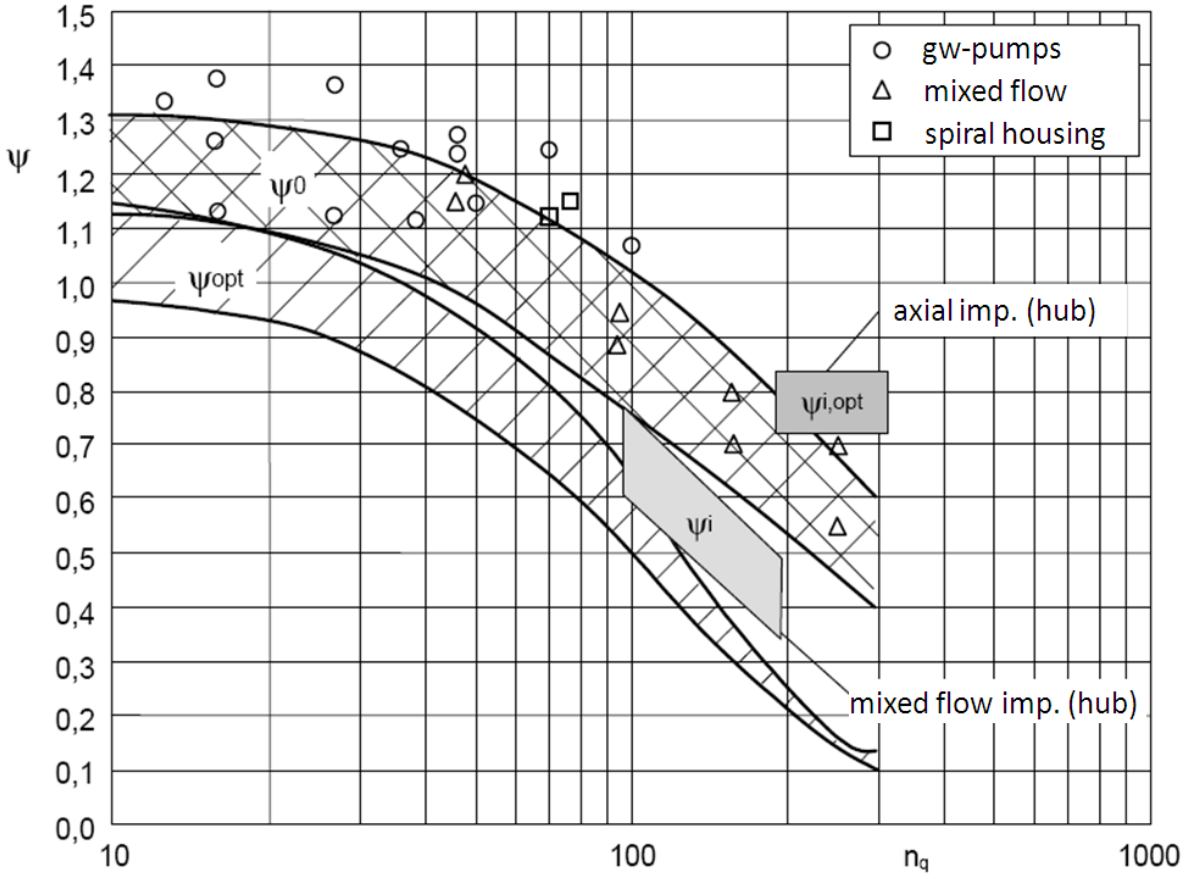

Figure 2.2: Coefficient of pressure [4, p. 112]

The upper value for the head coefficient is 0.99, which will lead to a flat characteristic curve, yet the risk of instability will increase. The lower value is 0.84, which will lead to steeper characteristic curves. [4, p. 113]

In the present case, a flat characteristic curve is needed, and for this reason the head coefficient will be defined as 0.94 for further calculations. The outer diameter of the impeller is calculated as shown in equation 2.12.

$$d_{2o\_as} := \frac{1}{n_{shaft}\,\pi}\cdot\sqrt{\frac{2\cdot g\cdot H_{BEP}}{\psi_{BEP}}} = 343.9\cdot mm \qquad 2.12$$

The circumferential velocity at the outer diameter can be investigated by 2.13.

$$u_{2o\_as} := d_{2o\_as}\cdot\pi\cdot n_{shaft} = 26.84\,\frac{m}{s} \qquad 2.13$$

2.3.3 Delivery and power coefficient

The reference area is the projected area of the outer diameter of the impeller and is defined as follows in equation 2.14.

$$A_{ref} := \frac{d_{2o\_as}^{2}\cdot\pi}{4} \qquad 2.14$$

The delivery coefficient is referenced to this area in equation 2.15, and the same reference applies to the power coefficient in equation 2.16.

$$\phi_{BEP} := \frac{Q_{BEP}}{A_{ref}\cdot u_{2o\_as}} = 0.0479 \qquad 2.15$$

$$\lambda_{BEP} := \phi_{BEP}\cdot\psi_{BEP}\cdot\eta_{BEP} = 0.0391 \qquad 2.16$$

2.4 Efficiency and losses

2.4.1 Total efficiency

The reachable overall efficiency for centrifugal pumps can be estimated with equation 2.17 which is recommended by [4, p. 142]. These equations are used for single-stage and multi-stage centrifugal pumps with different specific speeds. The exponent m_x is the same and is calculated with Q_{ref}=1 m³/s and factor a=1, when Q_{BEP} is lower than 1 m³/s.

$$m_x := 0.1 \cdot \left(\frac{Q_{ref}}{Q_{BEP}}\right)^{0.15} \cdot \left(\frac{45}{n_q}\right)^{0.06} = 0.14 \qquad 2.17$$

In order to estimate the overall efficiency of a single-stage centrifugal pump with a specific speed lower than 100, equation 2.18 can be used.

$$\eta_{total\_100} := 1 - 0.095 \cdot \left(\frac{Q_{ref}}{Q_{BEP}}\right)^{m_x} - 0.3 \cdot \left(0.35 - \log\left(\frac{n_q}{23}\right)\right)^2 \cdot \left(\frac{Q_{ref}}{Q_{BEP}}\right)^{0.5} = 85.2 \cdot \% \qquad 2.18$$

In order to estimate the overall efficiency of a multi-stage centrifugal pump with a specific speed lower than 60, equation 2.19 can be used.

$$\eta_{total\_60} := 1 - 0.116 \cdot \left(\frac{Q_{ref}}{Q_{BEP}}\right)^{m_x} - 0.4 \cdot \left(0.26 - \log\left(\frac{n_q}{25}\right)\right)^2 = 84 \cdot \% \qquad 2.19$$

The maximum total efficiency reachable can be estimated less than 85%, lower than the maximum total efficiency of 87% required by the customer. This means, that the hydraulic efficiency and also the mechanical efficiency have to be very high, to fulfil the requirements.

2.4.2 Hydraulic efficiency

The formula for the hydraulic efficiency by Gülich [4, p. 142] is calculated in equation 2.21.

$$m_h := 0.08 \cdot \left(\frac{Q_{ref}}{Q_{BEP}}\right)^{0.15} \cdot \left(\frac{45}{n_q}\right)^{0.06} = 0.11 \qquad 2.20$$

$$\eta_{h\_BEP} := 1 - 0.055 \cdot \left(\frac{Q_{ref}}{Q_{BEP}}\right)^{m_h} - 0.2 \cdot \left(0.26 - \log\left(\frac{n_q}{25}\right)\right)^2 \cdot \left(\frac{Q_{ref}}{Q_{BEP}}\right)^{0.1} = 92.8 \cdot \% \qquad 2.21$$

2.4.3 Volumetric efficiency

The inlet diameter of the impeller depends on the total flow rate through the impeller at the best efficiency point and on the cavitation behaviour. The total flow rate through the impeller Q_{run} is composed of the delivery flow rate which is required by the customer Q_{BEP}, the leakage flow rate of the wear ring sealing Q_{gap}, the leakage flow rate in case of axial force compensation Q_L and the flow rate, which is used for other purposes Q_h. The volumetric efficiency is defined as follows see equation 2.22.

$$\eta_V = \frac{Q_{BEP}}{Q_{BEP} + Q_{gap} + Q_L + Q_h} = \frac{Q_{BEP}}{Q_{run}} \qquad 2.22$$

The flow rate though the gap depends on the gap ring diameter, the gap ring clearance (which is defined by API 610), the length of the gap, the geometric shape of the clearance and the pressure difference.

The diameter of the gap ring is assumed to be 230 mm and the maximum diametric clearance of the wear ring is defined by the standard API 610 to be 0.53 mm [6, p. 39].

The length of the gap sealing has to be 50 times longer than its clearance [4, p. 97].

$$L_{gap\_min} := 50 \cdot s_{gap\_API} = 13.25 \cdot mm \qquad 2.23$$

$$L_{gap} := 20 \cdot mm$$

The realised gap ring length is at least 20 mm and bigger than 50 times the gap ring clearance.

To investigate the pressure difference at the wear ring sealing, the static pressure at the impeller outlet H_p must be known. At the best efficiency point, the total pressure at the

impeller outlet consists of a static and a dynamic part. The static pressure at the impeller outlet can be estimated by $H_p=H_{BEP}*R_G$ (with H_{BEP}, the delivery head at best efficiency point, R_G and the degree of reaction. The degree of reaction is the ratio between the static pressure production in the impeller and the static pressure production of the stage. This ratio is normally between 0.6 and 0.75 for centrifugal pumps [8, p. 57]. In order to be on the safe side, in this case $R_G=0.75$ will be used for further calculations.

$$H_p := H_{BEP} \cdot R_G = 25.88\,m \qquad 2.24$$

The Reynolds-number is based on the circumferential velocity (equation 2.25) at the outer diameter of the impeller, the outer diameter itself and the kinetic viscosity of water at 18°C. The values for the kinetic viscosity of water have been taken from [9, p. Dba2], and are interpolated between 15 and 18°C.

$$Re_{u2} := \frac{u_{2o\_as} \cdot d_{2o\_as}}{2 \cdot \nu_{H2O}} = 4.36 \times 10^{6} \qquad 2.25$$

In Order to consider the centrifugal force of the rotating fluid in the side chamber of the impeller (located between the rotating impeller and the stationary casing, Figure 2.3), a rotation factor will be needed, which can be calculated as shown in equations 2.26 and 2.27 for inwards flowing leakage.

$$y_{gap} := Re_{u2}^{0.3} \cdot \frac{s_{gap\_API} \cdot d_{gr}}{d_{2o\_as}^{2}} \cdot \sqrt{\frac{s_{gap\_API}}{L_{gap}}} = 0.01 \qquad 2.26$$

$$k := 0.9 \cdot y_{gap}^{0.087} = 0.58 \qquad 2.27$$

The pressure difference at the wear ring sealing ΔH_{gap} depends on the static pressure at the impeller outlet and the rotating velocity of the leakage flow between the impeller and the housing (equation 2.28).

$$\Delta H_{gap} := H_p - k^2 \cdot \frac{u_{2o\_as}^{2}}{2 \cdot g} \cdot \left(1 - \frac{d_{gr}^{2}}{d_{2o\_as}^{2}}\right) = 19.2\,m \qquad 2.28$$

The volumetric flow rate through this wear ring depends on the hydraulic friction losses and can be calculated in the same way as it can be done for pipes.

$$\Delta H_{gap} = \frac{c_{ax}^{2}}{2 \cdot g} \cdot \zeta_{gap} \qquad 2.29$$

The friction coefficient also has the same structure and is investigated by means of the coefficient for in- and outlet friction losses ξ_{EA} and the friction losses in the gap λ_{gap} (equation 2.30). The detailed calculations referring to these coefficients are shown in Appendix A.

$$\zeta_{gap} = \zeta_{EA} + \lambda_{gap} \cdot \frac{L}{d_h} \qquad 2.30$$

The mean axial velocity of the leakage flow is given by the relationship shown in equation 2.29.

$$c_{ax} := \sqrt{\frac{2 \cdot g \cdot \Delta H_{gap}}{\zeta_{EA} + \frac{\lambda_{gap} \cdot L_{gap}}{2 \cdot s_{gap\_API}}}} = 9 \frac{m}{s} \qquad 2.31$$

With this information, the leakage flow rate through the wear ring in reference to the cross section of the clearance is calculated as shown in equation 2.32.[4, p. 137]

$$Q_{gap} := \pi \cdot d_{gr} \cdot s_{gap} \cdot c_{ax} = 6.9 \cdot \frac{m^3}{h} \qquad 2.32$$

The volumetric efficiency is defined in equation 2.22 and can be evaluated to be 98.42%,see equation 2.33.

$$\eta_{V\_BEP} := \frac{Q_{BEP}}{Q_{run}} = 98.4 \cdot \% \qquad 2.33$$

2.4.4 Friction losses of the rotating disk

The friction losses of the wear- and cover-disk of the impeller are mainly depending on:

1) the Reynolds-number
2) the roughness of the disk
3) the roughness of the stationary casing
4) the axial gap between disk and housing
5) the geometrical design and the size of the impeller side chamber
6) the influence of the boundary layer
7) the leakage flow
8) the part-load recirculation
9) the impulse exchange

At the best efficiency point the precision of this approach to calculate the friction losses of the rotating impeller is +/- 25 %. [4, p. 89]

The following calculation is an example and should show the approach to estimate the friction losses of the impeller disks.

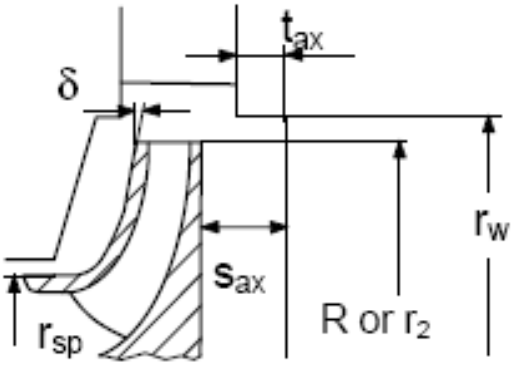

Figure 2.3: Impeller and housing, friction losses [4, p. 136]

The friction losses of a rotating disk are defined in equation 2.34, whereas k_{RR} is the coefficient of the friction, δ is the angle shown in Figure 2.3, d_{2o} the outer diameter of the disk and d_n the inner diameter of the disk.

$$P_{RR} = \frac{k_{RR}}{\cos(\delta)} \cdot \rho_{H2O} \cdot \omega^3 \cdot \left(\frac{d_{2o}}{2}\right)^5 \left[1 - \left(\frac{d_n}{d_{2o}}\right)^5\right] \qquad 2.34$$

The coefficient of friction at the wear disk for roughness of Ra=12.5 µm is the curve drawn as a full line; for Ra=6.3 µm the curve is drawn as a pointed line plotted against the axial gap between the disk and the stationary casing, beginning at 0 mm and ending at 10 mm (Figure 2.4).

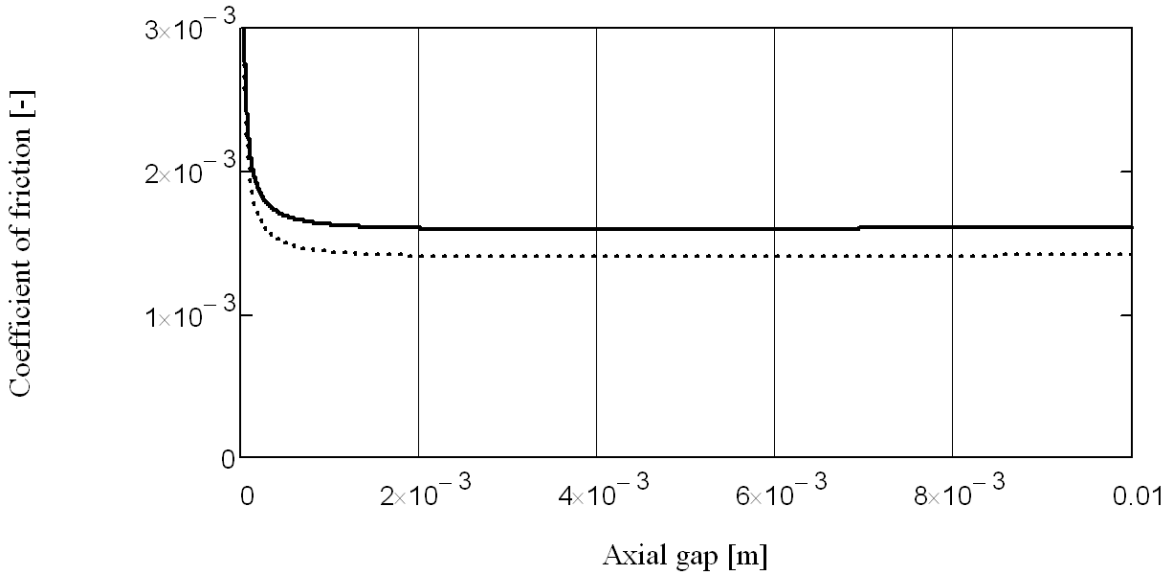

Figure 2.4: Coefficient of friction k_{RR}

In the same way, the friction loss in the form of power loss is plotted against the gap between the disk and the stationary casing (Figure 2.5).

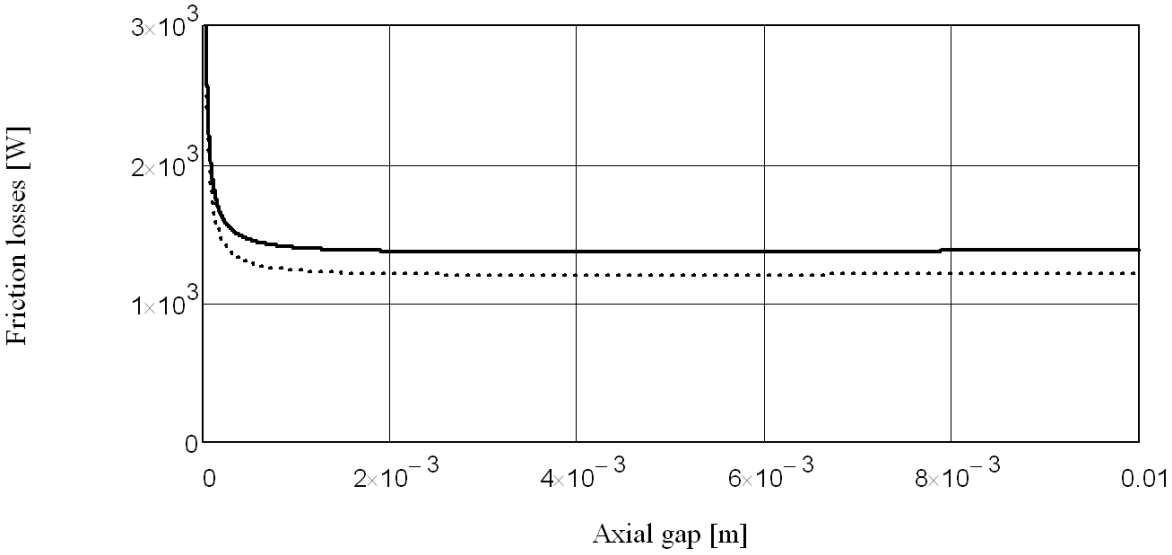

Figure 2.5: power losses in case of friction of rotating disk P_{RR}

In the considered case regarding production an axial gap at the back side of the impeller of 5 mm and at the front side (cover disk) an axial gap of about 7 mm will be realised. In this case, the friction loss of different roughnesses is calculated by means of the equations 2.35 and 2.36.

$$P_{RR\_12.5\_total} := P_{RR\_ps\_12.5}(5 \cdot mm) + P_{RR\_ss\_12.5}(7 \cdot mm) = 1372\,W \quad 2.35$$

$$P_{RR\_6.3\_total} := P_{RR\_ps\_6.3}(5 \cdot mm) + P_{RR\_ss\_6.3}(7 \cdot mm) = 1208\,W \quad 2.36$$

The friction losses with a roughness of 12.5 µm are 13.6% higher than the friction losses with a roughness of 6.3 µm. In order to achieve a better overall efficiency of the test rig and to reach a higher precession of the geometrical form of manufactured parts, the accurate surface of 6.3 µm will be realised for all wetted parts of the pump.

2.4.5 Mechanical efficiency

The mechanical efficiency includes the losses related to the bearing unit, the sealing unit or for example the losses in order to rotating oil inside the bearing unit. To meet the requirements by the customer, the mechanical losses have to be beneath the limit calculated in equation 2.37.

$$P_{m\_max} := P_P - \left(\frac{\rho_{H2O} \cdot g \cdot H_{BEP} \cdot Q_{BEP}}{\eta_{h\_BEP} \cdot \eta_{v\_BEP}} + P_{RR\_6.3\_total} \right) = 984\,W \quad 2.37$$

$$\eta_m := 1 - \frac{P_P - P_{m\_max}}{P_P} = 2.1 \cdot \% \quad 2.38$$

The concept of the bearing unit, the sealing unit and other components, which are responsible for friction losses, has to be as efficient as possible in order to have less friction torque as shown in the equation below.

$$M_{m\_max} := \frac{P_{m\_max}}{\omega} = 6.3 \cdot N \cdot m \quad 2.39$$

2.5 Main dimension and meridional design

The main dimension and the meridional design of the impeller and the diffuser are a very important information for the further optimisations in Ansys-CFX as well as for the generation of the general test rig design. The one-dimensional design of the impeller and the diffuser provide the initial boundaries for ongoing numerical optimisations in Ansys CFX. The concept of the test rig can be influenced by the meridional design of the impeller and the diffuser, especially with reference to the sealing and bearing unit, which are very important for attaining the mechanical efficiency.

2.5.1 Impeller - meridional design

The outer diameter of the impeller has already been defined in 2.3.2 with equation 2.12. The next step is, to define the meridional layout of the impeller according to the specific speed which has been calculated in 2.7, n_q=36.17 min^{-1}.

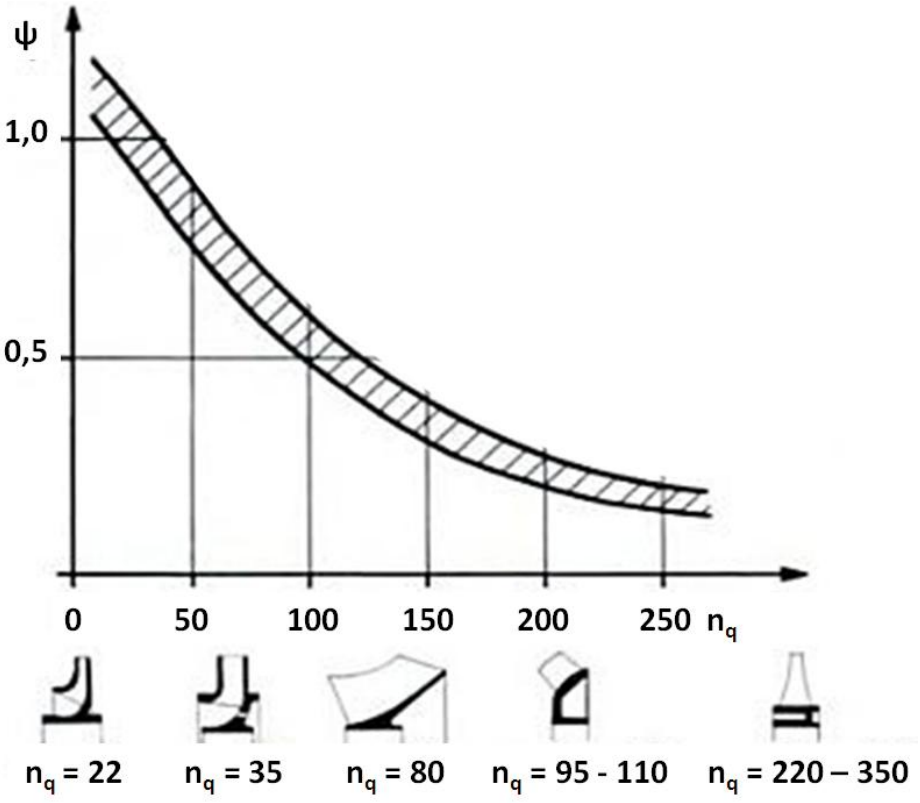

Figure 2.6: Impeller design and specific speed [10, p. 29]

Figure 2.6 shows the meridional design of the impeller with reference to the specific speed and the head coefficient. For the first layout a handmade drawing (Figure 2.7) helps to define the meridional design and to determine the geometrical measurements for further calculations, see Figure 2.8.

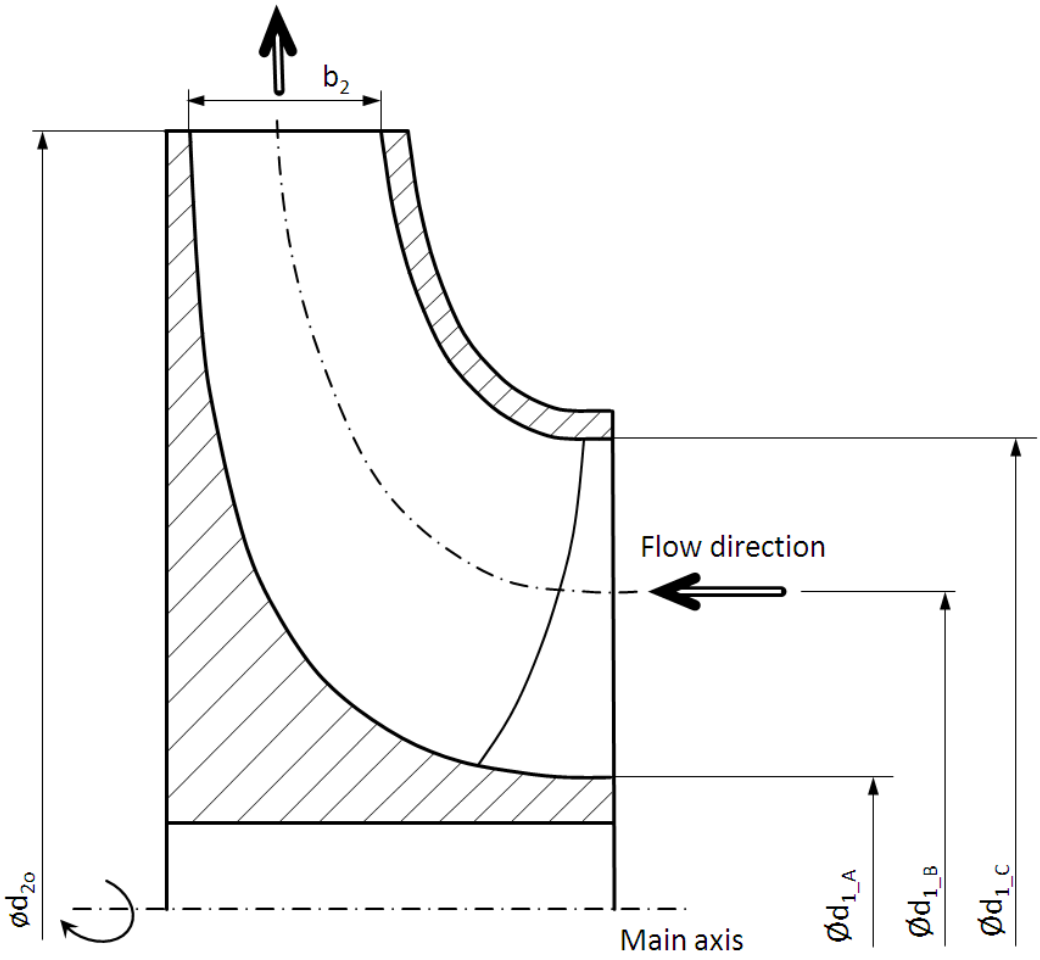

Figure 2.7: Meridional layout of the impeller

2.5.2 Diffusor - meridional design

The diffuser after the impeller has two very important tasks:

1) to convert kinetic energy into potential energy (e.g. static pressure) [4, p. 27]
2) to lead the flow to the next stage free of swirl

The aim is, to design a diffusor which manages these two tasks in a very efficient way.

The area of the inlet section of the diffusor depends on the outlet area of the impeller, and the area of the outlet section of the diffusor has to be the same as the inlet area of the impeller because the diffusor has to be suitable for multistage application.

The length of the stage (impeller and diffusor) has to be lower than 130 % of the outer diameter of the impeller. This is important for the design of the meridional layout of the diffusor and also influences the diffusor length for the calculation. A second dimension which has been limited with 130% of the outer impeller diameter is the outer diameter of the diffusor. In general, these dimensions define the deflection directly after the inlet of the diffusor.

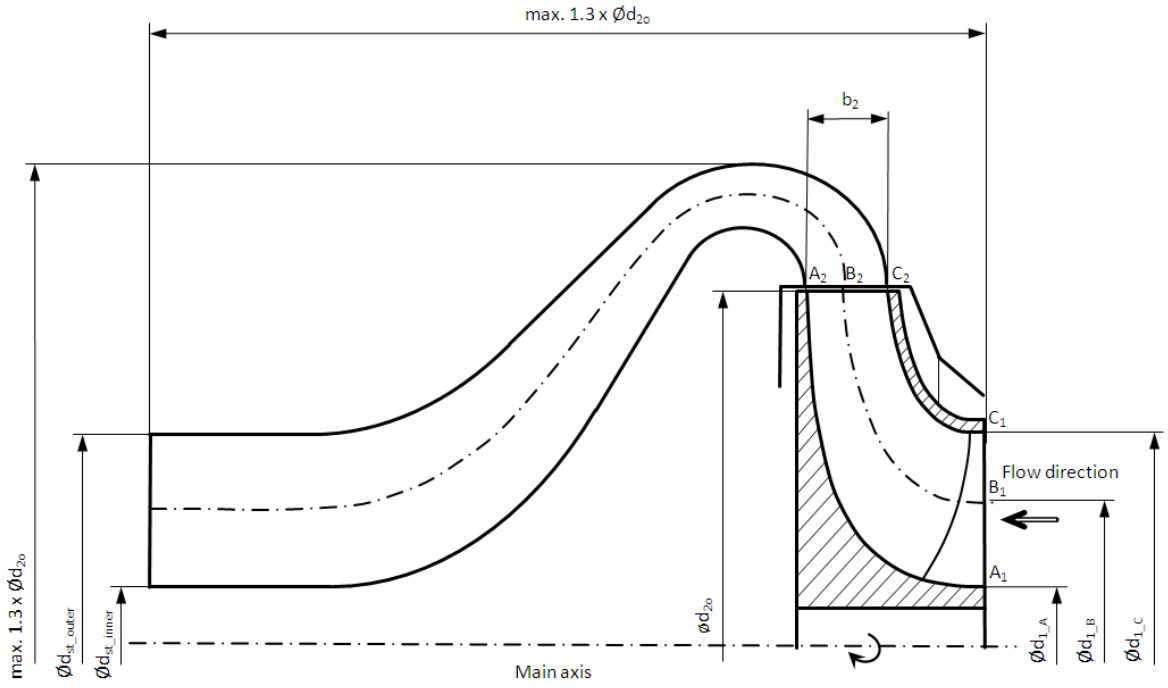

Figure 2.8: Diffusor and impeller with measurements (first section)

2.5.3 Number of blades

The number of blades of the runner has been selected very carefully, as it can influence the behaviour of the pump. The following criteria have to be pointed out:

1) the pressure pulsations as of the interaction between impeller and diffusor has to be avoided;
2) a well-defined hydrodynamic blade load;
3) more than 8 blades are not recommended, as of the instability of the characteristic curve (however pump turbines could have more than 8 blades)
4) less than 5 blades lead to an inhomogeneous deflection flow of the impeller at a delivery head of more than 100 m

Most of the radial and mixed-flow centrifugal pumps with a specific speed between 10 and 120 have five to seven blades on the impeller. [4, p. 345]

For the decision on the number of blades for the impeller, finally two criteria were defined:

1) the number of blades has to be between 5 and 8;
2) the pulsations of pressure have to be avoided within a wide range.

In order to avoid the accuracy of pressure pulsations, parameter m_{ij} (equation 2.40) must not have the value m=0 and m=1 up to the third order, that is to say i=j=3.

Parameter m=0 causes intense pressure pulsations and fluctuations of the axial load, parameter m=1 induced oscillating uncompensated radial forces which lead to vibrations of the housing.[4, p. 648]

$$m_{ij} = \left| i \cdot z_{run} - j \cdot z_{dif} \right| \qquad 2.40$$

The evaluation of the parameter m for the number of blades at the runner beginning at 5 and ending at 8 in combination with the number of blades at the diffusor beginning at 4 and ending at 10 shows that only three combinations meet the requirements.

1) z_{run}=6 and z_{dif}=8
2) z_{run}=6 and z_{dif}=10
3) z_{run}=7 and z_{dif}=9

If the parameter m=2 is chosen for the solution, the combination z_{run}=7 and z_{dif}=9 has this number only one time shown as beneath.

$$m_{11} := \left|1 \cdot z_{run} - 1 \cdot z_{dif}\right| = 2 \quad m_{12} := \left|1 \cdot z_{run} - 2 \cdot z_{dif}\right| = 11 \quad m_{13} := \left|1 \cdot z_{run} - 3 \cdot z_{dif}\right| = 20$$

$$m_{21} := \left|2 \cdot z_{run} - 1 \cdot z_{dif}\right| = 5 \quad m_{22} := \left|2 \cdot z_{run} - 2 \cdot z_{dif}\right| = 4 \quad m_{23} := \left|2 \cdot z_{run} - 3 \cdot z_{dif}\right| = 13$$

$$m_{31} := \left|3 \cdot z_{run} - 1 \cdot z_{dif}\right| = 12 \quad m_{32} := \left|3 \cdot z_{run} - -2 \cdot z_{dif}\right| = 39 \quad m_{33} := \left|3 \cdot z_{run} - 3 \cdot z_{dif}\right| = 6$$

Finally, the number of blades for the impeller is 7 and for the diffusor it is 9.

2.5.4 Suction diameter

The cross section at the impeller inlet influences the mean velocity in this region and has an important impact on the cavitation behaviour of the centrifugal pump. The customer has exactly defined the cavitation behaviour at the best efficiency point with the so-called "suction specific speed" n_{ss}. This suction specific speed is a characteristic number as already mentioned in chapter 1.4.3.

The cross-section at the inlet of the impeller is a circular ring with an inner diameter of 90 mm and an outer diameter which depends on the requirements regarding cavitation behaviour.

The following relation is applied to describe the cavitation behaviour with the meridional velocity and relative velocity in connection to the factors λ_c and λ_w. Factor λ_c is used to

consider the head losses of the inlet and is suggested to be λ_c=1.1 for an axial inflow. [4, p. 287].

Factor λ_w is used to include the decrease of pressure at the blades and is typically between 0.1 and 0.3 for the cavitation criteria 3% loss of delivery head and a swirl free inflow. [4, p. 287]

$$NPSH_3 = \lambda_c \cdot \frac{c_{1m}^2}{2g} + \lambda_W \cdot \frac{w_1^2}{2g} \qquad 2.41$$

This relation for $NPSH_{3\%}$ has to be plotted against the suction diameter, beginning at 175 mm and ending at 235 mm with different values of λ_w (see Figure 2.9) to check the sensibility with reference to the change of λ_w. As λ_w is not known, a curve has to be found, which has the minimum at the required $NPSH_{3\%}$ of 3.38 m for the best efficiency point. This will be manageable with λ_w=0.16193, which has the minimum at $NPSH_{3\%}$=3.38m and a suction diameter of about 218mm. Furthermore, the curve is rather flat at the lowest point, which is the reason why the suction diameter can vary between 215 mm and 225 mm without a significant decrease of $NPSH_{3\%}$.

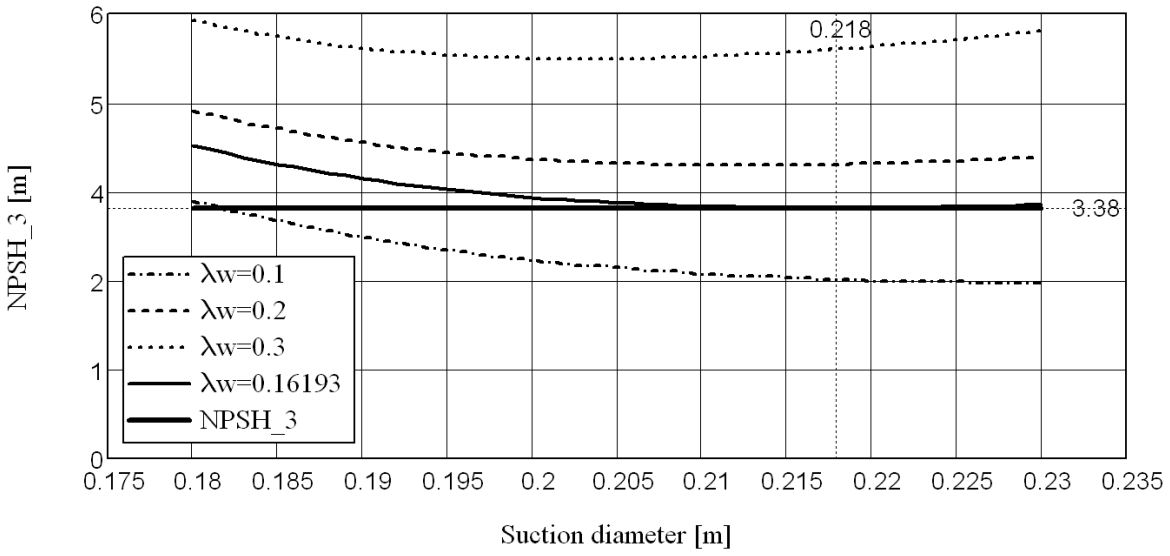

Figure 2.9: $NPSH_{3\%}$ for different values of λ_w against the suction diameter

For further calculations, a suction diameter of about 218 mm is defined with reference to λ_c=1.1 and λ_w=0.16193.

2.5.5 Blade angles at inlet

For the blade design at the inlet of the impeller, the calculation of the blade angle at three different circular surfaces, the inner surface "A", the outer surface "C" and the middle surface "B" was realised. The inner surface has the diameter d_{1_A}=90 mm and the outer surface has the diameter d_{1_C}=218 mm. The diameter of the middle surface divides the delivery flow rate into two partial flow rates Q_{run_p1} and Q_{run_p2}, which have exactly the same size (equation 2.42).

$$Q_{run\_p1} = Q_{run\_p2} = \frac{Q_{run}}{2} \qquad 2.42$$

Due to this fact, the relation between Q_{run_p1} and Q_{run_p2}, shown in equation 2.43 , can give the connection to the diameter of the middle circular surface in equation 2.44.

$$\frac{\left(d_{1\_B}^{2} - d_{1\_A}^{2}\right)\cdot\pi}{4}\cdot c_{m1} = \frac{\left(d_{1\_c}^{2} - d_{1\_B}^{2}\right)\cdot\pi}{4}\cdot c_{m1} \qquad 2.43$$

$$d_{1\_B} := \sqrt{\frac{d_{1\_A}^{2} - d_{1\_C}^{2}}{2}} = 140.4\cdot mm \qquad 2.44$$

Furthermore, the blade angles for the different circular surfaces at the inlet of the impeller without blades can be calculated and lead to the values shown in equation 2.45.

$$\beta_{1\_A} := \operatorname{atan}\left(\frac{c_{1m\_A}}{u_{1\_A}}\right) = 13\cdot°$$

$$\beta_{1\_B} := \operatorname{atan}\left(\frac{c_{1m\_B}}{u_{1\_B}}\right) = 19.7\cdot° \qquad 2.45$$

$$\beta_{1\_C} := \operatorname{atan}\left(\frac{c_{1m\_C}}{u_{1\_C}}\right) = 29.2\cdot°$$

The thickness of the blades at the inlet of the impeller is 4 mm, with an assumption of the blade angle whereas the obstruction caused by the blades could be calculated for example at streamline "A" in equation 2.46.

$$\tau_{1\_A} := \left(1 - \frac{z_{run}\cdot e_1}{\pi\cdot d_{1\_A}\cdot\sin\left(\beta_{1B\_A\_as}\right)\cdot\sin\left(\lambda_{1run\_A}\right)}\right)^{-1} = 1.18 \qquad 2.46$$

The final blade angle does not only depend on the obstruction caused by the blades, an "incidence" also has to be considered. The "incidence" is the difference between the blade angle and the flow angle including the obstruction of the blades. For the first layout, an incidence has to be defined for streamline "A" i_{1_A}=0°, for streamline "B" i_{1_A}=-2° and for streamline "A" i_{1_C}=-5°. This assumption has to be adapted in the following CFD-optimisation.

$$\beta_{1B\_A} := \beta'_{1\_A} + i_{1\_A} = 15.26\cdot^\circ$$

$$\beta_{1B\_C} := \beta'_{1\_C} + i_{1\_C} = 29.15\cdot^\circ \qquad 2.47$$

$$\beta_{1B\_B} := \beta'_{1\_B} + i_{1\_B} = 21.14\cdot^\circ$$

Figure 2.10 shows the velocity triangle at impeller inlet at plane A without pre-swirl as an example for plane B and C.

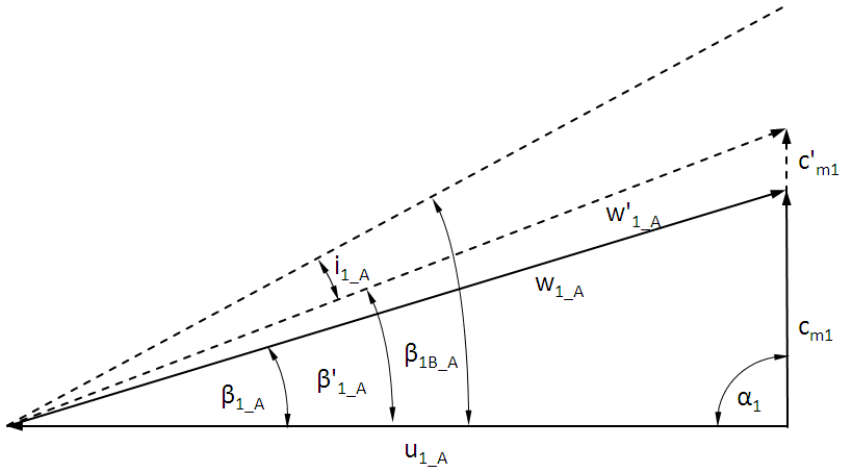

Figure 2.10: Velocity triangle at impeller inlet plane A (free of swirl)

2.5.6 Opening impeller outlet

In combination with the opening of the impeller outlet and the number of blades, the blade angle is responsible for attaining the required delivery head of the pump, in other words, to achieve the expected head coefficient and a stable characteristic curve.[4, p. 347]

A prediction of these theoretical relations is not reliable, hence a calculation based on experience is used to forecast the width of the opening at the impeller outlet. Therefore, equation 2.48 (nq_{ref}=100) is used as follows:

$$b_2 := d_{2o}\cdot\left[0.017 + 0.262\frac{n_q}{n_{q.Ref}} - 0.08\cdot\left(\frac{n_q}{n_{q.Ref}}\right)^2 + 0.0093\cdot\left(\frac{n_q}{n_{q.Ref}}\right)^3\right] = 35\cdot mm \qquad 2.48$$

2.5.7 Blade angles at outlet

The blade angle at the outlet of the impeller is responsible for attaining the required delivery head of the pump. This angle often lies between 20° and 27° for impellers with a blade number between 5 and 7 blades. The deviation angle is used to compensate the gap between the theoretical delivery head of the pump and the real delivery head. This deviation angle must not be larger than 14° to avoid an inhomogeneous flow distribution. The detailed calculation is shown in Appendix A. [4, p. 349]

$$\beta_{2B} := 22.8°$$

The flow angle at the outlet of the impeller is the relation between the meridional velocity at the outlet without the obstruction of the blades and the circumferential component of the relative velocity. The circumferential component of the relative velocity is the difference between the circumferential velocity and the circumferential component of the absolute velocity, which is used in the "Euler-Equation" to define the theoretical delivery head of the centrifugal pump as shown in the following equation 2.49.

$$H_{th} = \frac{1}{g}\cdot\left(u_2\cdot c_{u2} - u_1\cdot c_{u1}\right) \qquad 2.49$$

For swirl free inflow into the impeller, c_{u1}=0 m/s and the circumferential component of the absolute velocity can be investigated in equation 2.50.

$$c_{u2} := \frac{H_{th}\cdot g}{u_2} = 13.59\,\frac{m}{s} \qquad 2.50$$

The flow angle without obstruction of the blades is shown in equation 2.51, and the deviation can be calculated as follows, see equation 2.52.

$$\beta_2 := \operatorname{atan}\left(\frac{c_{2m}}{w_{2u}}\right) = 13.6\cdot° \qquad 2.51$$

$$\delta := \beta_{2B} - \beta_2 = 9.2\cdot° \qquad 2.52$$

The velocity triangle at the impeller outlet is shown in Figure 2.11 schematically.

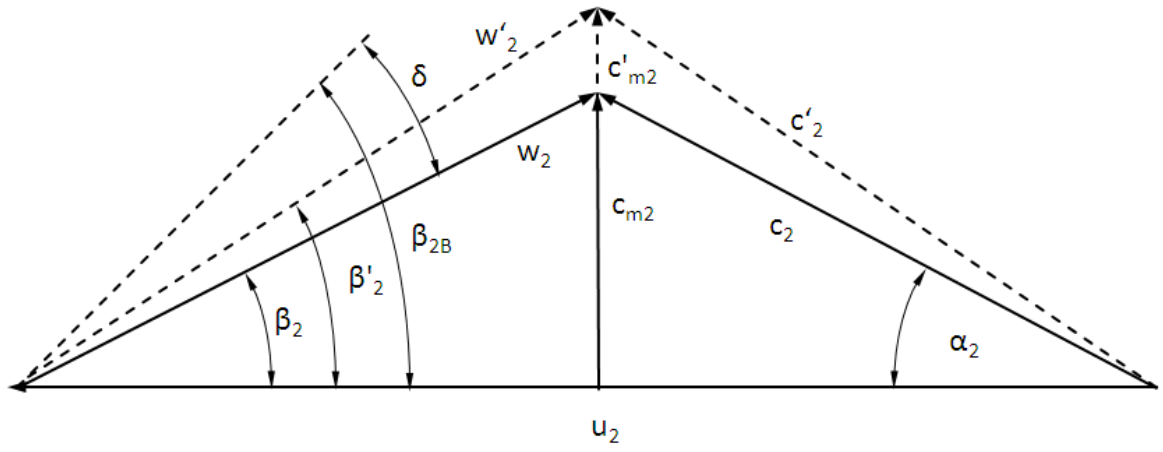

Figure 2.11: velocity triangle at impeller outlet

The main geometrical dimensions of the impeller are defined, and thus all information about the hydraulic components is given to design the first concept of the test rig. For the conception of the bearing and sealing unit more information will be needed, which is investigated in chapter 2.6.

2.6 Hydraulic load and pressure distribution

In this chapter, the pressure distribution behind and in front of the impeller is of interest, in order to define the correct specification for the sealing unit. Also, the axial load in case of the pressure distribution and other effects is very important information for the dimensioning of the bearing unit. The dimensions of and the concept for these units are directly influencing the overall concept of the test rig.

2.6.1 Increase of the static pressure at the impeller

For further calculations, the increase of pressure at the impeller is needed to investigate the pressure distribution behind and in front of the impeller. This static pressure is the potential component of the total pressure exactly after the impeller H_p as already explained in chapter 2.4.3. In equation 2.24, the reaction coefficient is used to estimate the static pressure increase at the impeller. As of the already known geometry of the impeller and the blades, the pressure difference can be calculated in the way as shown in equation 2.53.

$$\Delta p_{run} = p_{2\_run} - p_{1\_run} = \eta_{h\_run} \cdot \frac{\rho_{H2O}}{2} \cdot \left(u_2^2 - w_2^2 + c_2^2 \right) = \rho_{H2O} \cdot g \cdot H \cdot R_G \qquad 2.53$$

However, as the hydraulic efficiency of the impeller is not known, the calculation will be on the safe side, with η_{h_run}=1. Thus, the pressure difference could be calculated beginning

at $Q/Q_{BEP}=0$ going up to $Q/Q_{BEP}=1.6$ (equation 2.54), which is illustrated in Figure 2.12. [4, p. 534]

$$\Delta p_{run\_v}(Q) := \frac{\rho_{H2O}}{2} \cdot \left(u_2^{\,2} - w_{2\_v}(Q)^2 + c_{1\_v}(Q)^2 \right) \qquad 2.54$$

The characteristic curve of the pressure difference is used to estimate the pressure at the sealing unit and the axial load of the impeller at every operating point.

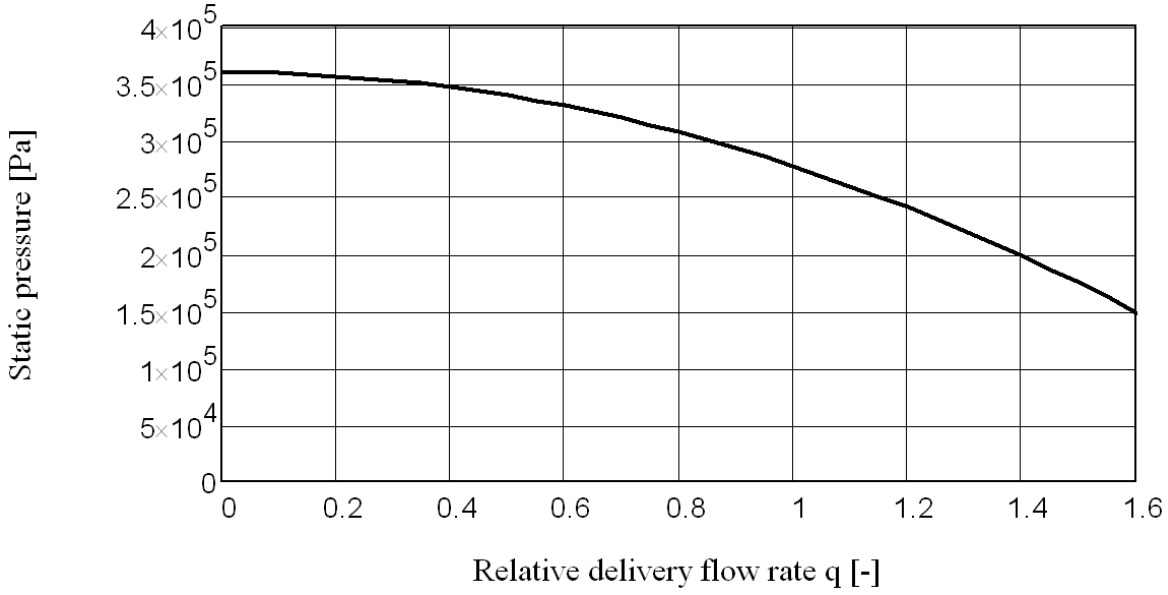

Figure 2.12: Pressure increase at the impeller [Pa]

2.6.2 Pressure distribution - impeller side chamber

Based on the pressure difference investigated in chapter 2.6.1, the pressure distribution behind the impeller in the side room could be calculated to get information about the pressure difference at the sealing unit in reference to the ambient pressure. This is very important information, which influences the decision on the final concept of the sealing unit in general.

The absolute static pressure at the impeller outlet is the pressure difference at the impeller (equation 2.53) plus the absolute static pressure at the inlet of the impeller see equation 2.55.

$$p_{2\_run}(Q) = p_{1\_run}(Q) + \Delta p_{run}(Q) \qquad 2.55$$

According to the "Bernoulli-equation" between the surface of tank water and the impeller inlet, the static pressure at the inlet of the impeller could be calculated. The final equation is shown below whereas the head difference between the tank water surface and the axis of the impeller H_{WT} is 1.5 m.

$$p_{1\_run}(Q) = p_{WT} + H_{WT} \cdot g \cdot \rho_{H2O} - \frac{\rho_{H2O}}{2} \cdot c_{ss}^{\,2} - H_{loss}(Q) \qquad 2.56$$

However, for further calculations, only the operating point Q_0 is of interest, as the highest static pressure is given at the impeller outlet. Therefore, the velocity in the suction pipe is zero and the pressure in the water tank will be the same as the ambient pressure in usual situation. The absolute pressure $p_{1\_run\_0}$ is shown in equation 2.57.

$$p_{1\_run\_0} = p_{amb} + H_{WT} \cdot g \cdot \rho_{H2O} \qquad 2.57$$

The local pressure in the side chamber according to the diameter is defined in equation 2.58 for the operating point Q_0. The pressure p_{CF} is based on the centrifugal force caused by the rotating fluid between the impeller and the housing.

$$p(d) = p_{2\_run\_0} - p_{CF}(d) \qquad 2.58$$

The rotating velocity depends on the diameter and is defined as half of the velocity of the impeller at this diameter. However, the rotating coefficient is assumed to be k_{RR}=0.5. With the final equation 2.59, the absolute pressure distribution can be illustrate as shown in Figure 2.13 for the operating point Q_0 with the highest Δp_{run}.

$$p_0(d) := \rho_{H2O} \cdot \left(\omega \cdot k_{RR}\right)^2 \cdot \frac{1}{2} \cdot \left[\left(\frac{d}{2}\right)^2 - \left(\frac{D_2}{2}\right)^2\right] + p_{2\_run\_0} \qquad 2.59$$

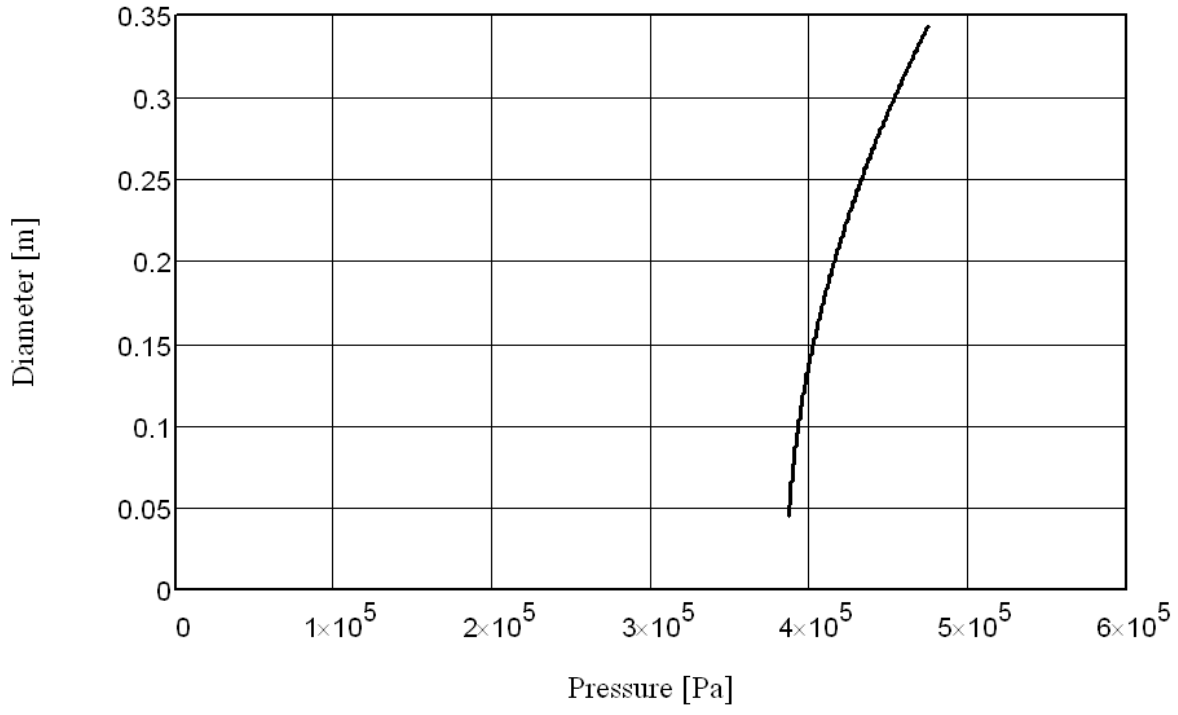

Figure 2.13: Pressure distribution at the impeller back side at Q_0

The maximum absolute pressure which has to be drained is at the operating point at the sealing diameter of 45 mm as calculated in equation 2.60.

$$p_{diff\_seal} := p_0(d_{seal\_r}) - p_{amb} = 2.86 \cdot bar \qquad 2.60$$

This is the pressure difference at the sealing, when the system pressure is the same as the ambient pressure. For measurements of the characteristic curve and also of the NPSH curves, the system pressure has to be higher than the ambient pressure. This is necessary to avoid undesired cavitation in the pump. Therefore, the pressure difference at the sealing unit is much higher than the pressure difference in case of a pressure increase of the impeller only. The maximum of the system pressure has to be defined as 2 bar over ambient pressure (p_{WT}=3 bar). Thus, the pressure difference at the sealing unit is defined at least with a minimum of 2.86 bar and a maximum of 4.86 bar.

$$p_{1\_run\_0} = p_{WT} + H_{WT} \cdot g \cdot \rho_{H2O} \qquad 2.61$$

2.6.3 Axial load of impeller

In case of different pressure distributions at the wear and cover disk of the impeller, the incentive force, the coupling force and the unbalanced load of the pump shaft have to be investigated. The axial load is used for the dimensioning of the axial bearing unit and the pump shaft. To reduce the axial load of the bearing unit, axial load compensation is applied. There are a large range of different methods to minimise and to avoid this axial load, but all these methods have a negative impact an the efficiency of the pump. With regard to the customers requirement, to reach a high overall efficiency of 87%, a very close look on the energy losses is necessary, if axial load compensation is used.

For the investigation of the axial load of the impeller, the different components will be investigated separately from each other (Figure 2.15).

First of all, it has to be defined that the positive direction of the force is against the direction of the flow in the suction pipe. The overall axial load is investigated in equation 2.62 and can be segregated into the pressure load at the wear disk F_{wd}, the pressure load at the cover disk F_{cd}, the incentive load, the coupling force and the unbalanced load of the pump shaft as shown in Figure 2.15.

$$F_{ax}(Q) := F_{wd}(Q) - F_{cd}(Q) - F_I(Q) + F_C + F_{shaft} \qquad 2.62$$

The pressure load at the wear disk F_{wd} is the pressure distribution integrated over the projected area of the impeller backside. The outcome of the integration is equation 2.63, which can be used to calculate the pressure load at any convenient point of operation. For the pressure load at the cover disk, the same approach can be used and leads to equation 2.64.

2.63

$$F_{wd}(Q) := \frac{\pi}{4}\cdot\left(d_{2o}^{\,2} - d_{seal\_r}^{\,2}\right)\cdot\left[\Delta p_{run\_v}(Q) - \frac{1}{16}\cdot\rho_{H2O}\cdot\omega^2\cdot k_m^{\,2}\cdot\left(d_{2o}^{\,2} - d_{seal\_r}^{\,2}\right)\right]$$

2.64

$$F_{cd}(Q) := \frac{\pi}{4}\cdot\left(d_{2o}^{\,2} - d_{gap\_s\_r}^{\,2}\right)\cdot\left[\Delta p_{run\_v}(Q) - \frac{1}{16}\cdot\rho_{H2O}\cdot\omega^2\cdot k^2\cdot\left(d_{2o}^{\,2} - d_{gap\_s\_r}^{\,2}\right)\right]$$

The incentive load depends on the deflection of the fluid flow through the impeller, which has an axial direction at the beginning and a radial direction ε_2=90° at the end.

$$F_I(Q) := \rho_{H2O}\cdot Q\cdot\left(c_{1\_v}(Q) - c_{2m\_v}(Q)\cdot\cos\left(\varepsilon_2\right)\right) \qquad 2.65$$

The force with regard to the clutch is F_C=0 N, and according to the pressure difference between the pressure at the suction side directly at the impeller cup and the ambient pressure with reference to the projected area ,the unbalanced force of the shaft. The pressure p_{1_stat} at the suction side could not be calculated accurately, as the installation of the suction pipe was not defined at that moment. Hence, to be on the safe side, p_1=0 bar (absolute) is used in the corresponding equation 2.66.

$$F_{shaft} := \left(p_{amb} - p_1\right)\cdot\frac{d_{seal\_r}^{\,2}\cdot\pi}{4} = 161\,N \qquad 2.66$$

Figure 2.14 shows the axial load against the relative flow rate of the test rig and each component.

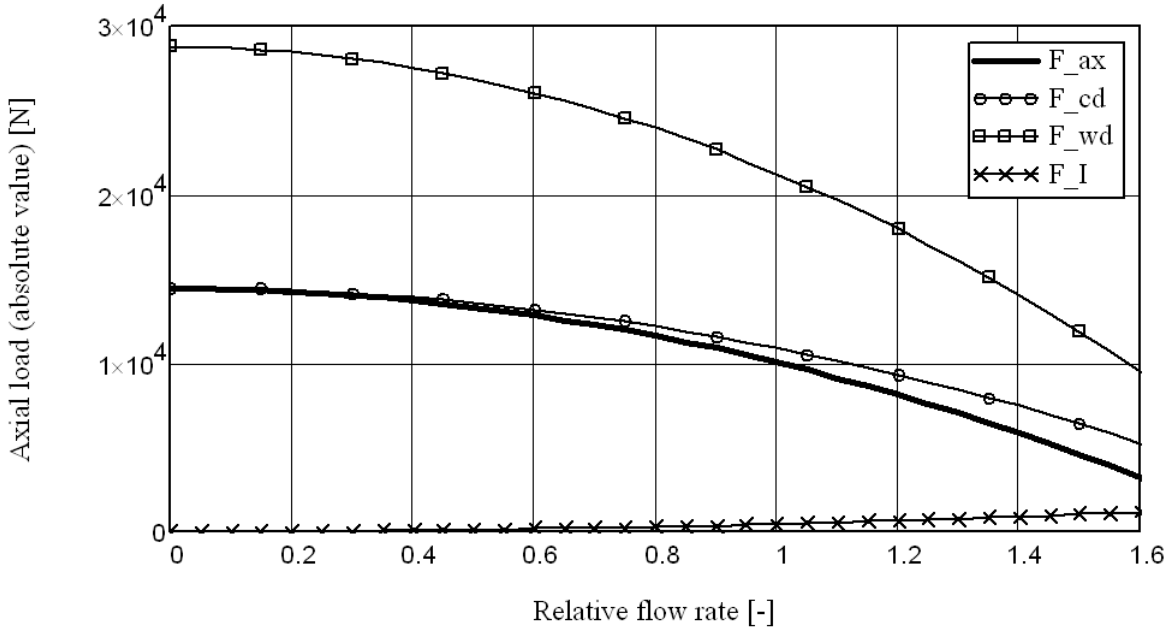

Figure 2.14: Axial load of the impeller and components

The axial load at the point of best efficiency is 10 059 N, at Q=0 m³/s it is 14 429 N.

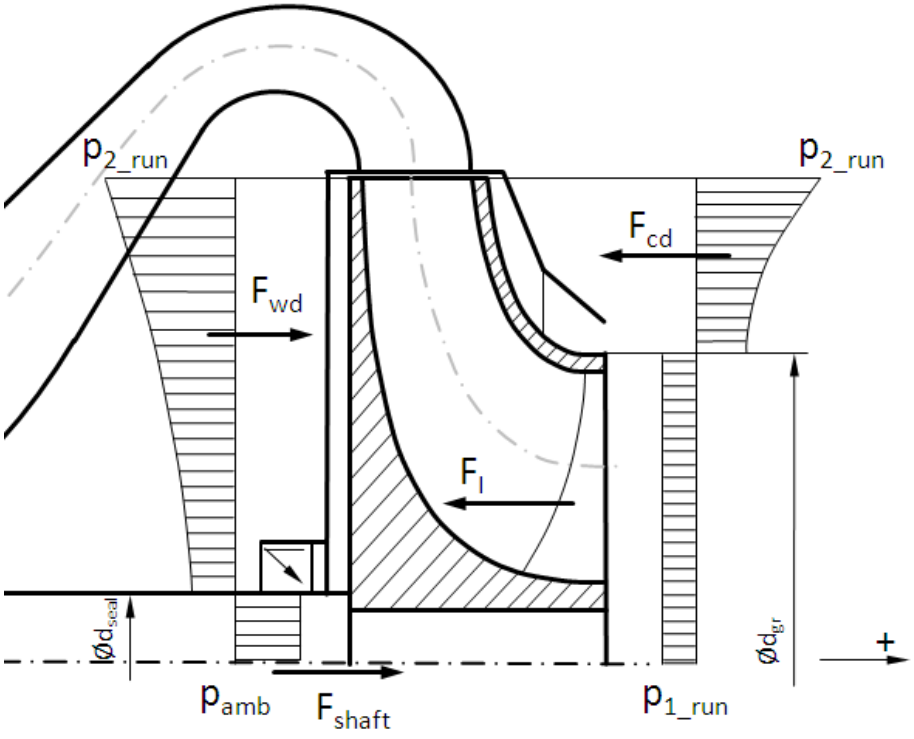

Figure 2.15: Pressure distribution and axial forces at the impeller [4, p. 529]

2.6.4 Radial force

The radial force is needed for the dimensioning of the radial bearing unit and the pump shaft with reference to the deflection and stiffness. The reason for a radial force is unbalanced pressure distribution at the impeller inlet and around the impeller outlet. This unbalanced pressure distribution is a consequence of non-rotationally symmetrical flow.[4, p. 543]

This non-rotationally symmetrical flow is caused by a non-rotationally symmetrical diffusor for example a spiral housing. The diffusor used on this test rig is rotationally symmetrical with nine blades, which are identical and have the same distance to each other. As of this construction of the diffusor, no radial force can be expected, because the non-symmetric pressure distribution offsets one another.

In order to be on the safe side, a radial force as it can be investigated for single spiral housings is assumed.

The calculation of this radial load is shown in detail in Appendix "A". In Figure 2.16, the radial force against the relative flow rate shows a minimum at the best efficiency point which is the design point of the spiral housing and shows a maximum at Q=0 m³/s.

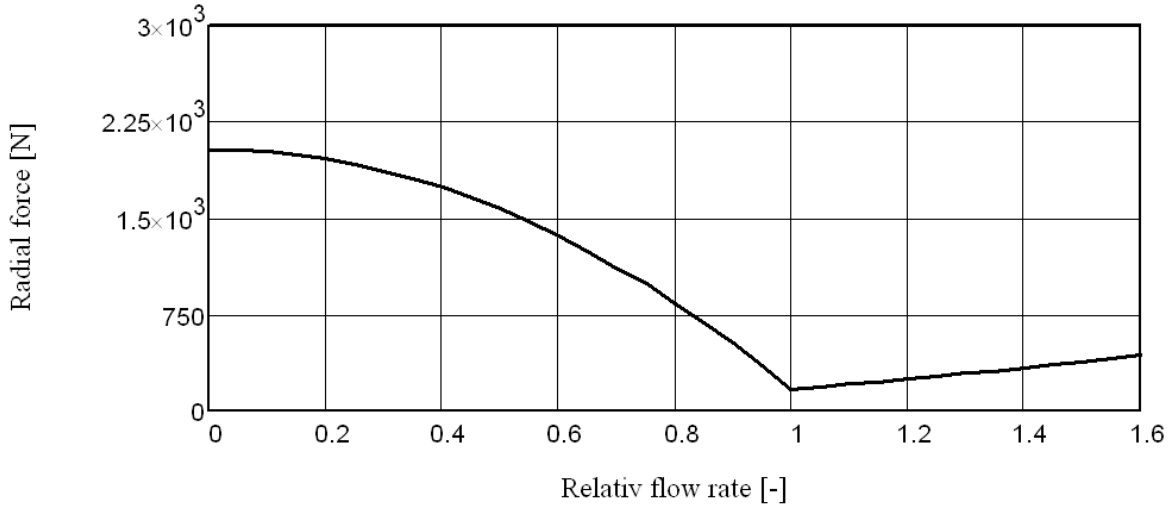

Figure 2.16: radial force of single spiral housing

The radial load at the best efficiency point is 169 N, at Q=0 m³/s it is 2018 N.

3 Construction

The fundamental information for the process of construction is the dimensional design, the loads on the pump shaft and also the pressure load inside the pump and pipes. This information is used to create the first layout including all the other important information in order to fulfil the customer requirements. Therefore, a lot of layouts are needed to show all the different solutions, in order to sort out the most convenient one. These layouts are drawings of the meridional cross-section of the test rig and are mostly made by hand. After that step, the 3D-CAD-model with all single parts and details has to be created, in order to merge all the components. For the construction the 3D-CAD drawing the system ProEngineer Wildfire 5.0 is used, which can be used for "top down design" and short analyses. The generated 3D-CAD model is used to deviate all single parts as well as the assembling drawings for the manufacturing. Finally, there a lot of modifications of some details as of different manufacturing methods or disposability of outsourced items have to be realised.

3.1 Basic considerations

A lot of different important requirements have to be met, which in most of the cases have an impact on the design and the construction. These requirements are shown in the following list:

1. Meridional section according to n_q
2. Dimension of impeller and diffusor according to the hydraulic design
3. Placement of pressure sensor according to ISO 9906
4. Constructional consideration of the rotating speed of 1490 rpm
5. Minimum of mechanical losses, due to the guaranteed overall pump efficiency
6. Wear ring seal clearance according to API 610
7. Wear ring exchangeable to investigate the influence of the gap-sealings
8. Pressure resistance up to 2 bar relative system pressure to ensure cavitation free operation in a wide range
9. Maximum stage length $1.3xd_2$
10. Shaft diameter at hub cap: 75 mm
11. Hub diameter at hub cap: 90 mm
12. For multi-stage useage
13. Placement of transient pressure sensor
14. Placement of torque sensor

These points are used for the evaluation of the different layouts in order to select the best one for this test rig. During the course of this development, 9 different layouts were needed to consider all above-named points.

3.2 Concept finding

In this chapter the way of finding the final concept for the test rig is described. For this purpose, all layout designs are illustrated with a short description of each. In the beginning, Figure 3.1 is used to give an overview about the structure and the main assemblies of the final test rig in order to facilitate understanding.

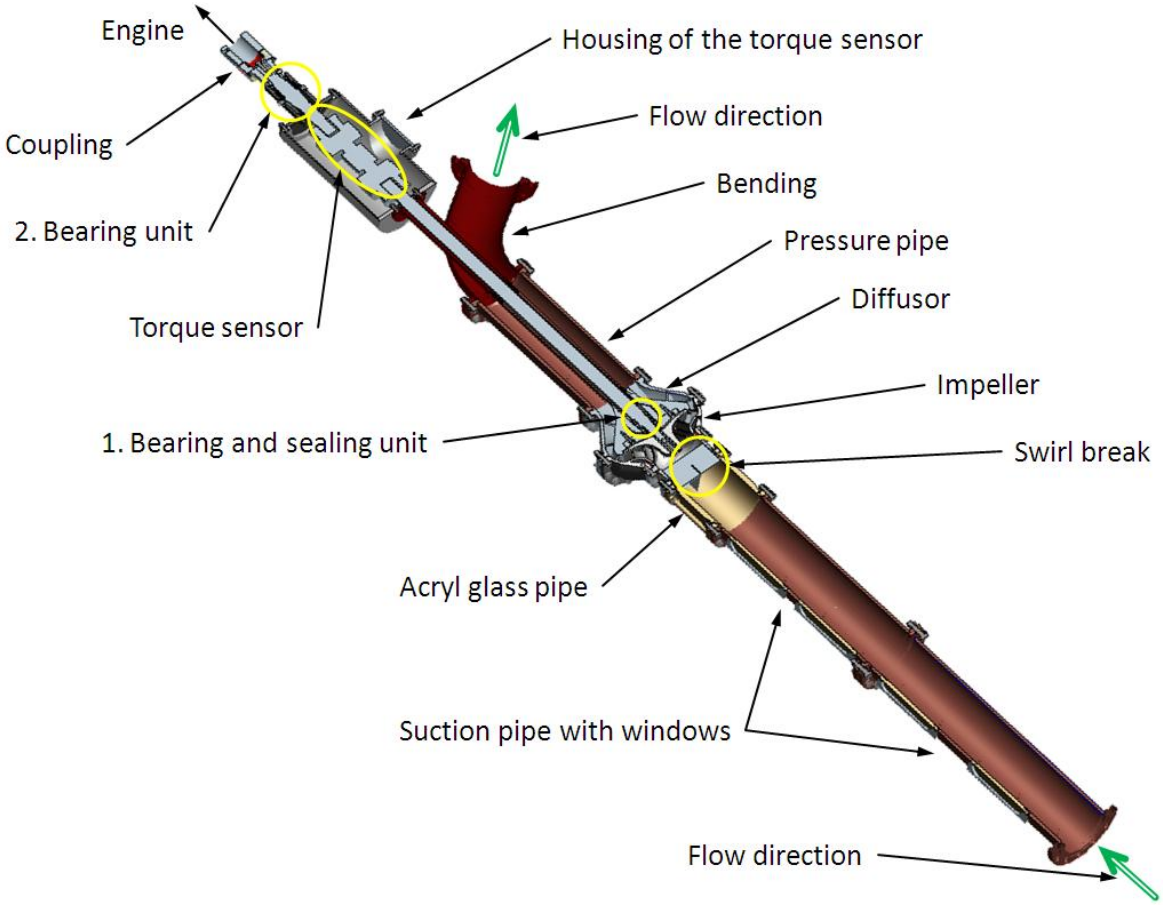

Figure 3.1: Overview of the test rig

The first layout is based on experiences made by the Institute of Hydraulic Fluid Machinery as well as on the concepts of Dipl.Ing. Hopfgardner [2] and Dipl.Ing. Handl [1]. Each of the following layouts is based on the preliminary layout and is an optimisation and often also an extension of the previous one. The layouts are designed in the same chronological order as shown below, and every layout design has been discussed at the Institute of Hydraulic Fluid Machinery.

3.2.1 The first layout

The first layout in Figure 3.2 shows the principal structure of the bearing unit, the sealing unit and the hydraulic components. The impeller consists of two parts, one is the wear disk with blades and the other one is the cover disk. These two components are connected by means of plug welds each blade. The same concept is used for the diffusor, where the inner part has the blades and the outer part is connected with plug welds. At the suction side and at the pressure side, a pipe made of steel is used to fix the pressure sensors. The bearing unit consists of two tapper roller bearings, running in oil. To drain off the water pressure of the pump, a slide ring sealing will be used, because this kind of sealing is the only one to manage the maximum pressure difference of 4.86 bar. To proof the oil of the bearing unit, two radial shaft seal rings can be used, because the pressure difference is not expected to be high. The bending and the positioning of the torque sensor will follow the same concept as Mr. Hopfgratner has used in his Master's Thesis [2, p. Appendix B1]. To reduce the axial load on the bearing unit, back blades at the impeller are applied, however these will lower efficiency.

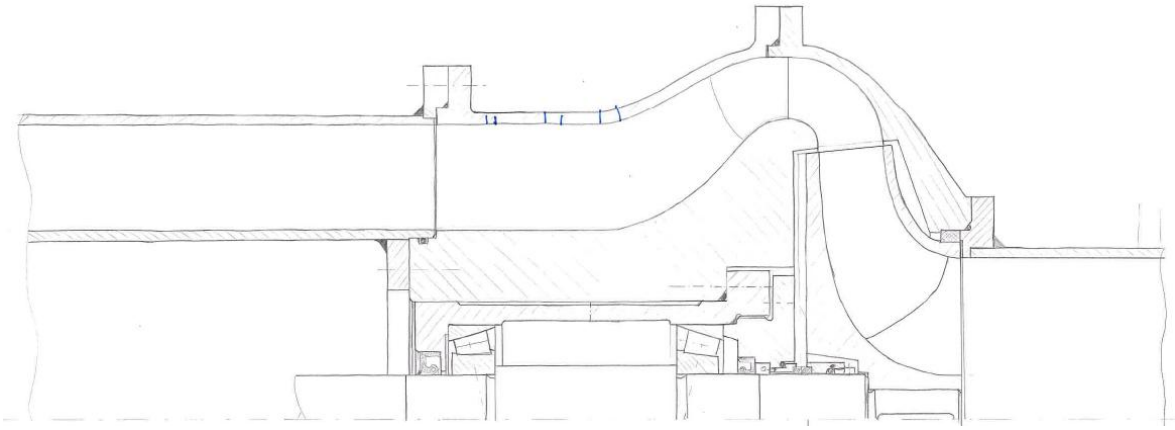

Figure 3.2: Layout 1

3.2.2 The second layout

This layout is based on the concept of the first layout, however enlarged by cooling fins and the leakage channel (Figure 3.3). The bearing unit, which is running in oil, and the sealing unit are producing heat, which has to be transported from the inside to the wetted surface of the diffusor. To increase efficiency of the forced convection at the inside of the bearing unit, the oil-wetted surface has to be maximised by means of cooling fins to hold the temperature on a constant level of about 70°C. The leakage channel enables the leakage fluid flow from the slide ring sealing to pass the bearing unit to the inner duct of the pressure pipe. Furthermore, protective sleeves are used as sliding surface for the radial shaft sealing ring.

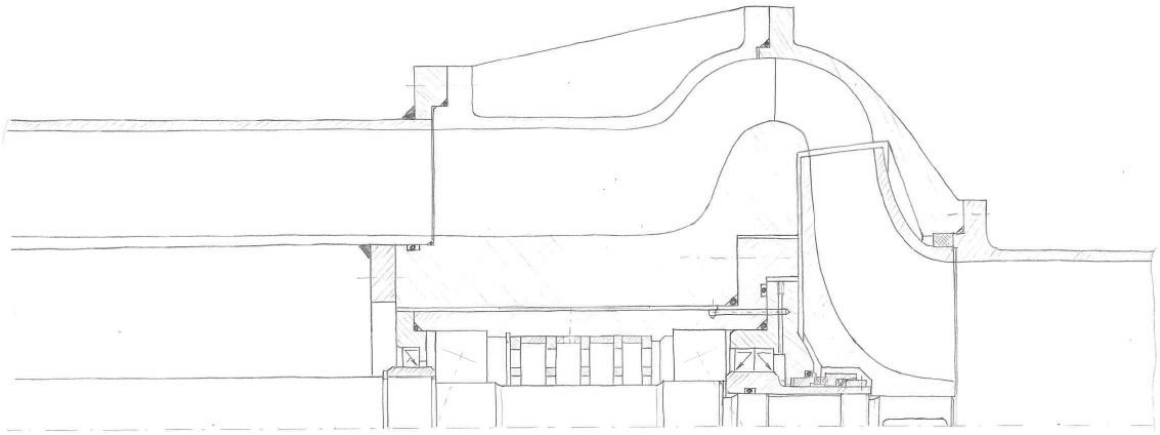

Figure 3.3: Layout 2

The energy losses from the tapper roller bearings running in oil and the friction losses of the slide ring sealing cannot be disregarded. In this case, the risk of failing to meet the requirements of 87% overall efficiency is too high. The alternative concept, to minimize the friction losses in the bearing and sealing unit, leads to the third layout.

3.2.3 The third layout

In the third layout, also tapper roller bearing are used, but not as in the layouts before running in oil, as they are now running in grease. This should result in less energy losses as it was the case with the bearing unit running in oil. To avoid the leakage of grease from the bearings, so-called “nilos rings” are used, since they provide fewer friction losses as radial shaft sealing rings. The slide ring sealing is substituted by a radial shaft ring sealing, which causes also less friction losses as the slide ring sealing. However, the difference in pressure, which could be drained with this radial shaft ring sealing, is not as high as it is at the slide ring sealing. The maximum pressure mainly depends on the rotating speed of the pump shaft and on the diameter of the sealing lip (Figure 3.5).

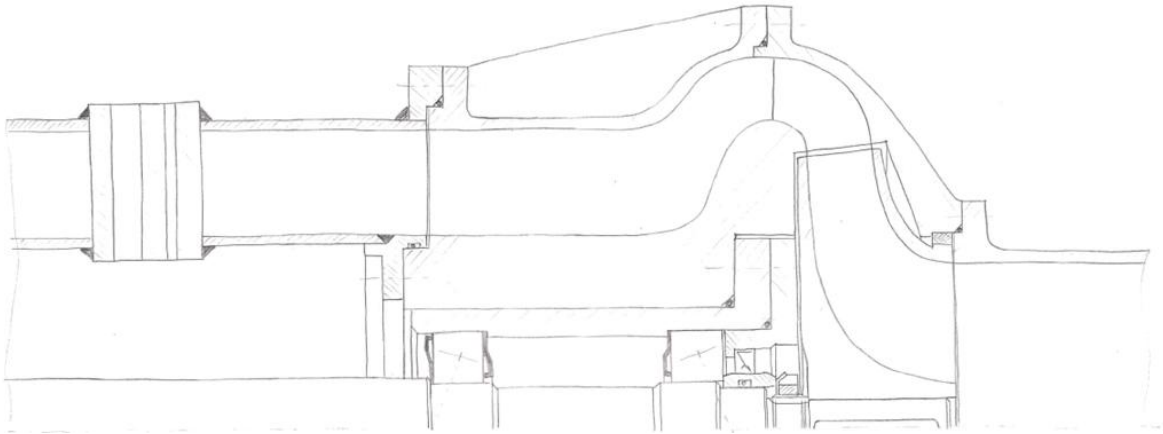

Figure 3.4: Layout 3

To give an example for the permitted pressure difference, a BABSL radial shaft seal ring by “Simrit” at a rotation speed of 1500 rpm and a sealing lip diameter of 40 mm, allow for a maximum permitted pressure of about 3 bar, see Figure 3.5. This is lower than the maximum pressure of 4.86 bar defined in chapter 2.6.2. In order to reduce the pressure at the radial shaft seal ring, different methods can be used.

Furthermore, to reduce mechanical losses, which are measured with the torque sensor, it is useful to keep the distance between impeller and torque sensor as small as possible. This means, that the torque sensor is not positioned between the electric motor and the test pump; the torque sensor will be positioned between the bending and the first bearing unit after the impeller (see Figure 3.9). This will reduce the measured friction losses and the overall efficiency will be higher. To realise this position of the torque sensor, the electrical power supply for the torque sensor will lead through the stiffening between the outer and the inner pipe at the pressure side of the pump.

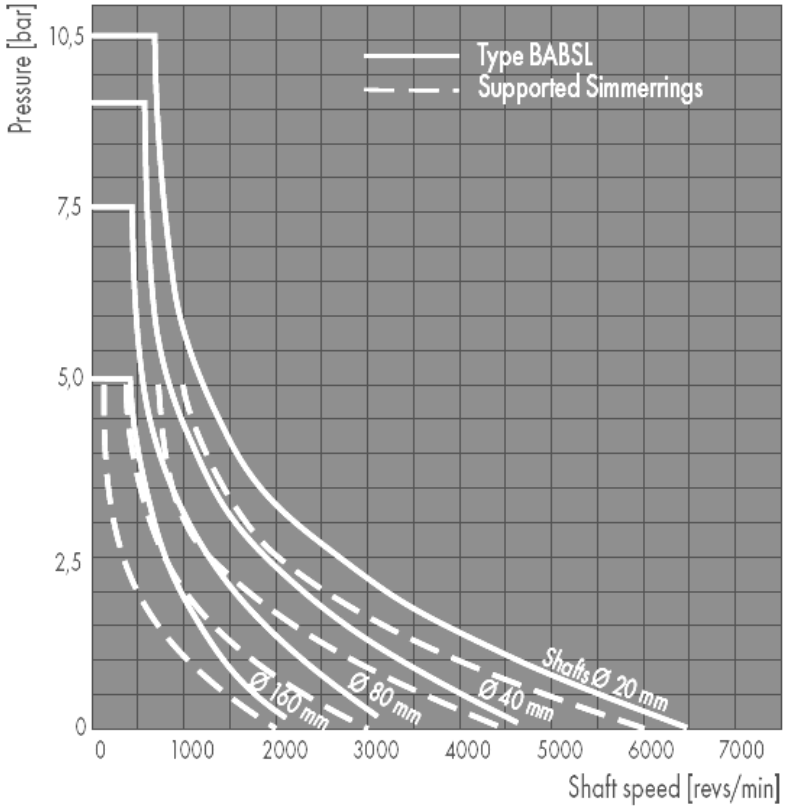

Figure 3.5: Permissible pressure type BABSL [11, p. 41]

3.2.4 The fourth layout

In this layout, back vanes are used to reduce the pressure at the radial shaft seal ring, and as a result of this to reduce the axial load of the impeller. The lower axial load on the bearing unit allows for conventional deep groove ball bearings. They have the advantage to be available at any time and to provide less friction losses than tapper roller bearings. Referring to the lower hydraulic efficiency of the pump in case of the back vanes, this layout will not meet the overall efficiency requirements.

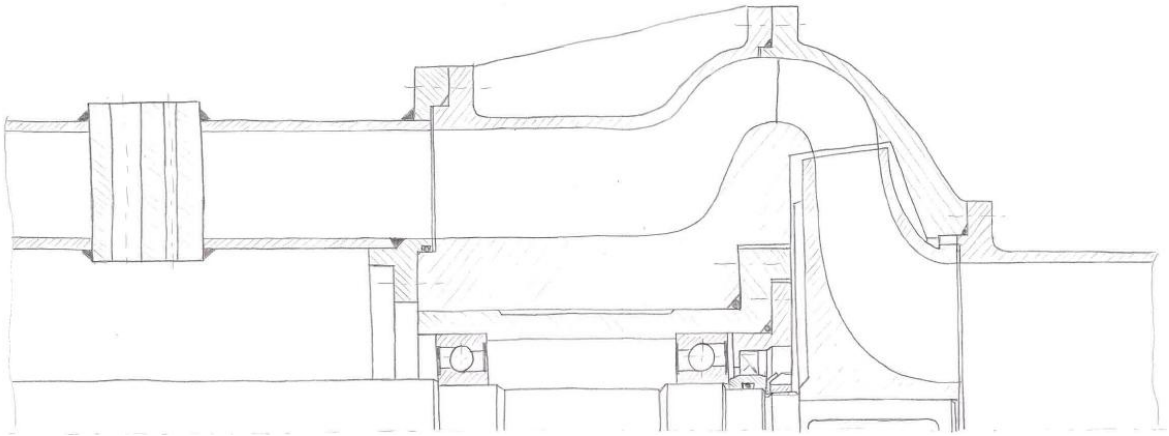

Figure 3.6:Layout 4

3.2.5 The fifth layout

The fifth layout uses the method based on a wear ring sealing at the back side of the impeller and relief wells, see Figure 3.7. As an alternative solution to the roller and ball bearings, in this layout a slide bearing unit will be used, which is running in oil. This slide bearing unit will take up forces in both directions, radial and axial, and has the advantage to be more efficient than the ball and the roller bearings. The axial force has to be rather low, because there is not enough space for the axial slide bearing. With this method of axial load compensation, the axial force could be reduced to a minimum in the design point. Aside this design point, the axial force will grow, and the bearing unit is not able to take up this axial load. As a result, this concept could not be used for the test rig.

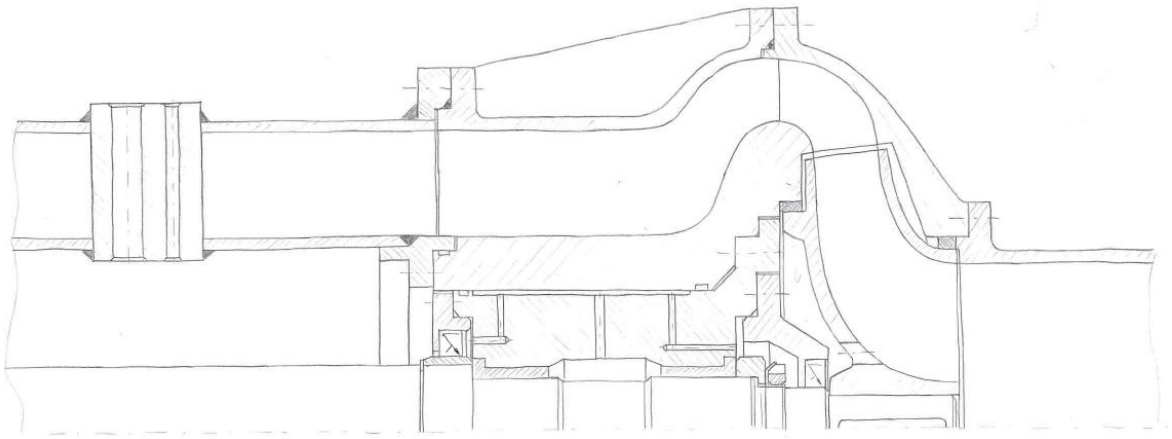

Figure 3.7: Layout 5

3.2.6 The sixth layout

The sixth concept is very similar to the third layout depicted in Figure 3.4. Here also a tapper roller bearings and a radial shaft seal ring are used. However, in this layout a second radial shaft seal ring is used to protect the bearing unit from leakage flow, if the first radial shaft sealing ring breaks. This leakage flow passes the bearing unit through the leakage channel to the backside, where it is collected and drained to the outside. The pressure difference at the first radial shaft seal ring is 4.86 bar, which and is too high, as no axial load compensation is used. To lower this difference in pressure at the radial shaft seal ring, the pressure at the back side of this sealing should be the same as the system pressure (maximum 2 bar above the ambient pressure). This could be realised by connecting the leakage flow channel with the water tank of the test rig. The difference in pressure at the radial shaft seal ring is not higher than the pressure caused by the delivery head of the impeller. The maximum delivery pressure at Q=0 m³/s is 2.86 bar and is thus lower than the maximum allowed difference in pressure of 3 bar for the radial shaft seal ring in this application.

In Figure 3.8, there are two lines, which have the same way, passing the bearing unit to the radial shaft seal ring. Thus, the leakage could flow out of the test pump, and the same way the system pressure of the water tank could get to the sealing unit.

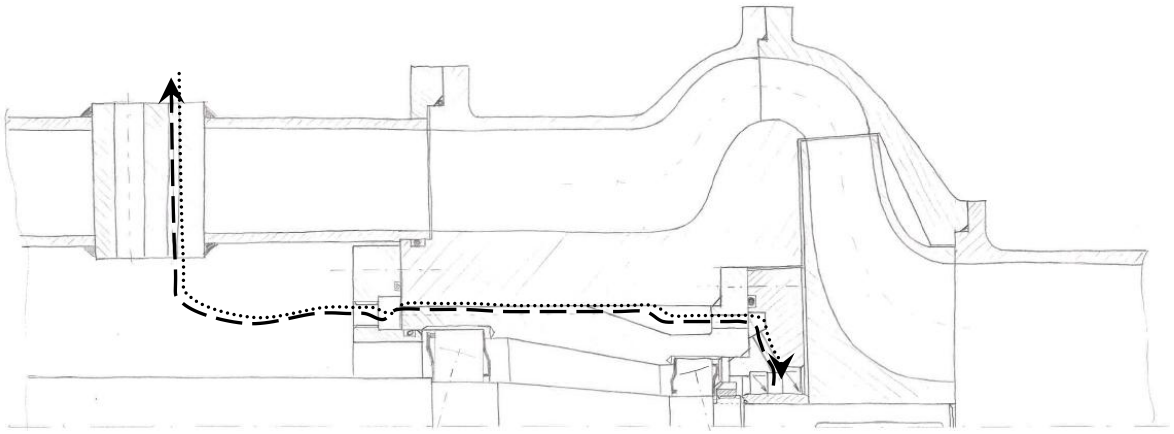

Figure 3.8: Layout 6

3.2.7 The seventh layout

The seventh layout consists of the sixth concept of the bearing and sealing unit and is extended by the concept of the torque sensor unit and the bending. Behind the bearing unit, a straight pipe has to be used for positioning the pressure sensors. The distance between the diffusor and the pressure sensors is two times the outer diameter of the pressure pipe. This outer diameter has to be the same as the diameter of the suction pipe as of multi-stage usage. To reduce the measured friction losses, the torque sensor is positioned as near as possible to the impeller. As a result of this, the pump shaft has a large overhang, which could have a negative impact on the running smoothness of the pump because of vibrations. The second pump shaft is connecting the torque sensor and the coupling and has to be lead through the bending to the outside of the pump. A second bearing and sealing unit will to be needed for this shaft. The efficiency of this power train is not important, because this power train does not influence the measured torque of the testing pump. This power train has only the task to house the second pump shaft and to be proof. The efficiency of this power train is not relevant for the overall efficiency of the test pump.

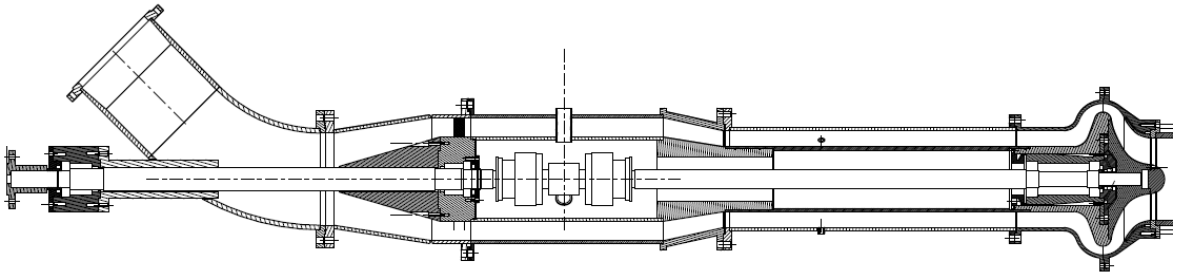

Figure 3.9: Layout 7

3.2.8 The eighth layout

The eighth layout has the same concept as the seventh layout, however the torque sensor is not placed between the bending and the bearing unit, it is positioned after the bending. The advantage of this construction is, that the cables for the torque sensor have not been led through the outer and inner pressure pipe. The disadvantage is, that a second deep groove ball bearing is used for stabilising the rather long pump shaft in order to avoid vibrations during operation. The torque sensor is located inside a housing which has to keep the left and the right pump shaft in position to each other. This housing has to be air-proof because the system pressure is present inside the whole pump. The second (left) pump shaft has two deep groove ball bearings and a slide ring sealing. This slide ring sealing has to drain off the system pressure inside the pump against the ambient pressure.

This construction has the great advantage, that it allows to use system pressure higher than 2 bar over the ambient pressure.

At the suction side, an acrylic glass pipe will be installed directly in front of the impeller for cavitation analysis. This acrylic glass pipe is used to be able to see the blades of the impeller during the NPSH-measurements in order to determine the $NPSH_i$-value (cavitation is visible the first time) and to take pictures with a high-speed camera for documentation purposes.

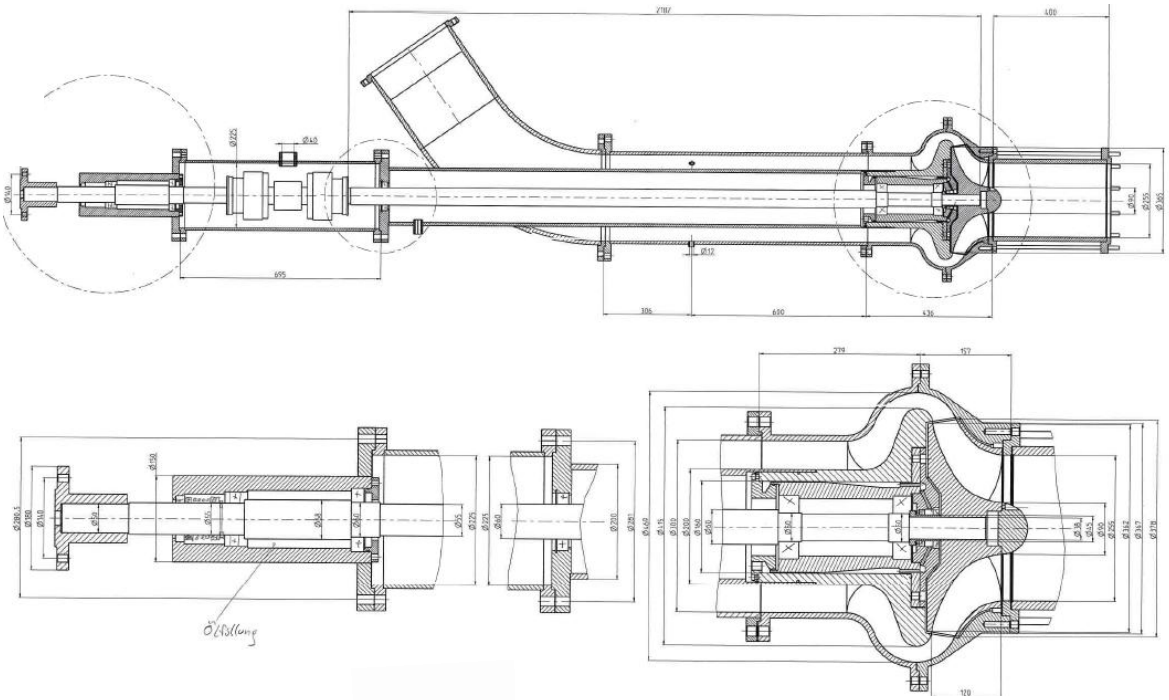

Figure 3.10: Layout 8

3.2.9 The ninth layout

The ninth layout is the last one and is compliant with the final construction of this test pump. The impeller and the diffusor have the same construction as in the layouts presented before. At the suction side, an acrylic glass pipe is used, and at the pressure side a pipe made of steel is used which has the same diameter as at the suction side. The inner pipe at the pressure side has a diameter of 90 mm, which is the same diameter as the inner diameter at the impeller inlet the hub diameter. This construction is used to enable a multi-stage assembling of this pump in final production and is the main difference between the layout eight and the layout nine. Therefore, the bearing unit has to be designed differently with reference to the layouts before. The bearing unit is positioned to have space for the axial and radial deep groove ball bearings and for the sealing unit, consisting of two radial shaft seal rings. The leakage channel has the same position aside the bearing unit. However, the leakage flow is not collected after passing the bearing unit, it flows inside of the inner pipe back to the outlet which is positioned directly before the second radial ball bearing after the bending (this is not shown in Figure 3.11). The pressure sensors at the pressure pipe have a distance of twice the diameter of the pipe. The bearing unit is filled with grease and in order to refill it, a grease fitting could be used, but it has to be replaced by a screw as grease fitting is not water-proof. The torque sensor is positioned behind the bending; the housing around the torque sensor is air-proof and is under system pressure. A grommet could be used as airtight closure to lead the cable for the torque sensor through the housing.

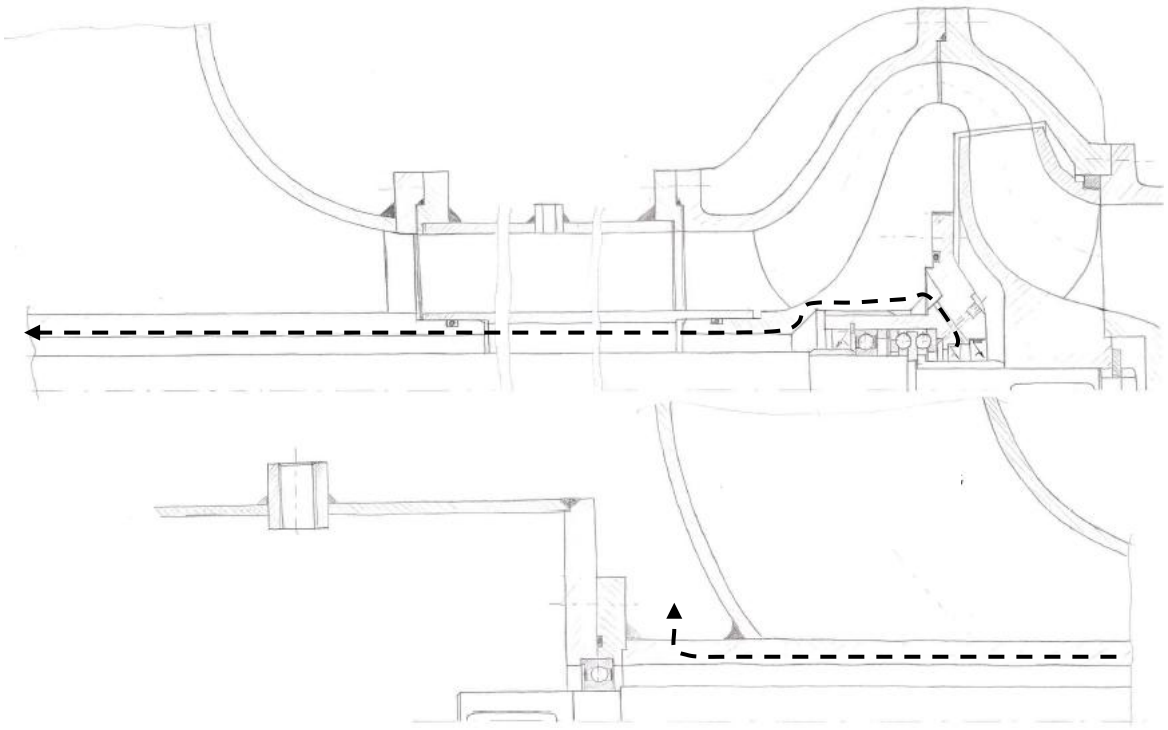

Figure 3.11: Final layout 9

The second pump shaft as well as its bearing and sealing unit follow the same construction design as it is used in layout eight. The leakage flow could pass the bearing unit as show with the dotted line and can leave the inside of the pump through a fitting to a tank made of acrylic glass. This provides additional safety, for the case that the first radial shaft seal ring breaks, which will then be visible immediately.

3.2.10 Pre-calculation

This final layout meets all construction requirements defined in the beginning of layout finding. In a next step, it is necessary to check all components which are exposed to a specific load shown in the list below.

- Pump shaft
- Bearing unit
- Sealing unit
- Pump shaft - impeller connection
- Screw at the pump shaft impeller connection
- In general all screw connection
- Acrylic glass pipe
- Pressure pipe (steel)

Before a detailed 3D construction can be realised, a pre-calculation of the above-listed components is necessary because the dimensions of different screws, the pump shaft, the bearing unit, the sealing unit and etc. have to be known. As of the low “degree of difficulty” of these calculations, they are not part of this Master`s thesis. However, a detailed stress analysis is provided in chapter 4.

3.3 Detail engineering

The final layout describes the overall concept of the test rig, which is also the basis for the 3D model. In this case, ProEngineer-Wildfire 5.0 is used to build the 3D model as this software offers two different methods of construction. The first method is the so-called “Top-Down-Method” and the second is the “Bottom-Up-Method”. These methods are used, in case where not only one part is used for the 3D model. The Top-Down-Method is starting from a rough layout that has to be defined in advance, right down to a greater level of detail. The first step of this method includes the transfer of the hand-drawn general overview to software sketch. This sketch of the overview is assembly all sketches of the single parts, which are used for the details of each component. It is called “skeleton model” and provides the basis for the 3D model. The great advantage of this method is, that in one overall sketch all relevant relations between different parts can be defined and that parameters can be easily implemented. If there is a change during the design process of an important parameter which influences a large range of different parts, it can be done very easily in the skeleton model and all parts will follow this parameter. In the Bottom-Up-Method, each component is designed separately, and does not have a connection to the leading parameter and to other influencing parts. In this case, it is necessary to enter design changes for each part separately, which means much more effort and is more error-prone. [12, p. 21]

3.3.1 Structure of the assembly model

The final layout asof chapter 3.2.9 is the basis for the skeleton model of the 3D model. This layout has been separated into the different parts and is extended with further details.

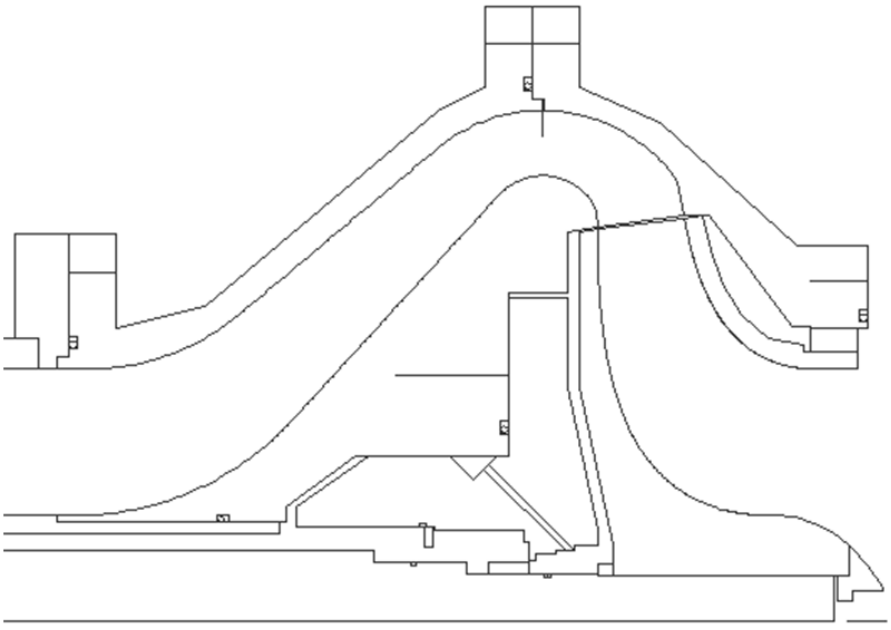

Figure 3.12: Skeleton sketch of the test pump

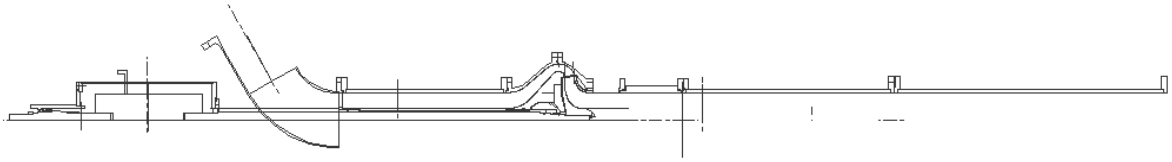

Figure 3.13: skeleton-sketch of the test rig

In Figure 3.12 (a detail of Figure 3.13), the meridional designs of the impeller, diffusor and the bearing holder are shown. In Figure 3.13, the overall skeleton sketch of the whole test rig is shown, with all important components having an influence. The single sketches summarised in this overall sketch represent the basis for the single part design of each component. The meridional design of the impeller and the diffusor are defined by the numerical optimisation and are imported sketches. The design of all other sketches is free.

3.3.2 The 3D model

After the single part design and a large range of changes as of manufacturing, assembly and cost aspects, the 3D assembly is generated automatically with reference to the skeleton model. In Figure 3.14, the 3D model of the test rig is shown, beginning at the suction pipe with acrylic glass windows and ending at the jaw clutch coupling for rotational energy transport. The 3D model of the whole test rig is divided into different sub-assemblies which also consist of different parts and components. These sub-assemblies are shown in detail in Appendix C.

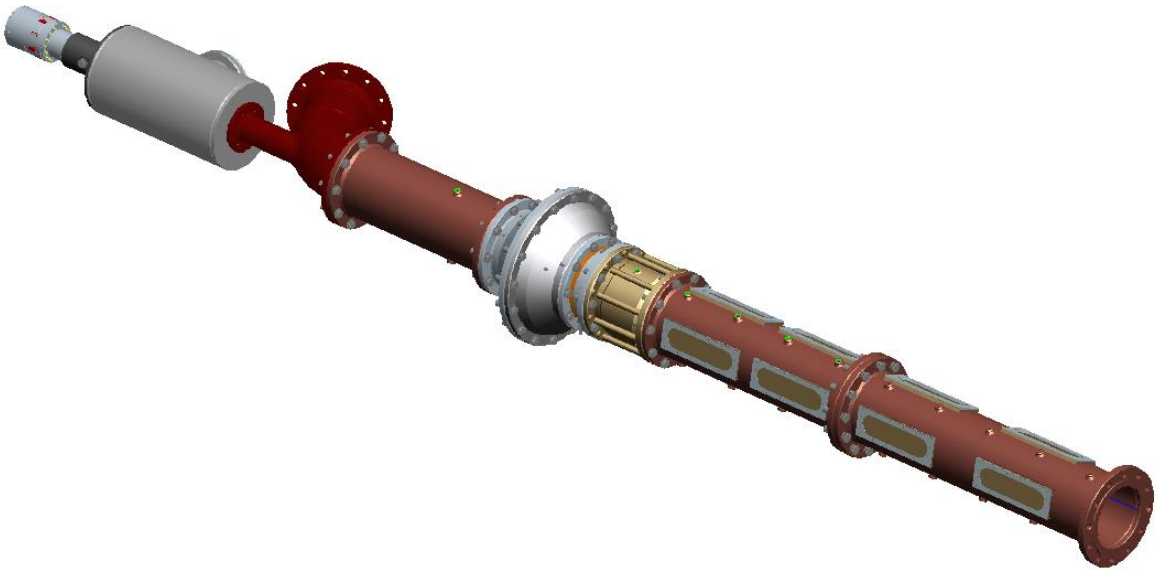

Figure 3.14 3D model of the test rig

The cross-section through all components of the test rig is shown in Figure 3.15. A detailed drawing of each area of this cross-section is shown in the overall assembly drawing in Appendix C.

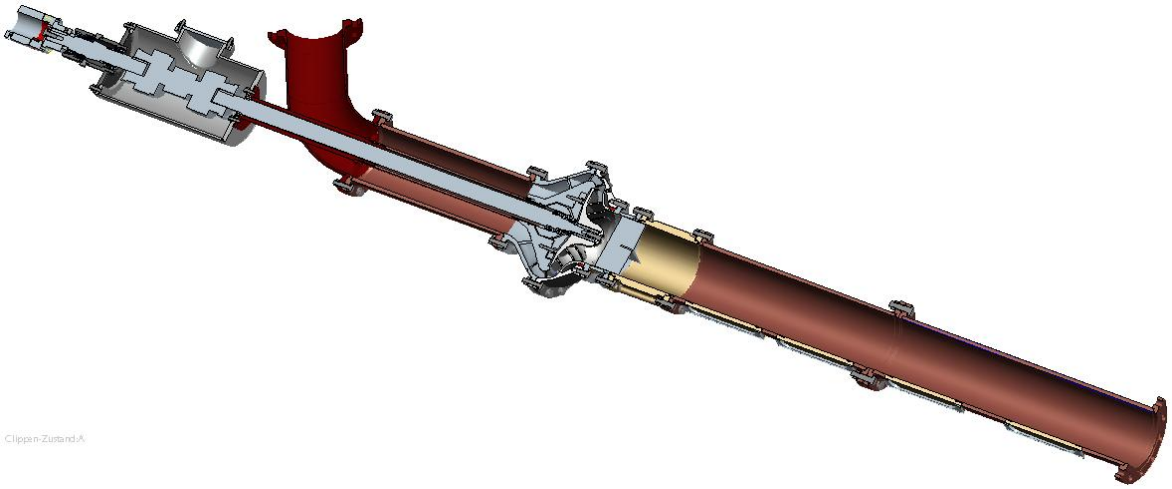

Figure 3.15: Cross-section of the test rig

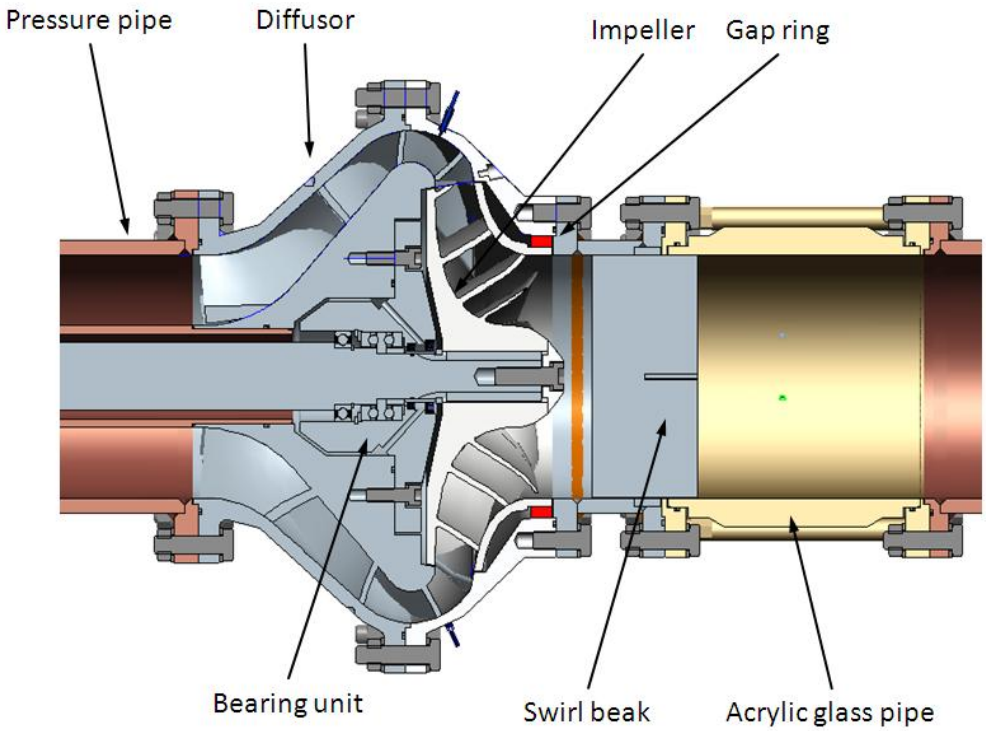

Figure 3.16: Cross section detail

3.3.3 Impeller

The impeller is made of aluminium and consists of two parts, on the one hand the wear disk with all blades and on the other hand the cover disk with the boreholes for the plug welds. The design of the impeller, especially the meridional design and the design of the blades are a result taken from the numerical optimisation, which was realised by DI Stefan Höller-Litzlhammer. The generated optimisation data were imported as Cartesian coordinates into the design software ProE, which was used to design the impeller surface. After manufacturing the different parts of the impeller, these were merged together by means of welding. In order to ensure dimensional accuracy, the cover disk with the plug welds was machined again to become concentric with the surface of the gap sealing.

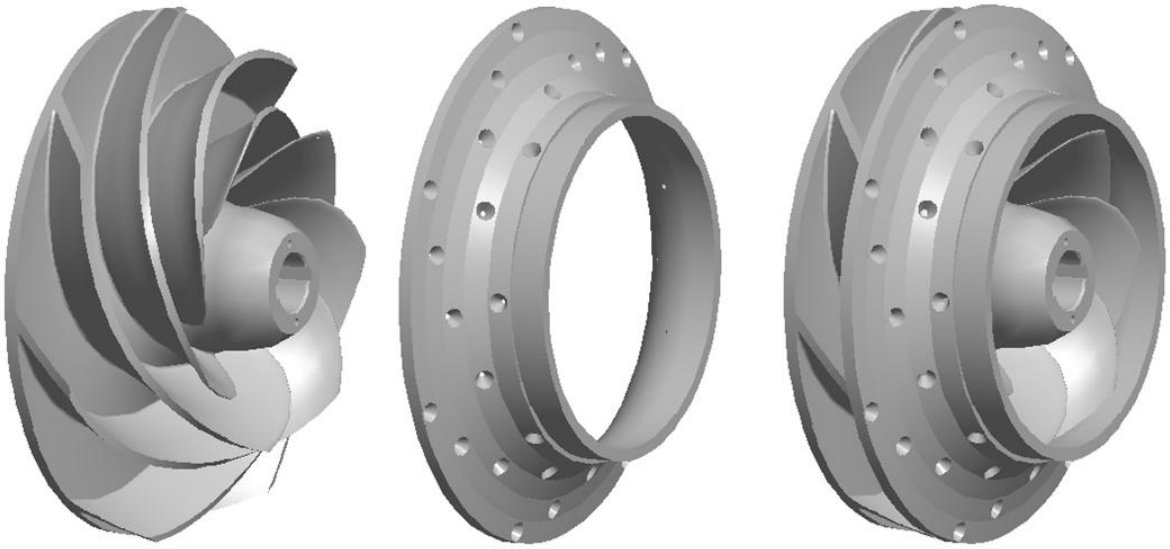

Figure 3.17: Left: wear disk with blades, middle: cover disk, right: assembled impeller

The bore holes for the plug welds are designed as shown in Figure 3.18.

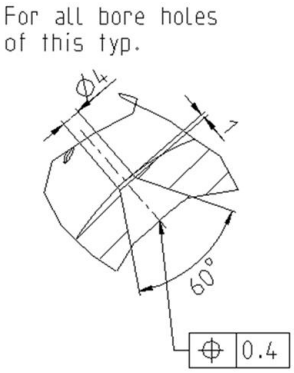

Figure 3.18: Bore holes for plug weld

The construction details of the impeller are indicated in Appendix C.

3.3.4 Diffusor

The diffusor has the same concept as the impeller, in other words, it also consists of two parts and is made of aluminium. The inner part of the diffusor has to wear the nine blades, is responsible for positioning the bearing unit and has to absorb the forces of the impeller. The outer impeller has two flanges, at the pressure side to fasten the pressure pipe and at the suction side to position the diffusor cover with the gap ring. The bore holes on the outer part of the diffusor are used to merge the inner part with the plug welds. The design for these bore holes is the same as shown in Figure 3.18. After merging these two parts together by welding, a fine finishing was necessary. To compensate the delay after the welding process a machining allowance was necessary to get finally the right measurements.

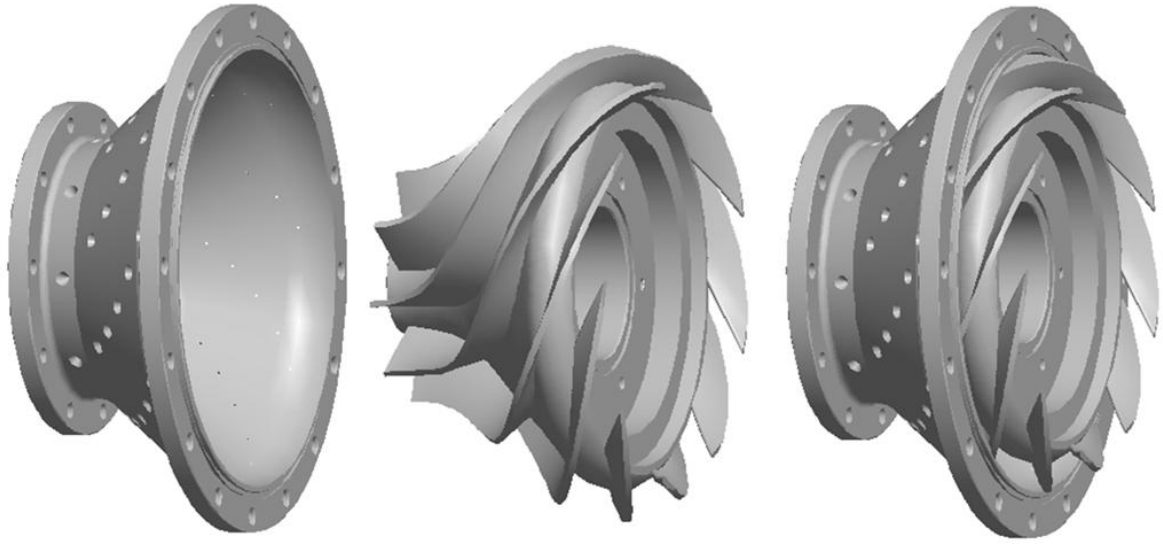

Figure 3.19: Left: outer diffusor, middle: inner diffusor, right: merged diffusor

3.3.5 Suction pipes

At the suction side of the pump, four different pipes with different tasks are used, see Figure 3.20.

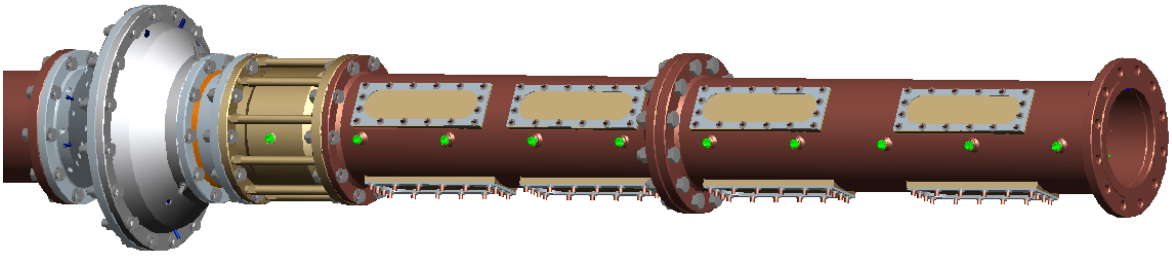

Figure 3.20: Suction side, pipes

The component directly in front of the pump is very short and has the task to fasten the swirl break. Different kinds of swirl breaks were tested, therefore the component has to be mountable and removable very easily. The next component is the acrylic glass suction pipe, which is used provide an insight into the inlet of the impeller for cavitation analysis. The second pipe on the right hand-side is much longer than the acrylic glass pipe and has windows made of acrylic glass, to make the swirl at the part load visible and allow for pictures. Furthermore, the measuring points for static pressure measurements for the characteristic curve of the pump are positioned in a distance of twice the suction pipe diameter from the inlet of the pump. The first pipe on the right-hand side also has acrylic glass windows which are used for the analysis of the pump pre-swirl. Along the entire suction pipe, there are thirty positions for high dynamic pressure sensors, ten planes whereas each of the planes is equipped with three sensors in a distance of one suction pipe diameter. The positions of all sensors used for the test rig are shown in chapter 3.3.9.

3.3.6 Bearing and sealing unit

The bearing support represents a central component, because it is the support for the radial shaft seal rings, the radial deep groove ball bearing and the axial deep groove ball bearing, and it defines the position between the diffusor and the impeller. Furthermore, it is responsible for the leakage flow in case of a breakdown of the first radial shaft seal ring and can consequently pass the bearing unit to the backside of the test pump to the inner pressure pipe.

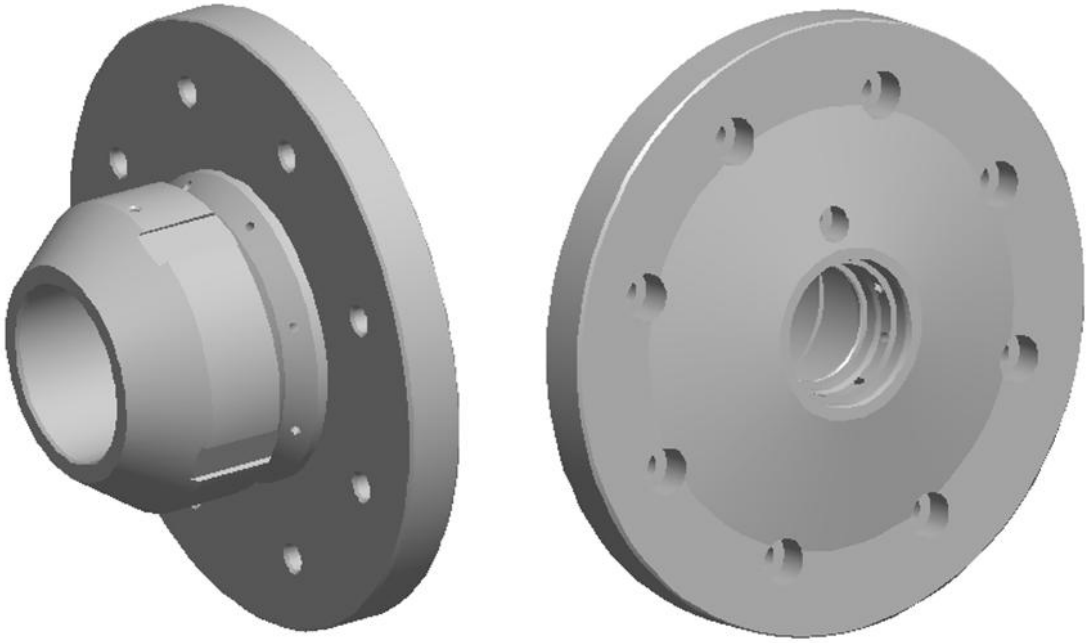

Figure 3.21: Bearing and sealing support

The first radial shaft seal ring has the task to drain the pressure difference in case of the delivery head of the impeller.

If this sealing breaks, the second radial shaft seal ring avoids for leakage to get into the bearing unit. Hence, the leakage has to pass the bearing unit via the boreholes and slots. These two radial shaft seal rings are running on an inner ring of a needle roller bearing as a shaft protection jacket.

The bearing unit consists of two deep groove ball bearings. One, only operating in radial direction, is a radial deep groove ball bearing, and the second one, operating in both axial directions, is an axial deep groove ball bearing. Both bearings together represent the fixed bearing unit of the pump shaft. To ensure low eccentricity of the impeller and to avoid an influence of the gap clearance, the bearing unit has to be very stiff. Therefore, two tapper roller bearings, as used in layouts 1, 2, 3, 6, 7 and 8, would be the best solution, as the radial clearance can be adjusted by a slotted round nut with a hook spanner. Due to the fact the unbalanced axial force is too high, so that the expected lifetime of 200 hours would not be reached with tapper roller bearings, this arrangement do not fulfil the requirement.

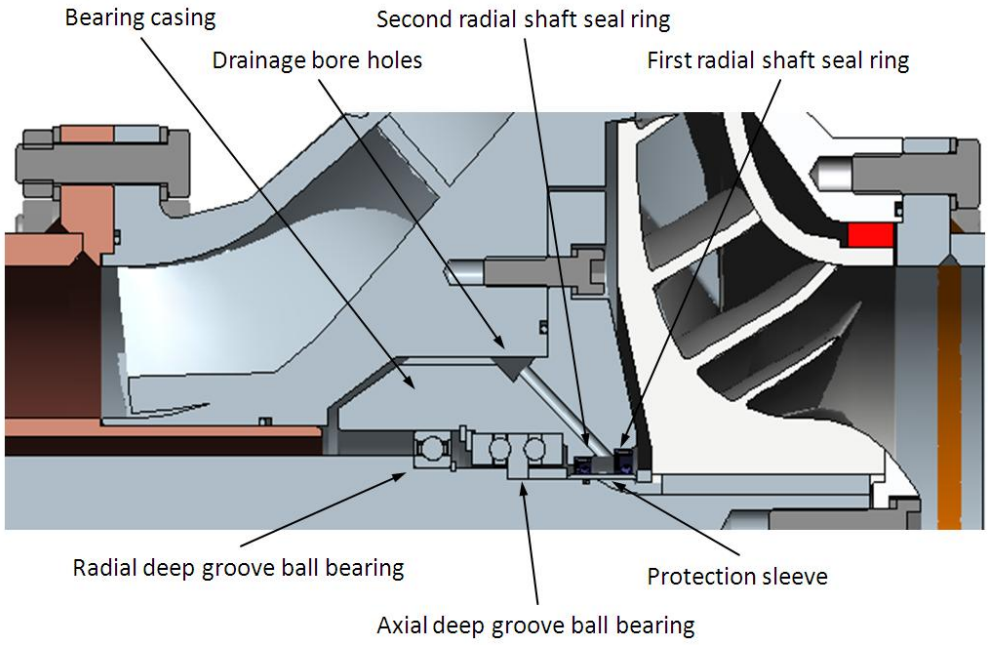

Figure 3.22: Bearing and sealing unit

3.3.7 Impeller fastening

For the torque transmission between the impeller and the pump shaft, two parallel keys are used. The reason for two parallel keys is the unbalanced mass in case of only one parallel key, which has to be sufficient with reference to the maximum allowable stress. The position of these two keys has an offset of exactly 180°, and not 120° as usual. Behind the impeller a shim is used to influence the final position of the impeller by changing this shim, see Figure 3.22. In front of the impeller, an impeller cap is used to transmit the axial force

to the central socket head screw. This impeller cap is made of the same material as the pump shaft.

3.3.8 Torque sensor housing and second bearing unit

The torque sensor housing has to meet different requirements. It has to be hermetically sealed in order to hold the system pressure inside the test rig as a counter pressure for the sealing unit at the pump side. Therefore, it is necessary to have an air-proof cable bushing as shown in Figure 3.24. Furthermore, the torque sensor housing has to adjust the second shaft (see Figure 3.23) exactly to the pump shaft in reference to the angular and axial offsets. For balancing offsets, the torque sensor is equipped with a curved teeth coupling at both sides.

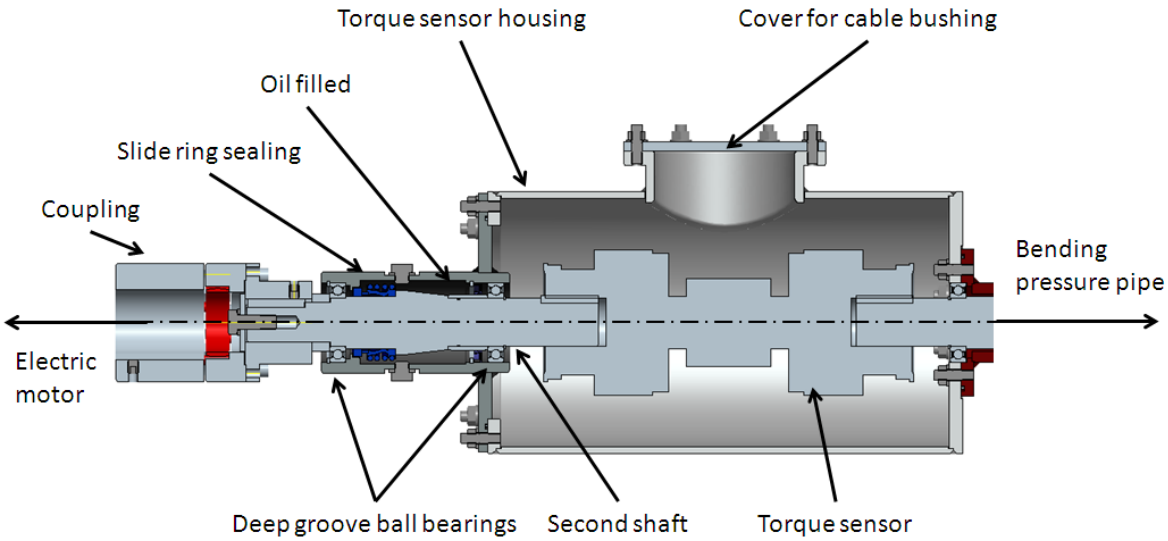

Figure 3.23: Torque sensor housing and bearing unit

The second pump shaft has two deep groove ball bearings, the left one is the fixed bearing and the right one is the floating bearing. These ball bearings are running in grease, as they are thus producing less head than running in oil. The slide ring sealing is used for tightening the system pressure against the ambient pressure and is able to manage a pressure difference as far as 16 bar. The concept of the slide ring sealing is a unbalanced MG1/60-G60 by EagleBurgmann (see datasheet in Appendix B). In order to compensate the angular and axial offsets between the electric motor and the second shaft, a jaw clutch by KTR is used. This enables an interruption of the torque transmission from the electric motor to the test pump without having to disassemble the motor, which is a great advantage as the adjustment of the motor takes a lot of time and can thus become redundant.

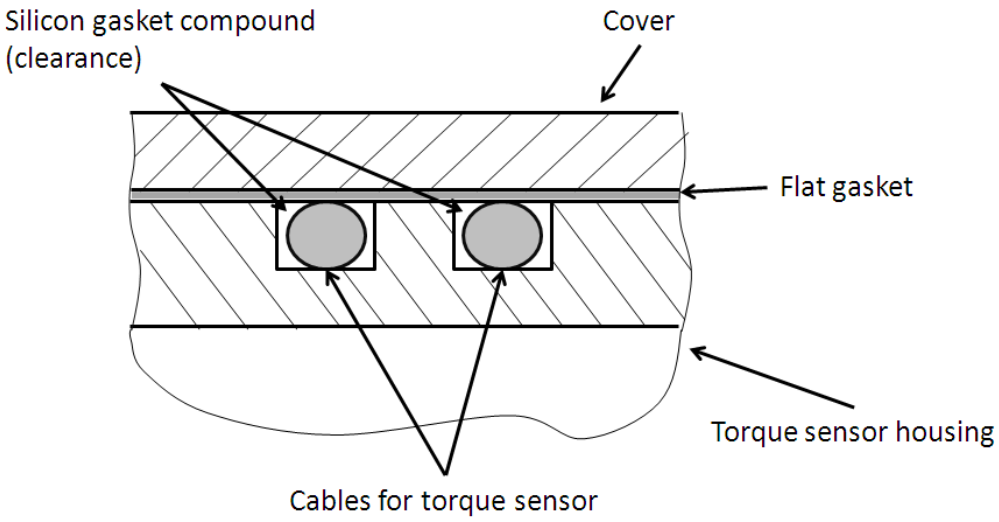

Figure 3.24: Cable bushing

3.3.9 Measurement points at the test rig

All sensors used have to be exactly named and positioned, in order to be able to allocate the measurement data to the position on the test rig. Two different pressure measurements have to be made and installed. On the one hand, a static pressure measurement for the head curve of the test pump, and on the other hand, a dynamic pressure measurement for vibration analysis needs to be set up.

The static pressure measurement has to stay installed all the time and has to be done at the suction side in a distance of two suction pipe diameters away of the inlet, see Figure 3.25 at plane “p_ss”. The same way installation has to be made at the pressure side of the pump also in a distance of two pressure pipe diameter away of the outlet of the pump, see Figure 3.25 at plane “p_ps”. At these two planes “p_ss” and “p_ps”, there are four pressure tappings with an offset of 90° to each other.

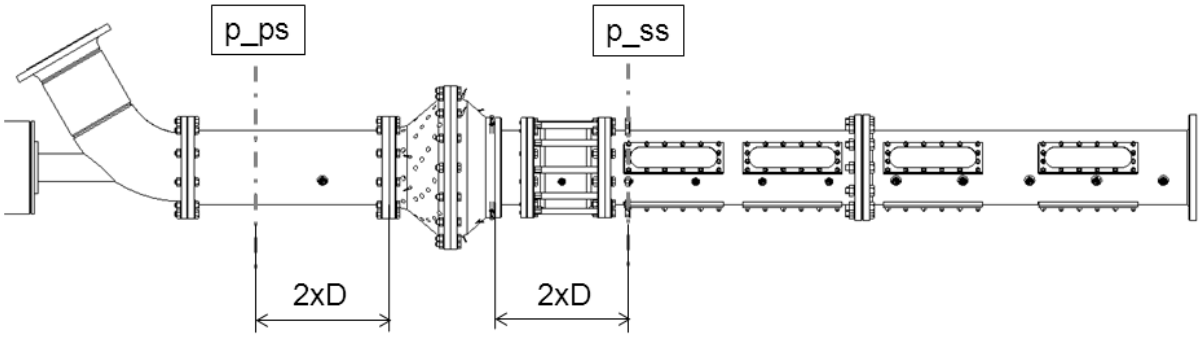

Figure 3.25: Static pressure measurement

The design of these pressure tappings is defined by DIN EN ISO 9906:2013-03 and has to be executed in the same way as shown in Figure 3.26.

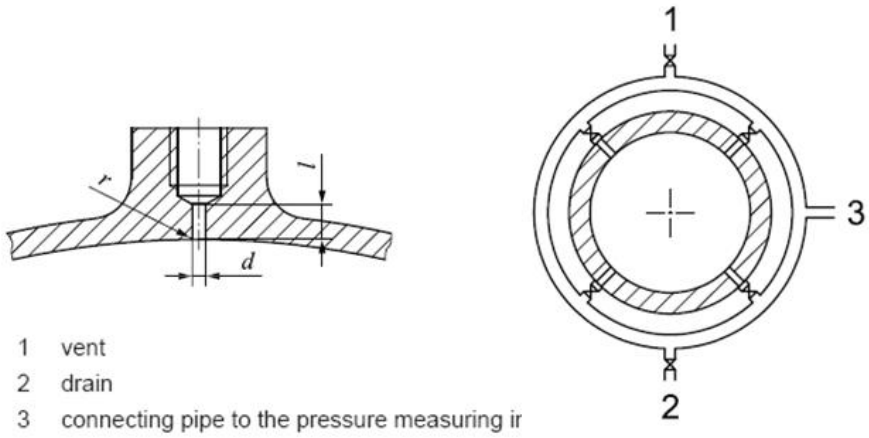

Figure 3.26: pressure tappings [13, p. 36]

These four pressure tappings are connected to a ring manifold, which leads the pressure to the pressure sensor.

For the dynamic pressure measurements special sensors are used, which have to be positioned directly at the point, of interest and do not have to be connected to a manifold. The reason for that is, to avoid influences as of the length of the measurement pipe and other effects on the result. The distance between the measurement point and the sensor has to be as short as possible, ideally it is installed as indicated in Figure 3.27.

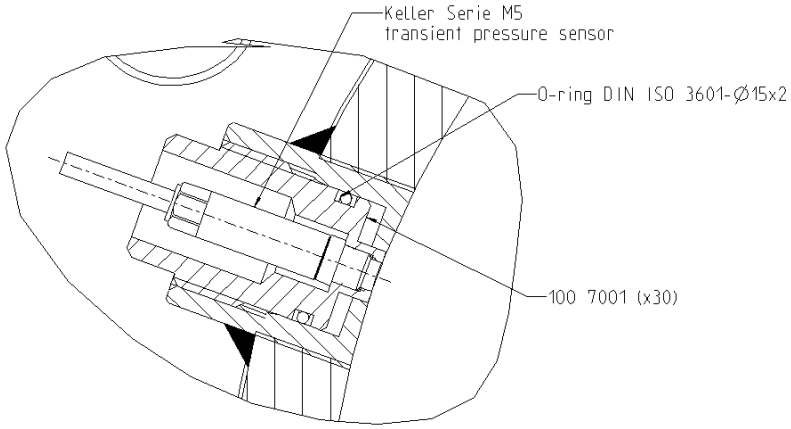

Figure 3.27: Installation of the dynamic pressure sensors

The pressure sensor “Kistler Serei M5” is mounted in a continuously adjustable part in order be able to move the top of the sensor exactly to the surface of the internal wall of the pipe, as shown in Figure 3.27. However, these pressure sensors are not just installed in the suction and pressure pipe of the test rig, they are also installed in the space between the impeller and the diffusor (vaneless space) and in the channels (between the blades) of the diffusor.

The positions and the names of these dynamic pressure sensors are shown in Figure 3.28, Figure 3.29 and Figure 3.30.

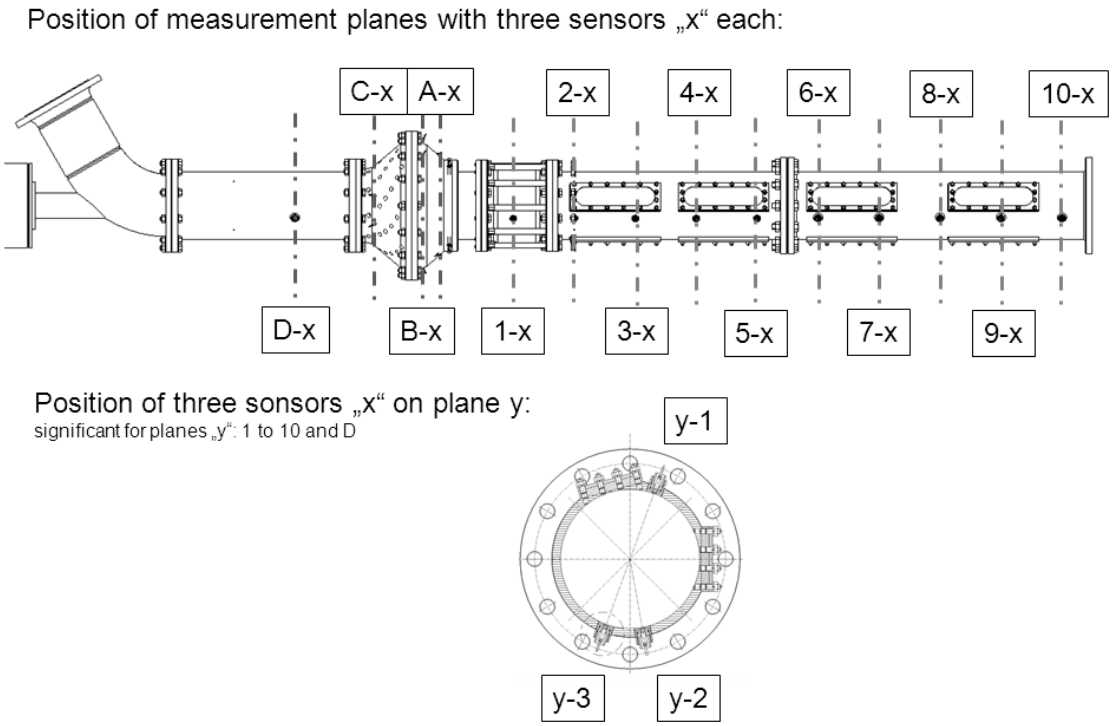

Figure 3.28: Denomination of the dynamic pressure sensors

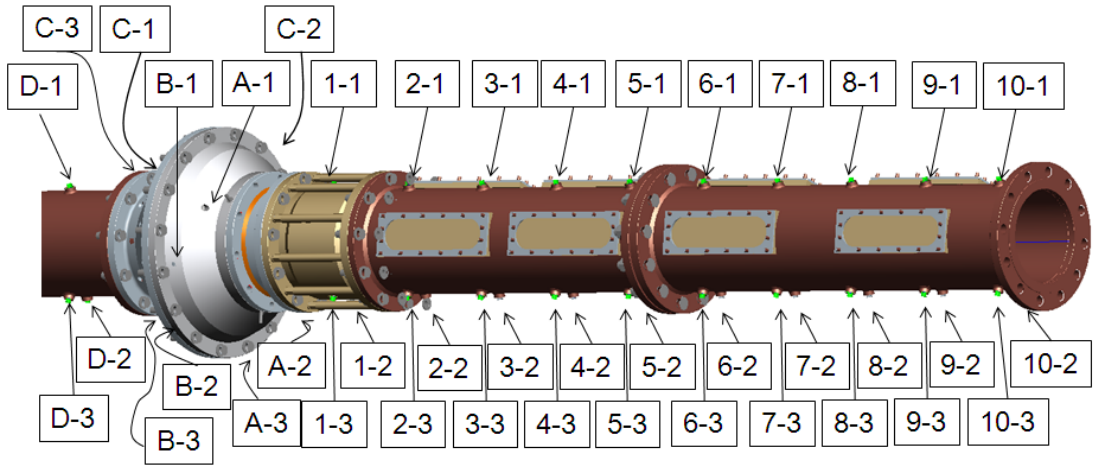

Figure 3.29: Position and denomination of all dynamic pressure sensors

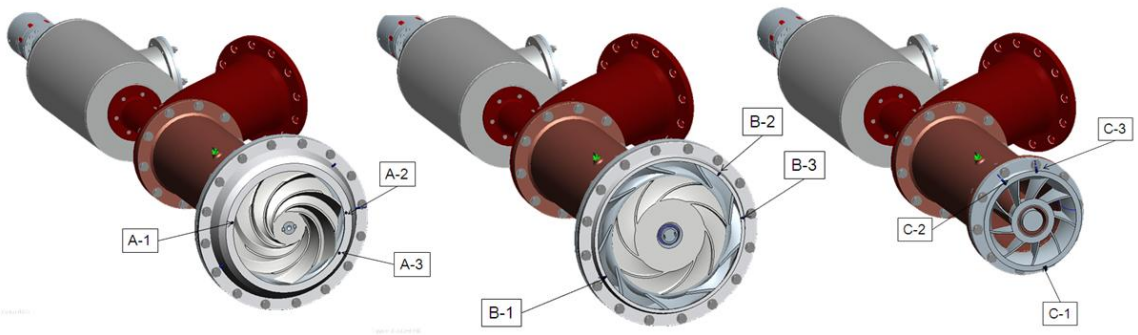

Figure 3.30: Position at plane A (left), plane B (middle) and plane C (right)

4 Stress analyses

In this chapter of the present Master Thesis, all single parts, which could cause failure in case of an overload, are calculated to reach the lifetime needed to realise all necessary measurements. Also, the deflection of the pump shaft, which has an influence on the clearance of the gap sealing and the critical bending speed, which are important for the overload of single parts and the running smoothness of the test rig, have to be calculated.

4.1 Forces and denominations

To realise the calculations of the bearing unit and the pump shaft, the reaction forces are needed. Therefore, a simplified model of the pump shaft, the impeller and the bearing unit is drawn to show and to define different forces and distances, see Figure 4.1. The distances in this model are specified in the 3D model and can be looked up in Appendix C. The distances between the bearing points at the model are in reference to the middle of the bearing unit and were given by measurements in the 3D model.

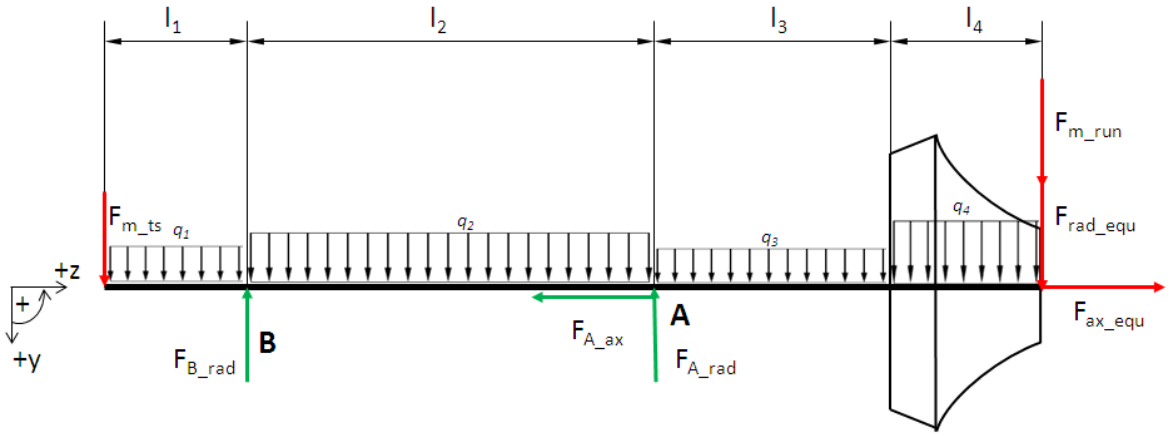

Figure 4.1: Forces at the pump shaft

The coordinate system will be defined as shown in Figure 4.1 and is valid for each of the following calculations.

The weight of the impeller and the torque sensor are considered as point loads F_{m_run} (impeller) and F_{m_ts} (torque sensor), and the pump shaft is divided into sections with different diameters and length. The application point of the weight of the impeller and the torque sensor is supposed to be on the safe side at the ends of the pump shaft. The weight of the pump shaft is approximated with 36 kg, for the torque sensor with 10 kg and for the impeller with 7.8 kg. The weight of each section is considered as a line load q_1 to q_4, which is calculated as the total weight of each section divided by its length. The geometrical model of the pump shaft is shown in Figure 4.2 whereas the length and the diameter of each section are defined. The different sections are simplifications and do not exactly reflect the

real model. Thus, it is possible that a section with a certain length and diameter in the model has more than one differing diameter at the real pump shaft. The simplifications are used to summarise a large number of different but similar sections of the real pump shaft to one section in the model in order to simplify the calculations.

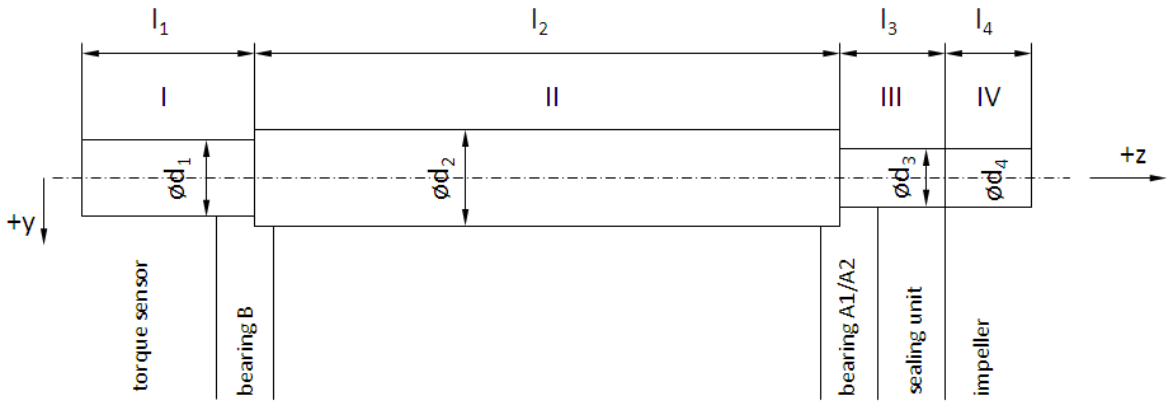

Figure 4.2: Geometrical model of the pump shaft

4.2 Bearing lifetime

As mentioned in chapter 3.3.6, the maximum lifetime of the bearing unit has to be 200 hours, which was claimed by the Institute of Hydraulic Machinery and is based on experiences. First of all, the reaction forces have to be investigated as the axial load, the radial load and the weights of the components are already known.

4.2.1 Reaction forces

The equilibrium conditions lead to the following equations, the detailed calculation is shown in Appendix A.

$$\Sigma M_A = 0 \qquad 0 = -F_{B\_rad}\cdot l_2 + F_{m\_ts}\cdot(l_2+l_1) + q_1\cdot l_1\cdot\left(l_2+\frac{l_1}{2}\right) + q_2\cdot l_2\cdot\frac{l_2}{2} - q_3\cdot l_3\cdot\frac{l_3}{2} \ldots \qquad 4.1$$
$$+ (-q_4)\cdot l_4\cdot\left(l_3+\frac{l_4}{2}\right) - (F_{m\_run}+F_{rad})\cdot(l_3+l_4)$$

$$F_{B\_rad}(Q_{BEP}) := \frac{1}{l_2}\cdot\left[\begin{array}{l} F_{m\_ts}\cdot(l_2+l_1) + q_1\cdot l_1\cdot\left(l_2+\frac{l_1}{2}\right) + q_2\cdot l_2\cdot\frac{l_2}{2} - q_3\cdot l_3\cdot\frac{l_3}{2} \ldots \\ + (-q_4)\cdot l_4\cdot\left(l_3+\frac{l_4}{2}\right) - \left(F_{m\_run}+F_{rad}(Q_{BEP})\right)\cdot(l_3+l_4)\end{array}\right]$$

$$\Sigma F_y = 0 \qquad 0 = -F_{A\_rad} + F_{m\_run} + F_{rad} + F_{m\_ts} - F_{B\_rad} \cdots + l_1 \cdot q_1 + l_2 \cdot q_2 + l_3 \cdot q_3 + l_4 \cdot q_4 \tag{4.2}$$

$$F_{A\_rad}(Q_{BEP}) := F_{m\_run} + F_{rad}(Q_{BEP}) + F_{m\_ts} - F_{B\_rad}(Q_{BEP}) \cdots + l_1 \cdot q_1 + l_2 \cdot q_2 + l_3 \cdot q_3 + l_4 \cdot q_4$$

$$\Sigma F_z = 0 \qquad 0 = F_{ax} - F_{A\_ax} \tag{4.3}$$

$$F_{A\_ax}(Q_{BEP}) := F_{ax}(Q_{BEP})$$

$$F_{B\_ax} := 0 \cdot N$$

4.2.2 Load spectrum

The application conditions of the test rig are not constant during the whole operating time because of measurement points, which have to be analysed very carefully, and other operating points, which are not of interest. The points of operation of high interest are at 0% Q_{BEP} in reference to the shut off-head, the Q_{BEP} in reference to the best efficiency point and the operation points at 70%, 100% and 130% of Q_{BEP} in reference to the $NPSH_{3\%}$ value. The majority of the lifetime of the test rig will be used for measurements at these guaranteed points; the rest of the lifetime is used for measurements of the characteristic curve at a constant distribution from 0% to 130% of Q_{BEP}. The axial and radial forces are calculated as mentioned in chapter 2.6.3 and 2.6.4 for the different points of operation and lead to 14.429 N at 0% BEP, 12.288 N at 70% BEP, 10.059 N at 100% BEP, 7.044 N at 130% BEP for axial load and 2.018 N at 0% BEP, 1.117 N at 70% BEP, 169 N at 100% BEP, 186 N at 130% BEP for radial load. Figure 4.3 displays the calculated axial and radial load spectrum in reference to the guaranty points.

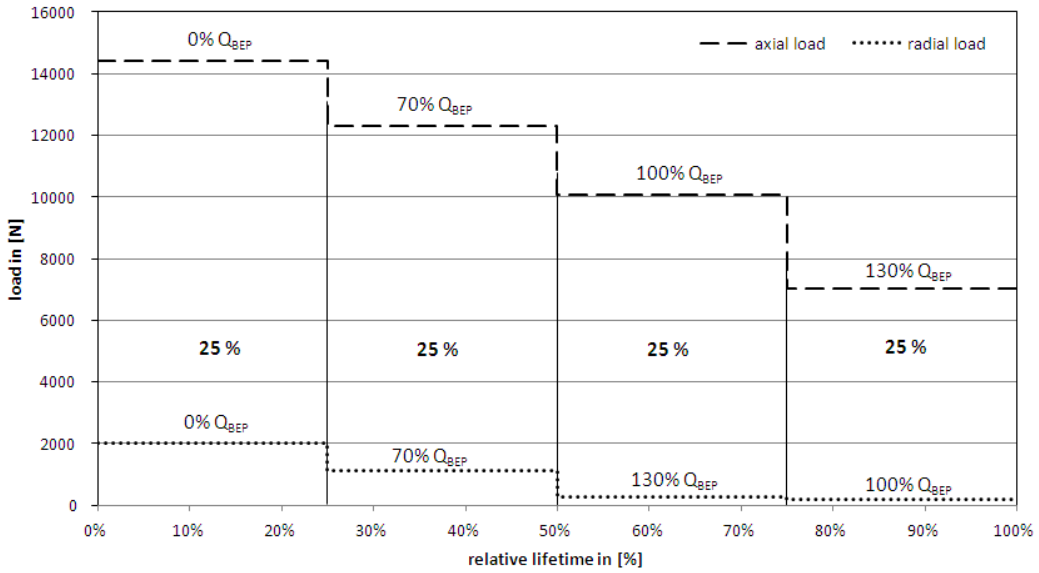

Figure 4.3: Axial and radial load spectrum

4.2.3 Load carrying capacity and lifetime

The geometrical dimensions of the bearings used are given by the pre-calculations and the 3D model. The data for the calculation of the load carrying capacity as well as the calculation of the maximum lifetime are shown in Table 4.1 and can be seen in Appendix B.[14]

In the non-rotating state of the test rig, the axial load is depending on the unbalanced shaft load and is rather low, whereas the radial load is only depending on the weight of the pump shaft, the torque sensor and the impeller. Therefore, the static load carrying capacity is not calculated. To calculate the dynamic load carrying capacity and the shortest lifetime, the equivalent dynamic load of each bearing in reference to the load spectrum is needed.

Table 4.1: Axial and radial deep groove ball bearing technical data[14]

A1: axial deep groove ball bearing	**52210**
basic dynamic load rating, axial	50 kN
basic static load rating, axial	106 kN
minimum load factor	0,07
limiting speed	4950 1/min
geometrical dimensions	40x78x39 dxDxB
A2: radial deep groove ball bearing	**6010-2RSR**
basic dynamic load rating, radial	22 kN
basic static load rating, radial	158 kN
limiting speed	5600 1/min
geometrical dimensions	50x80x16 dxDxB
B: radial deep groove ball bearing	**6011-2RSR**
basic dynamic load rating, radial	30 kN
basic static load rating, radial	212 kN
limiting speed	5000 1/min
geometrical dimensions	55x90x18 dxDxB

In order to consider the load variability represented by the load spectrum with constant rotating speed, the equivalent load of each bearing is calculated as shown in equation 2.44 and equation 4.5 with $q_i=\Delta t_i/T_{ges}$ and F_i being the effective load. [15, p. 157]

$$P^3 \cdot 100\% = \sum_i \left(q_i \cdot F_i^{\,3}\right) \tag{4.4}$$

$$P = \sqrt[3]{\frac{\sum_i \left(q_i \cdot F_i\right)}{100\%}} \tag{4.5}$$

This equation is used to calculate the equivalent load of each bearing and is applied to bearing unit A1 in equation 4.6, only for axial load,

$$P_{A1} := \sqrt[3]{\begin{matrix} q_{0\%} \cdot F_{a\_A1}\left(Q_{BEP} \cdot 0\right)^3 + q_{70\%} \cdot F_{a\_A1}\left(Q_{BEP} \cdot 0.7\right)^3 \ldots \\ + q_{100\%} \cdot F_{a\_A1}\left(Q_{BEP} \cdot 1\right)^3 + q_{130\%} \cdot F_{a\_A1}\left(Q_{BEP} \cdot 1.3\right)^3 \end{matrix}} = 11589\,N \qquad 4.6$$

bearing unit A2 in equation 4.7 , only for radial load,

$$P_{A2} := \sqrt[3]{\begin{matrix} q_{0\%} \cdot F_{r\_A2}\left(Q_{BEP} \cdot 0\right)^3 + q_{70\%} \cdot F_{r\_A2}\left(Q_{BEP} \cdot 0.7\right)^3 \ldots \\ + q_{100\%} \cdot F_{r\_A2}\left(Q_{BEP} \cdot 1\right)^3 + q_{130\%} \cdot F_{r\_A2}\left(Q_{BEP} \cdot 1.3\right)^3 \end{matrix}} = 1743\,N \qquad 4.7$$

bearing unit B in equation 4.8, only for radial load.

$$P_B := \sqrt[3]{\begin{matrix} q_{0\%} \cdot F_{r\_B}\left(Q_{BEP} \cdot 0\right)^3 + q_{70\%} \cdot F_{r\_B}\left(Q_{BEP} \cdot 0.7\right)^3 \ldots \\ + q_{100\%} \cdot F_{r\_B}\left(Q_{BEP} \cdot 1\right)^3 + q_{130\%} \cdot F_{r\_B}\left(Q_{BEP} \cdot 1.3\right)^3 \end{matrix}} = 194\,N \qquad 4.8$$

The exponent used for ball bearing units is 3 and the one for roller bearings it is 10/3. The basic rating life is the time which will be reached by 90% of the bearings, and which is calculated as shown in equations 4.9 to 4.11.

$$L_{A1h} := \left(\frac{C_{aA1}}{P_{A1}}\right)^3 \cdot \frac{10^6}{n_{shaft}} = 898 \cdot h \qquad 4.9$$

$$L_{A2h} := \left(\frac{C_{rA2}}{P_{A2}}\right)^3 \cdot \frac{10^6}{n_{shaft}} = 22509 \cdot h \qquad 4.10$$

$$L_{Bh} := \left(\frac{C_{rB}}{P_{A2}}\right)^3 \cdot \frac{10^6}{n_{shaft}} = 57077 \cdot h \qquad 4.11$$

The axial deep groove ball bearing is the bearing with the lowest lifetime of about 750 hours. In order to consider more than the equivalent load, a calculation of the expanded adjusted rating life is realised for bearing A1 in Appendix A. This calculation is done for a requisite reliability of 99% and a temperature of about 70° with typical contaminations, and leads to a maximum lifetime of about 280 hours, which is satisfying.

4.3 Pump shaft

The geometrical raw design of the pump shaft is defined in layout nine whereas the dimensions of the diameter and the length are limited by the torque sensor a the one hand, and by the impeller on the other hand whereas the diameter of the suction and the pressure pipe, which influences the distance between the diffusor and the bending. The shaft diameter at the impeller fastening and at the bearing section “A” seems to be critical because the bending torque and the normal internal force are rather high and additional a notch is weakening the cross section at this location, therefore it has to be analysed in detail. To do this, the trend of the internal forces and torques against the length of the pump shaft have to be calculated. The dead load of the torque sensor, the dead load and the radial load of the impeller are approached as point load at the end of the pump shaft. The dead load of the pump shaft itself is considered as line load, see chapter 4.1. As the pump shaft is very long, this could lead to a low critical bending speed. It is very important to avoid an overcritical operating point, because of high forces in case of resonance caused by the high density of the fluid used. Therefore, an analysis of the critical bending speed is necessary to avoid an overload of the pump shaft and other parts, and to avoid rough running. The radial and axial load of the impeller used for further calculations is the load at Q=0 m³/h. This is the highest possible force within the whole range of operation points and is realised in oder to be on the safe side during further calculations. The geometrical design of the pump shaft has already been realised as 3D design and is shown below.

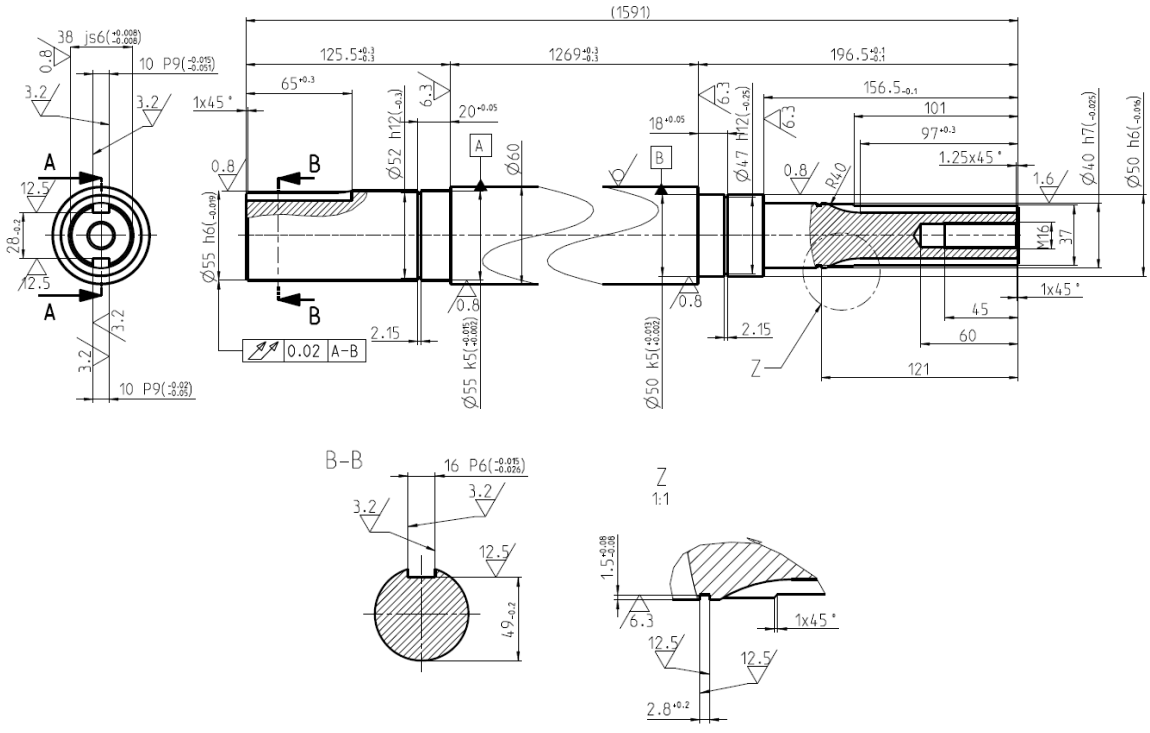

Figure 4.4: Design details of the pump shaft

4.3.1 Trends of internal forces

The first step is, to investigate the trends of the internal forces along the pump shaft in order to find highly stressed points and to ensure failure safety. Another important information is given by the deflection of the pump shaft. The deflection at the impeller influences the clearance at the gap sealing which could affect the leakage losses and the impeller could touch the gap ring in the worst case. Therefore, the pump shaft is divided into four different sections as mentioned above, and the equations for the trend of the internal forces are partially investigated as shown below for section two. All equations together are used to calculate the trend of the axial and shear forces and the bending torque along the pump shaft.

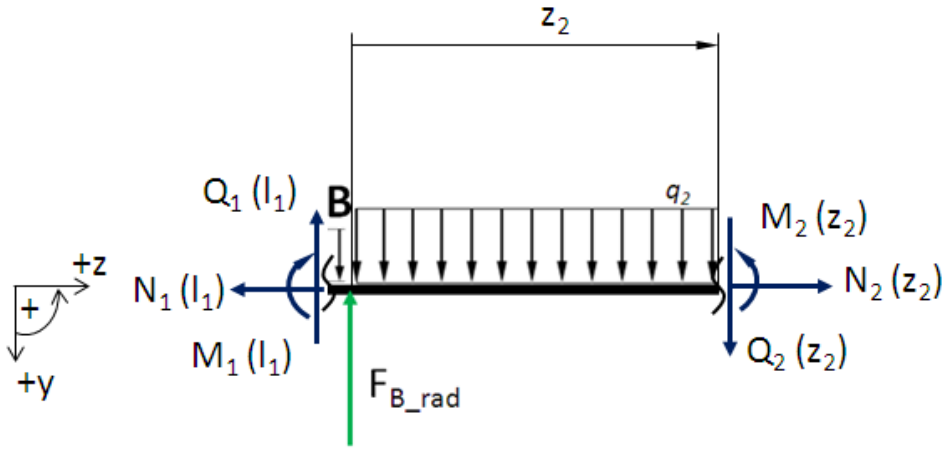

Figure 4.5: Section two of the pump shaft

$$N_2(z_2) := 0 \tag{4.12}$$

$$Q_2(F_{B\ rad}, q_2, z_2, Q_{1\ B}) := F_{B\ rad} - q_2 \cdot z_2 + Q_{1\ B} \tag{4.13}$$

$$M_2(M_{1\_B}, F_{B\_rad}, q_2, z_2, Q_{1\_B}) := M_{1\_B} + \int_0^{z_2} Q_2(F_{B\_rad}, q_2, z_2, Q_{1\_B})\, dz_2 \tag{4.14}$$

The whole calculation is presented in Appendix A, the results are shown in Figure 4.6, Figure 4.7 and Figure 4.8.

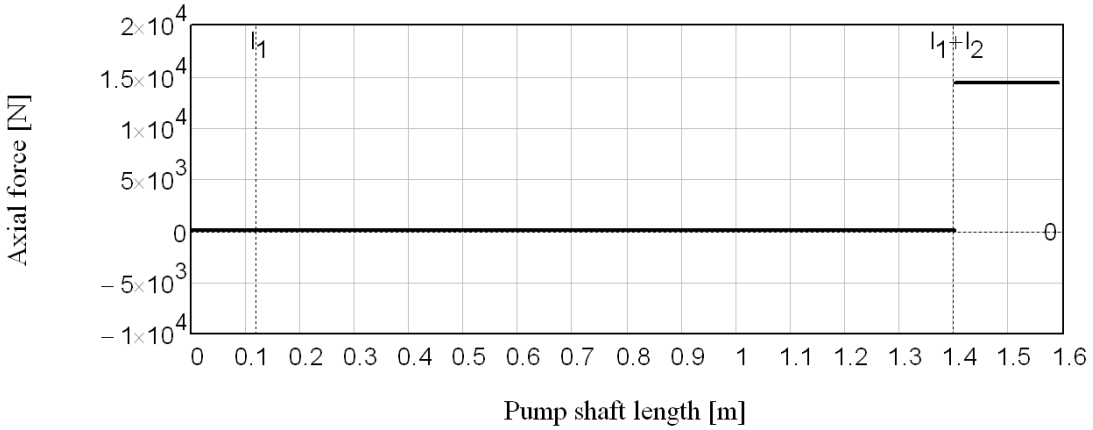

Figure 4.6: Axial force along the pump shaft

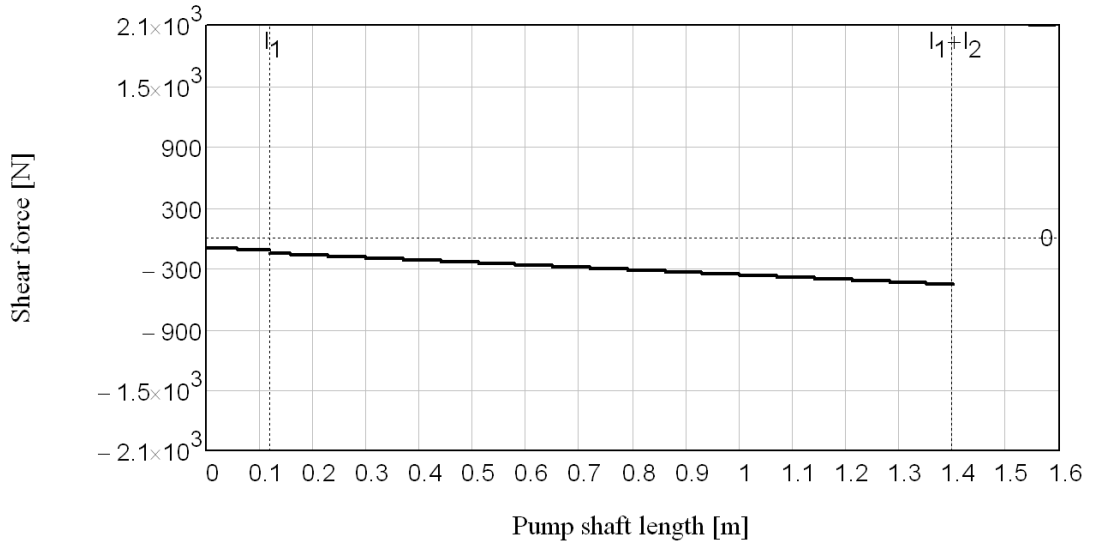

Figure 4.7: Shear force along the pump shaft

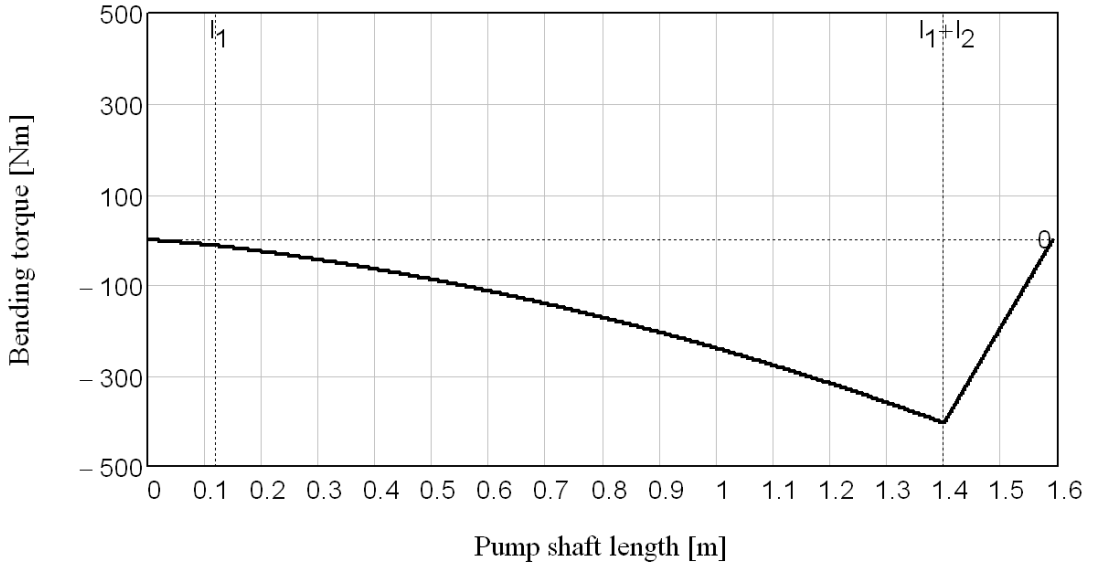

Figure 4.8: Bending torque along the pump shaft

4.3.2 Stress verification

The calculation in chapter 4.3.1 shows, that the highest stressed section at the pump shaft is between the position of bearing A and the impeller. In this chapter, the stresses within the sections three and four (Figure 4.2) are going to be analysed in detail. The detailed calculation is presented in Appendix A, the results of this calculation are shown below. This part of the pump shaft is divided into new sections drawn, as in Figure 4.9.

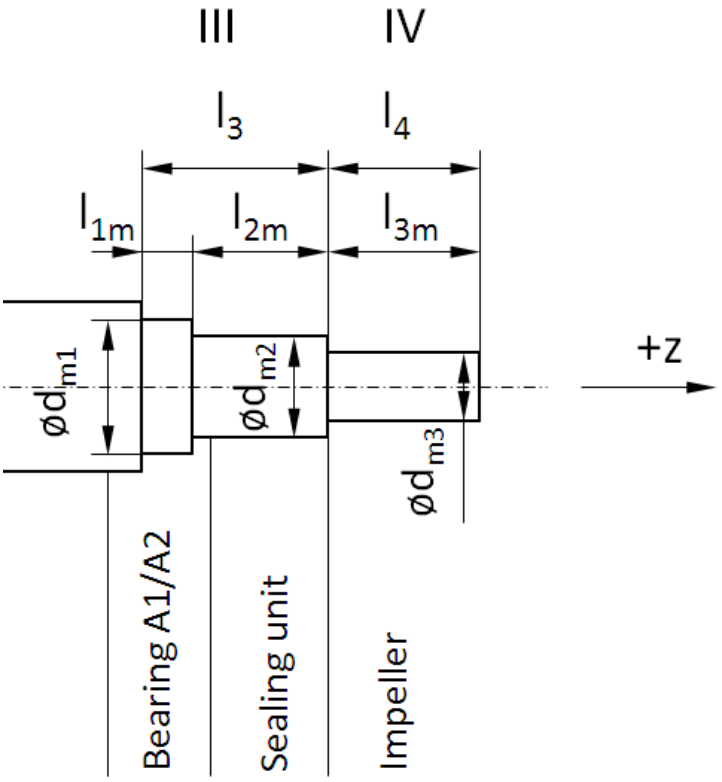

Figure 4.9: Section three and four in detail

The following diagrams show the trend of the normal and shear stress within the sections three and four. The deflection stress is alternating with the rotating speed of the pump shaft because the direction of the weights and the radial load from impeller are assumed as unvaried. The mean stress is the static part of the stress of each cross-section and the maximum stress is the sum of the static (mean stress) and the dynamic parts (deflection stress).

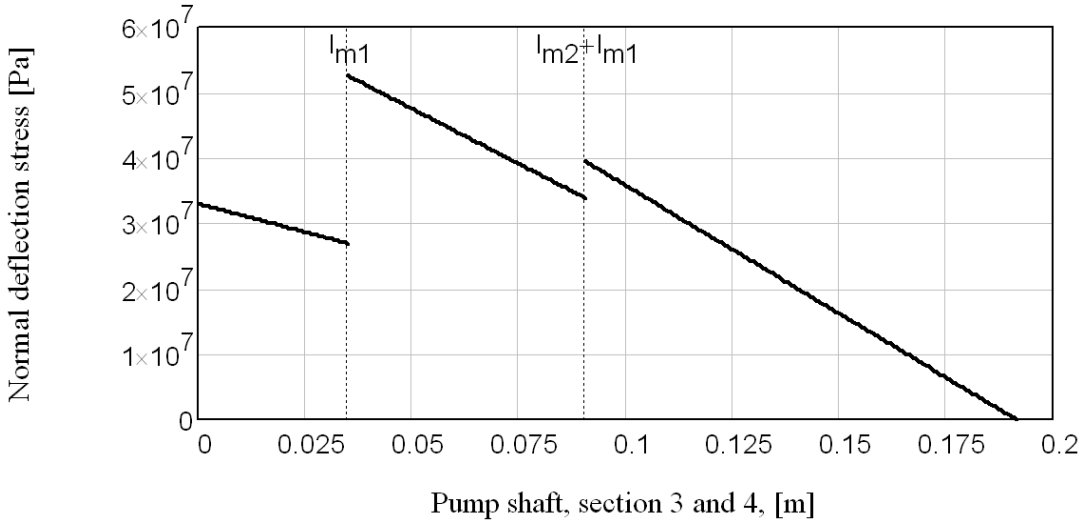

Figure 4.10: Normal deflection stress, dynamic

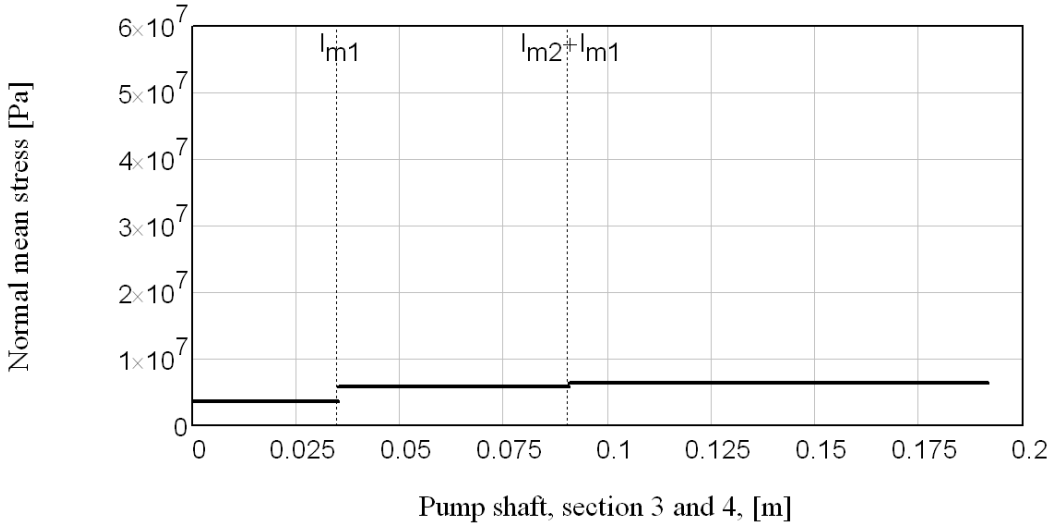

Figure 4.11: Normal mean stress, static

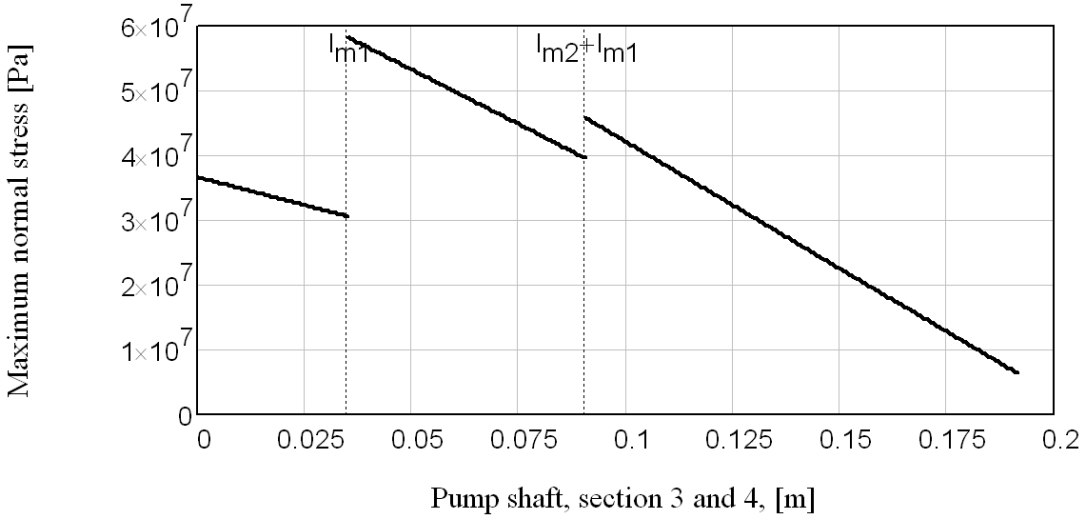

Figure 4.12: Maximum normal stress

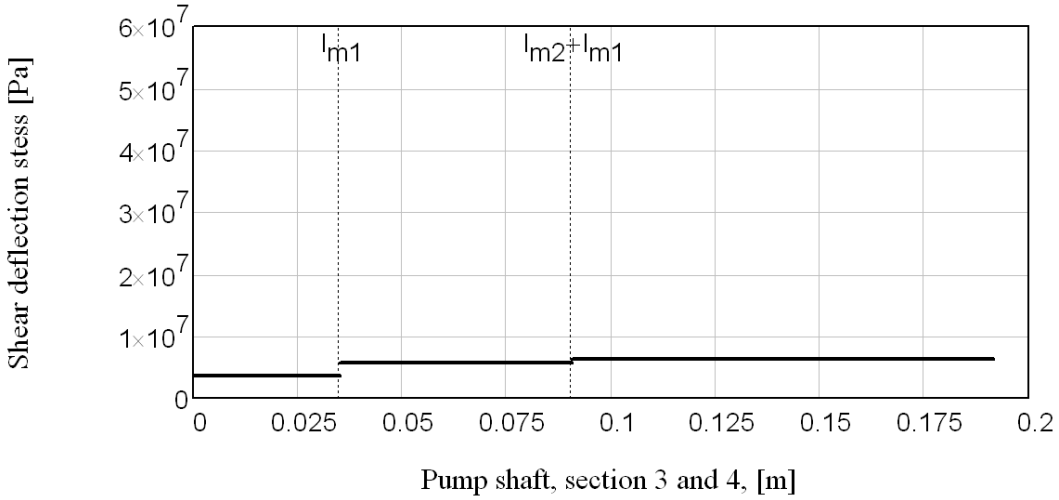

Figure 4.13: Shear deflection stress

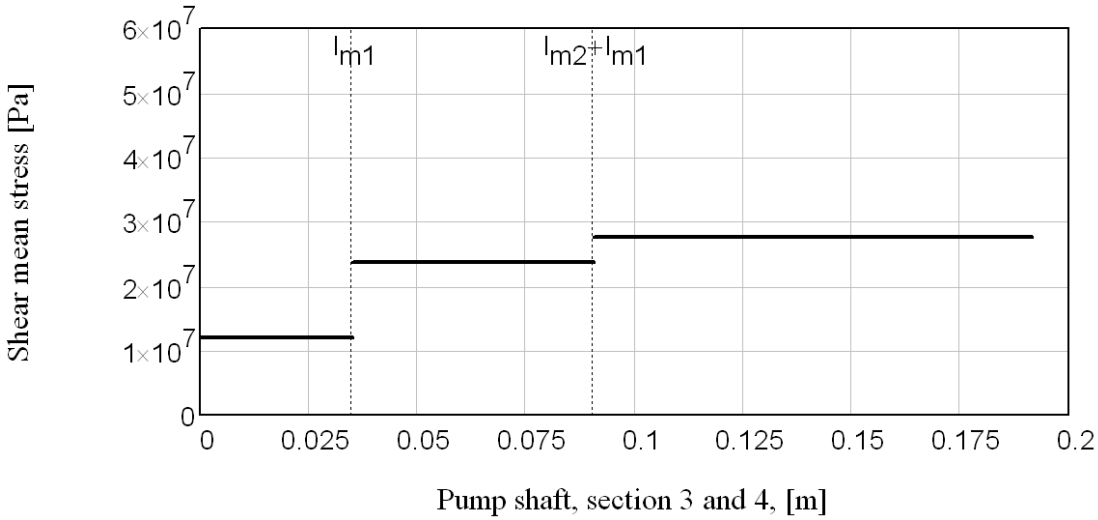

Figure 4.14: Shear mean stress

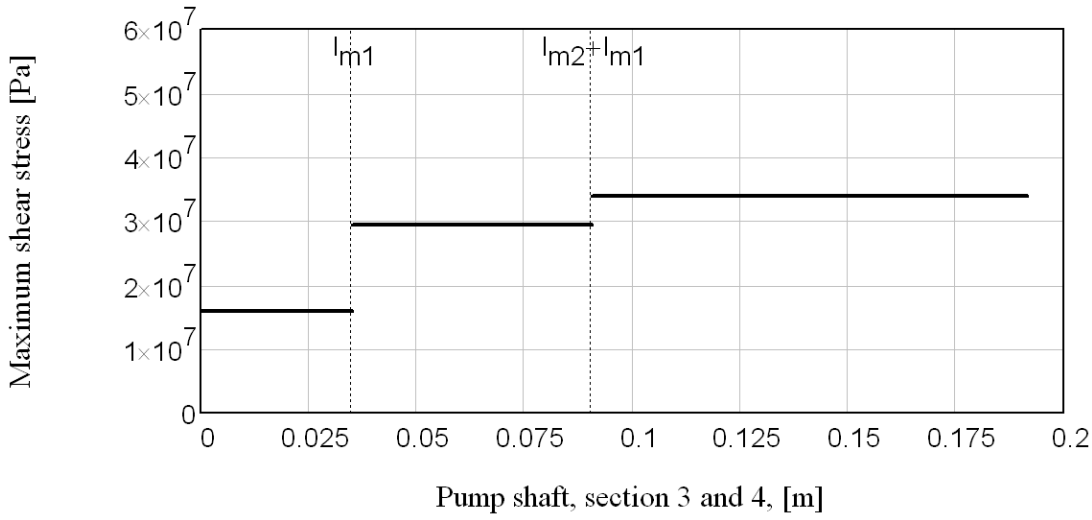

Figure 4.15: Maximum shear stress

4.3.3 Creep resistance

Referring to a period of use of maximum 200 hours, the number of load cycles during this time could be estimated to 1.8 10^7. This is the reason why a creep resistance design of the pump shaft is used, as it provides more than 10^7 load cycles see [16, p. 47]. Therefore, all points at sections three and four of the pump shaft are going to be analysed, which seems to be critical in reference to notches. Figure 4.16 shows the points, which are of interest for this kind of analysis.

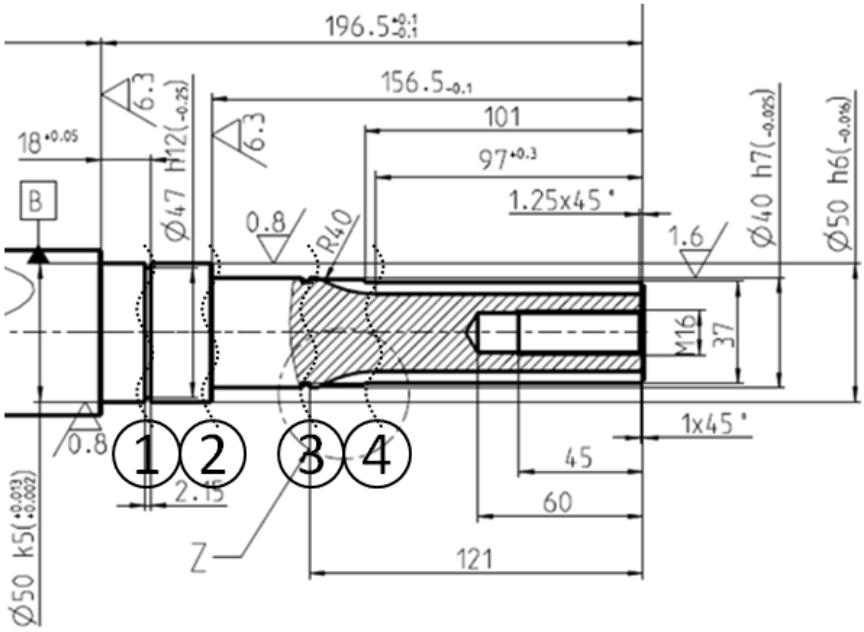

Figure 4.16: Creep resistance, critical cross-sections

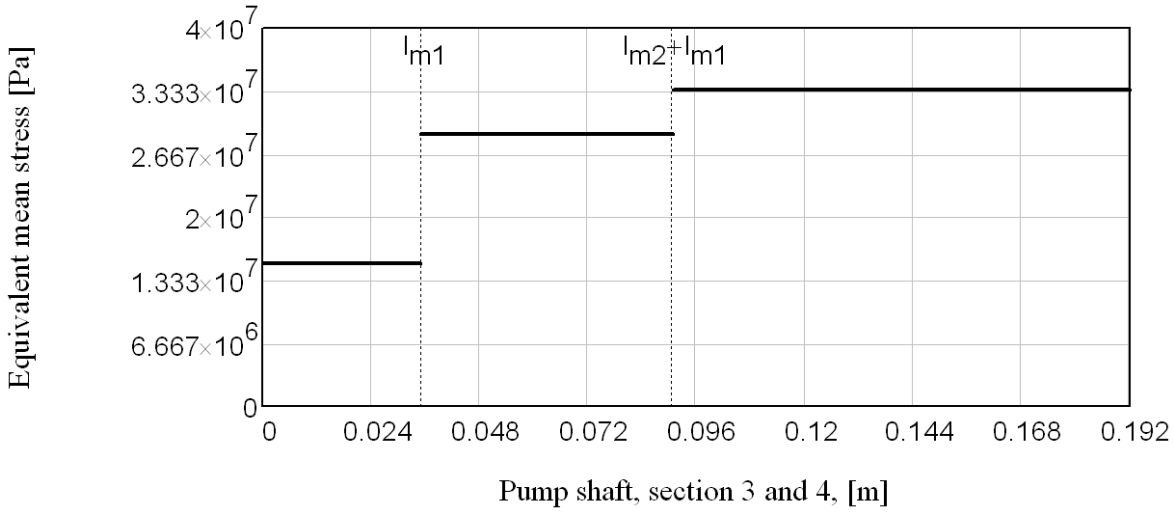

Figure 4.17: Equivalent mean stress

In Figure 4.17, the equivalent mean stress σ_{vm} along the pump shaft sections three and four is displayed, which is used to calculate the deflection strength σ_A and τ_A with the help of the Haigh-diagram. The deflection strength reduced by the kerfs factors leads to the nominal deflection strength σ_{NA} and τ_{NA} which indicate the maximal stress allowed in reference to the notches at each section. The minimum criterion to be creep resistance is that the nominal deflection stress σ_{NA} has to be higher than the equivalent deflection stress of each notch, which finally leads to safety against fatigue failure as shown below.

$$S_1 := \frac{\sigma_{NA\_1}}{\sigma_{va\_1}} = 5 \qquad S_2 := \frac{\sigma_{NA\_2}}{\sigma_{va\_2}} = 3 \qquad S_3 := \frac{\sigma_{NA\_3}}{\sigma_{va\_3}} = 4 \qquad S_4 := \frac{\sigma_{NA\_4}}{\sigma_{va\_4}} = 5$$

The detailed approach and calculation of this method are presented in Appendix A.

4.3.4 Deflection of the pump shaft

The deflection of the pump shaft is used for investigating the lowest critical bending speed on the one hand, and on the other hand it is used for the specification of the coupling as well as the definition of the lowest possible clearance at the gap sealing. Therefore, the calculation of the deflection is also done piecewise for each of the sections one to four as defined in chapter 4.3.1. First of all, the differential equations have to be defined for each section. Equations 4.15 to 4.19 show the differential equations for section four.

$$E_{steel} \cdot I_{y4} \cdot w''''_4(z_4) = q_4 \tag{4.15}$$

$$E_{steel} \cdot I_{y4} \cdot w'''_4(z_4, C_{13}) = q_4 \cdot z_4 + C_{13} = -Q_4(z_4) \tag{4.16}$$

$$E_{steel} \cdot I_{y4} \cdot w''_4(z_4, C_{13}, C_{14}) = q_4 \cdot \frac{z_4^2}{2} + C_{13} \cdot z_4 + C_{14} = -M_4(z_4) \tag{4.17}$$

$$E_{steel} \cdot I_{y4} \cdot w'_4(z_4, C_{13}, C_{14}, C_{15}) = q_4 \cdot \frac{z_4^3}{6} + C_{13} \cdot \frac{z_4^2}{2} + C_{14} \cdot z_4 + C_{15} = -E \cdot I_{y4} \cdot \alpha_4 \tag{4.18}$$

$$E_{steel} \cdot I_{y4} \cdot w_4(z_4, C_{13}, C_{14}, C_{15}, C_{16}) = q_4 \cdot \frac{z_4^4}{24} + C_{13} \cdot \frac{z_4^3}{6} + C_{14} \cdot \frac{z_4^2}{2} + C_{15} \cdot z_4 + C_{16} \tag{4.19}$$

The differential equations for all sections lead to 16 equations with 16 unknown variables. Therefore, 16 different boundary conditions are needed to solve this linear system of equations (equation 4.20).

$$A \cdot C = b \tag{4.20}$$

$$C = A^{-1} \cdot B \tag{4.21}$$

Table 4.2: Boundary conditions

$M_1(0)=0$	$M_3(l_3)= M_4(0)$	$w_3(0)=0$	$w_3(l_3)'= w_4(0)'$
$M_4(l_4)=0$	$w_1(l_1)=0$	$w_3(l_3)= w_4(0)$	$Q_1(0)=-F_{m\_ts}$
$M_1(l_1)= M_2(0)$	$w_2(0)=0$	$w_1(l_1)'= w_2(0)'$	$Q_1(0)=-F_{m\_run}+F_{rad}$
$M_2(l_2)= M_3(0)$	$w_2(l_2)=0$	$w_2(l_2)'= w_3(0)'$	$Q_3(l_3)= Q_4(0)$

Table 4.2 shows the list of boundary conditions, which are inserted into the different differential equations. The result is a 16x16-matrix "A", in which all factors of the unknown coefficients C_1 to C_{16} are included as well as a coefficient matrix "x" and a vector "B", see equation 4.22.

$$\begin{pmatrix} a_{1.1} & a_{1.2} & \cdots & a_{1.16} \\ a_{2.1} & a_{2.2} & \cdots & a_{2.16} \\ \cdots & \cdots & \cdots & \cdots \\ a_{16.1} & a_{16.2} & \cdots & q_{16.16} \end{pmatrix} \cdot \begin{pmatrix} C_1 \\ C_2 \\ \cdots \\ C_{16} \end{pmatrix} = \begin{pmatrix} b_1 \\ b_2 \\ \cdots \\ b_{16} \end{pmatrix} \tag{4.22}$$

This linear system of equations could be solved with the inverse matrix A^{-1}, and the coefficients C_1 to C_{16} were calculated. The detailed calculation is shown in Appendix A, the bending line equations are estimated in the equations 4.23 to 4.26 for each section.

$$w_{1.}(z_1) := \frac{-1}{E_{steel} \cdot I_{y1}} \cdot \left(fq \cdot q_1 \cdot \frac{z_1^4}{24} + C_{1.} \cdot \frac{z_1^3}{6} + C_{2.} \cdot \frac{z_1^2}{2} + C_{3.} \cdot z_1 + C_{4.} \right) \tag{4.23}$$

$$w_{2.}(z_2) := \frac{-1}{E_{steel} \cdot I_{y2}} \cdot \left(fq \cdot q_2 \cdot \frac{z_2^4}{24} + C_{5.} \cdot \frac{z_2^3}{6} + C_{6.} \cdot \frac{z_2^2}{2} + C_{7.} \cdot z_2 + C_{8.} \right) \tag{4.24}$$

$$w_{3.}(z_3) := \frac{-1}{E_{steel} \cdot I_{y3}} \cdot \left(fq \cdot q_3 \cdot \frac{z_3^4}{24} + C_{9.} \cdot \frac{z_3^3}{6} + C_{10.} \cdot \frac{z_3^2}{2} + C_{11.} \cdot z_3 + C_{12.} \right) \tag{4.25}$$

$$w_{4.}(z_4) := \frac{-1}{E_{steel} \cdot I_{y4}} \cdot \left(fq \cdot q_4 \cdot \frac{z_4^4}{24} + C_{13.} \cdot \frac{z_4^3}{6} + C_{14.} \cdot \frac{z_4^2}{2} + C_{15.} \cdot z_4 + C_{16.} \right) \tag{4.26}$$

The assembled bending lines plotted against the pump shaft length are shown in Figure 4.18. The maximum deflection could be detected at the end of the pump shaft, at the impeller inlet and accounts for w=-0.17 mm. This is similar to the position of the gap ring, which lead to the fact that the maximum gap ring clearance has to be higher than this maximum deflection, in order to avoid material contact in the gap ring. Therefore, the minimum clearance of the gap ring has to be 0.2 mm. The deflection at the other side of the pump shaft, at the coupling side, is 0.02 mm, it is much lower than at the impeller side, and it is not within a critical dimension.

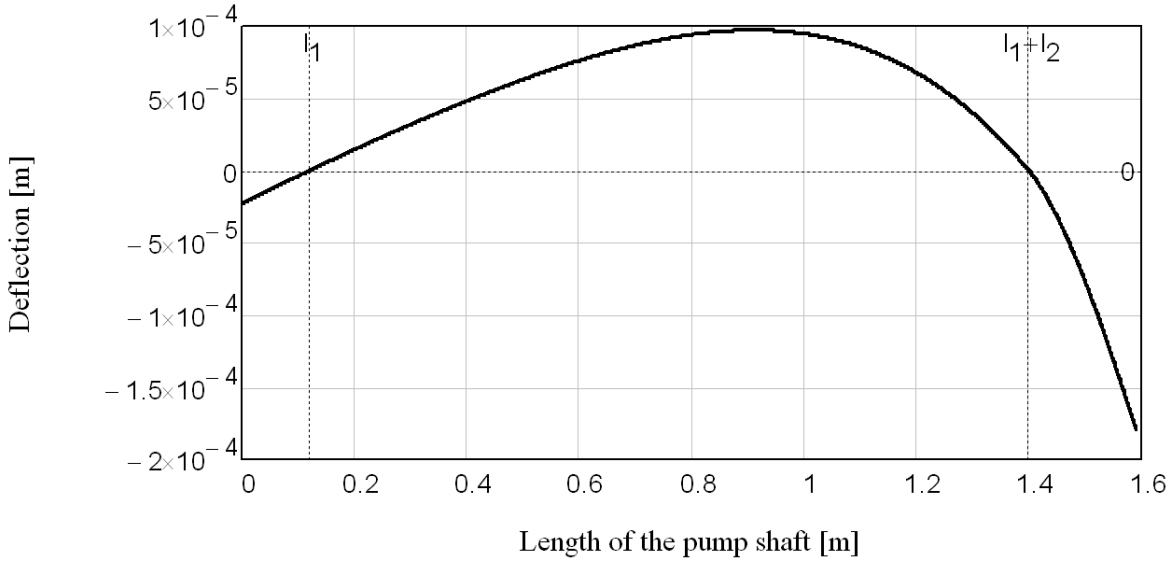

Figure 4.18: Deflection of the pump shaft

4.3.5 Critical bending speed

It is very important to have information about the critical bending speed, in order to avoid resonance vibrations and part failure in reference to overload. Furthermore, the critical bending speed could influence the smoothness of running enormously, if it is too low. The condition to avoid overload of single parts and to avoid vibrations in case of resonance is, to have a higher critical bending speed as the rotating speed of the pump shaft, which is actually 24.83 Hz (1490 rpm).

For the calculation of the lowest critical bending speed of a shaft with two bearings and more different single masses, the Dunkerley method could be used, see equation [16, p. 339].

$$\frac{1}{\omega_{crit}^2} = \frac{1}{\omega_{c0}^2} + \frac{1}{\omega_{c1}^2} + \frac{1}{\omega_{c2}^2} \qquad 4.27$$

However, first the natural frequency of the pump shaft without any single masses and the frequency of each single mass, without the mass of the pump shaft, have to be calculated.

Therefore, the deflections of each case are calculated separately. The mere deflection caused by the mass of the pump shaft is 0.06 mm, by the mass of the torque sensor it is 0.009 mm and by the mass of the impeller it is 0.015 mm. The natural frequency for each case is calculated in equation 4.28 for mass only, in equation 4.29 just for torque sensor and in equation 4.30 just for impeller only.

$$\omega_{c0} := \sqrt{\frac{g}{|w_{2\_max\_mass}|}} = 402 \cdot Hz \qquad 4.28$$

$$\omega_{c1} := \sqrt{\frac{g}{|w_{2\_max\_ts}|}} = 1030 \cdot Hz \qquad 4.29$$

$$\omega_{c2} := \sqrt{\frac{g}{|w_{2\_max\_run}|}} = 786 \cdot Hz \qquad 4.30$$

The critical speed investigated by means of the Dunkerly method is calculated in equation 4.31 and leads to a critical speed of about 20 300 rpm, which is much higher than 1490 rpm, the normal rotating speed.

$$\omega_{crit} := \sqrt{\frac{1}{\frac{1}{\omega_{c0}^{2}} + \frac{1}{\omega_{c1}^{2}} + \frac{1}{\omega_{c2}^{2}}}} = 338 \cdot Hz \qquad 4.31$$

The estimated lowest critical bending speed is expected to be 5% to 10% lower than it will be in reality, see in [16, p. 339]. Furthermore, the rigidities of the bearings and also the restraining effect of the fluid around the impeller are not included in this calculation. With regard to these aspects, the critical bending speed seemed to be lower as calculated before, but high enough to avoid failure and vibrations.

4.4 Impeller

The impeller is mounted with a central socket head screw; for torque transmission two fitting keys are used.

4.4.1 Fitting key

The force to transmit the torque between shaft and impeller has to be considered with an application factor k_A=1.25. This factor includes the typical conditions for power supply by an electrical engine and can be looked up in [17]. By means of equation 4.32 the force of each fitting key could be calculated with n_p=2 (two fitting keys) and a basic load rating of about 75% (p_p=0.75).

$$F_{key} := \frac{M_t \cdot k_A \cdot 2}{d_{shaft\_run} \cdot n_p \cdot p_p} = 13038\,N \qquad 4.32$$

The maximum stress at each component, the pump shaft and the impeller could calculated as follows, and whereas it has to be lower than the maximum stress allowed for each component.

$$p_{shaft} := \frac{F_{key}}{t_{1\_run} \cdot l_t} = 33 \cdot \frac{N}{mm^2} \qquad 4.33$$

$$p_{run} := \frac{F_{key}}{t_{2\_run} \cdot l_t} = 54 \cdot \frac{N}{mm^2} \qquad 4.34$$

The maximum stress allowed for the pump shaft is 480 N/mm² and for the impeller 470 N/mm².

4.4.2 Seating stress at impeller cap

The seating stress between impeller cap and washer is calculated as follows:

$$p_{washer} := \frac{F_{ax}\left(Q_{BEP} \cdot 0\right) \cdot k_A}{A_r} = 79 \cdot \frac{N}{mm^2} \qquad 4.35$$

The seating stress between the impeller cap and the impeller is calculated by equation 4.36.

$$p_{cap} := \frac{F_{ax}\left(Q_{BEP} \cdot 0\right) \cdot k_A}{A_{r\_cap}} = 8 \cdot \frac{N}{mm^2} \qquad 4.36$$

4.4.3 Impeller mounting screw

For the impeller fastening a central socket head screw is used, which has to fix the impeller in its position and has to transmit the unbalanced axial force of the impeller to the pump shaft. A detailed analysis of this screw connection is needed in order to get information on how high the tightening torque has to be. The maximum axial force during the operation is calculated at the operating point Q=0 m³/h to 15160 N.

The function lines shown in Figure 4.19 describe the single parts affected when the screw axial load of the pressure distribution behind the impeller is acting and when also the pre-load force of the screw is acting. The following drawing shell illustrate all the single parts, which have an effect on the screw connection.

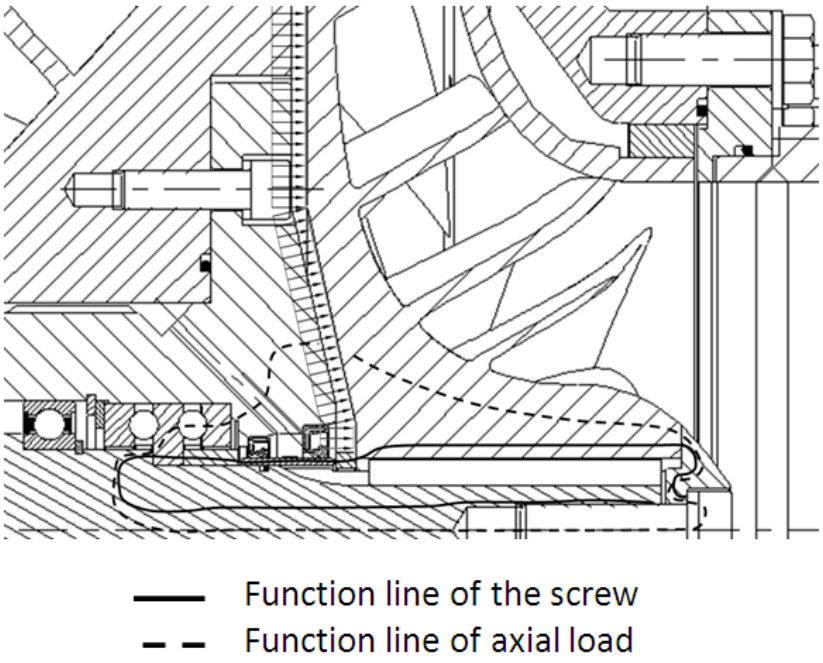

Figure 4.19: Function lines of the screw and the axial load

These single parts affecting the screw connection are shown in Figure 4.20 and have to be considered in the calculation.

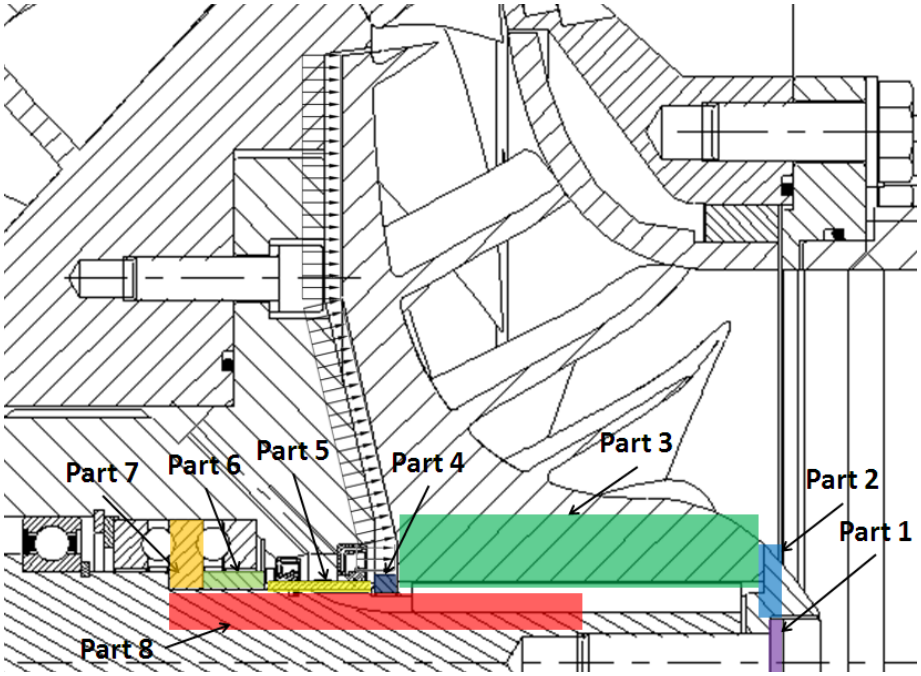

Figure 4.20: Denomination of the different parts for calculation purpose

In the next step, all compliances of the parts one to eight and the screw are needed and have to be summed up.

The compliances of all stretching parts (when the operating force acts) are summed up as shown in 4.37.

$$\delta_{stress} := \delta_{p3} + \delta_{p2} + \delta_{p1} + \delta_{screw} + \delta_{p8} = 1.95 \times 10^{-6} \cdot \frac{mm}{N} \qquad 4.37$$

The compliances of all compressing parts (when the operating force acts) are summed up as follows.

$$\delta_{compress} := \delta_{p7} + \delta_{p6} + \delta_{p5} + \delta_{p4} = 7.39 \times 10^{-7} \cdot \frac{mm}{N} \qquad 4.38$$

These compliances and a tightening moment of 180 Nm leads to the following diagram, see Figure 4.21.

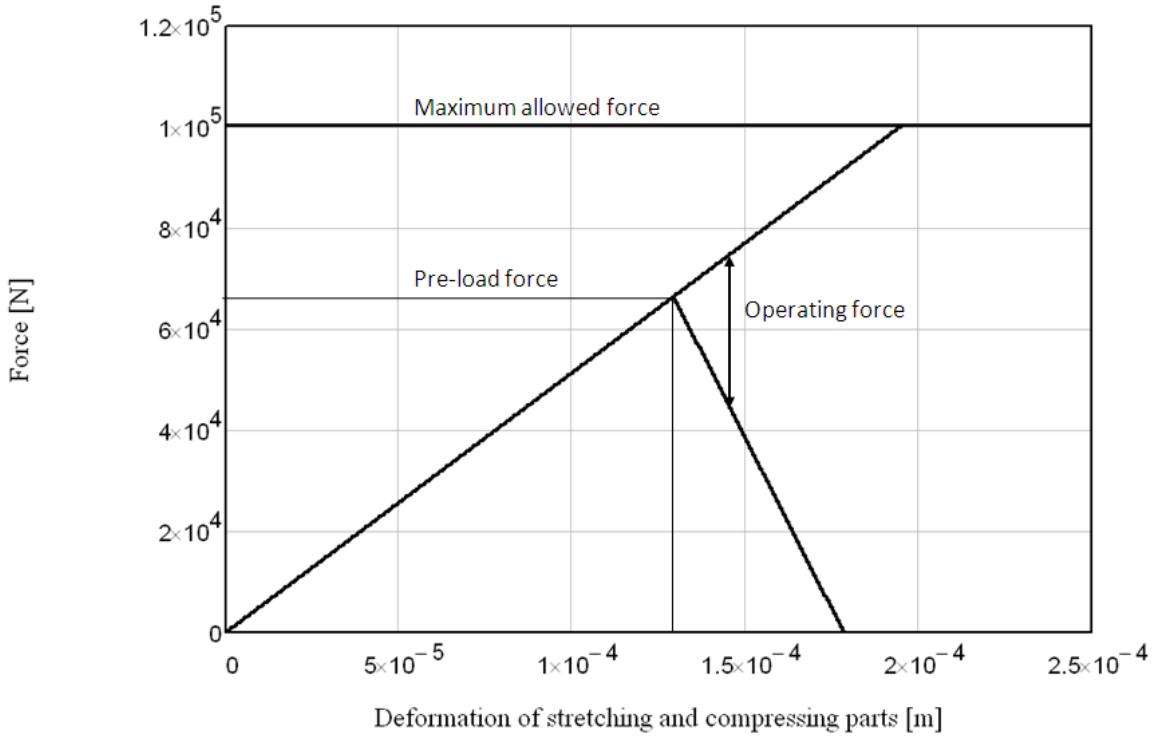

Figure 4.21: Force and elongation

This diagram shows that the operating force leads to an additional force in the screw. However, the maximum force during the operation is lower than the highest allowable force of the screw. Furthermore, the operating force initiates a tension relief of the compressed parts, but the pre-load force is high enough to avoid a gap.

5 Measurement

The present chapter refers to the installation of the test rig, the measurement devices, the measurements uncertainties, the measurement results and the completion of the requirements.

5.1 Installation

The Institute of Hydraulic Machinery has an existing pump and turbine test rig, which can be adapt to different installations. Figure 5.1 shows the installation of the entire test rig already adapted to the actual measurement task. The flow measurement device is permanently installed and is used for both flow directions. The main pump is linked out and is not used for this measurement.

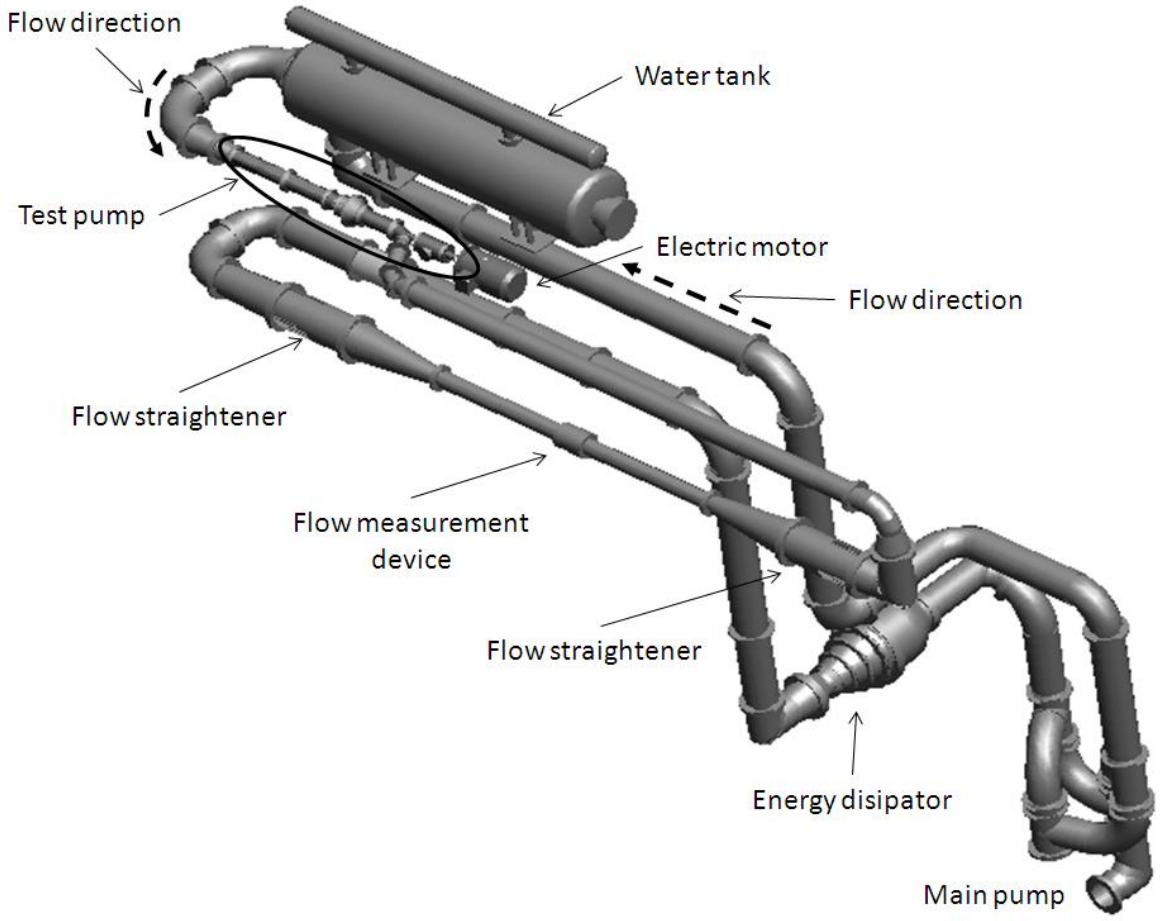

Figure 5.1: Installation of the test rig

The water tank has a collector pipe at the top, which is used lead the air out of the system. Therefore, the water has to flow through the whole water tank very slowly, in order to provide enough time for outgassing. In the actual installation, the water flows into the tank at the left end and leaves the tank at the same end.

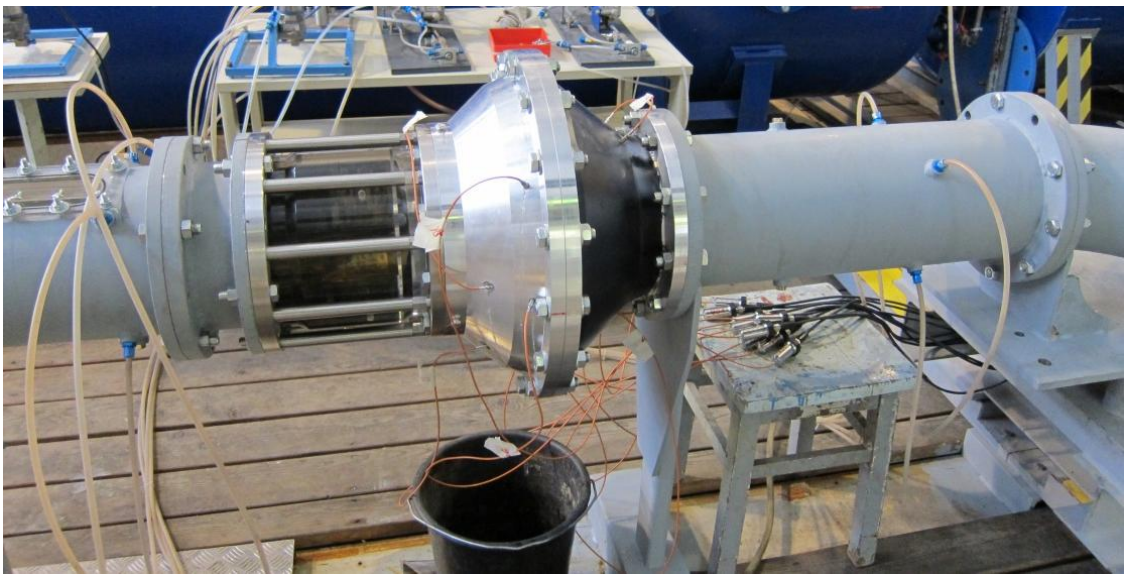

Figure 5.2: test rig installation [3]

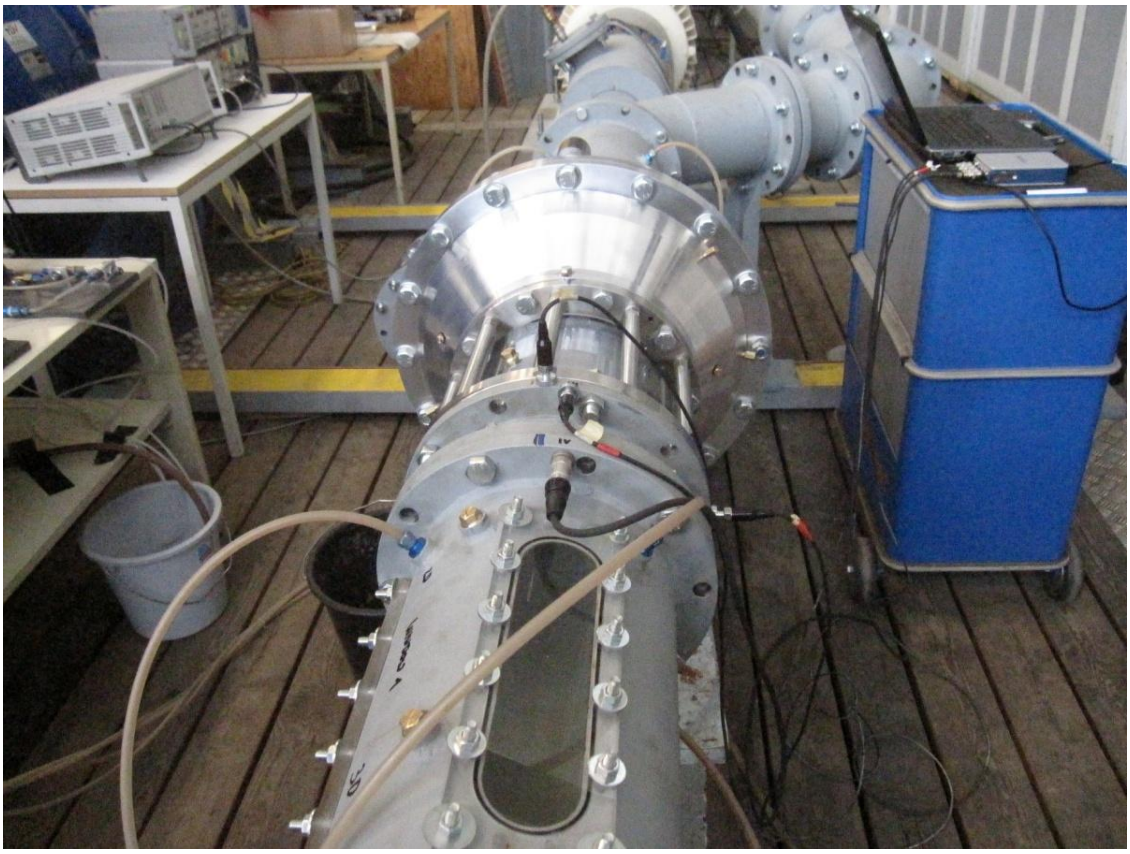

Figure 5.3: test rig installation [3]

5.2 Measurement equipment

The measuring devices needed are defined by the measurement data needed for this task: Q, H, P_{mech}, $NPSH_3$ and η. The following list shows the necessary measurement data:

- Absolute pressure at suction side
- Difference pressure between suction and pressure side
- Torque
- Rotating speed
- Discharge
- Temperature of fluid

In order to manage these measurements, the devices presented in the following are necessary.

5.2.1 Pressure measurement

As already mentioned in chapter 3.3.9, the design of the pressure measuring taps is according to ISO 9906. The positions of the pressure measurement taps are two times the diameter of the pipe away from each flange. The static pressure tappings are disposed symmetrically at each section and have an offset to each other of 90°. The offset in reference to the vertical axis is 45°, in order to avoid measurement tapping at the highest position, were air from the system might be collected and get into the measurements pipes. Each single measuring tap is equipped with a valve and connected to a manifold. This allows for reading out each single tap separately (Figure 5.4). The installation of the pressure measurement pipes provides different valves, which can be used to flush pipes in order to avoid air inside the measurement pipes (Figure 5.5).

In Figure 5.4, two differential pressure transmitters and one absolute pressure transmitter are shown. The absolute pressure transmitter is used to measure the absolute pressure at the suction side of the pump. This absolute pressure is later on needed to calculate the NPSH values and has the specifications as shown in Table 5.1. The first pressure transmitter is used for the measurement of the differential head between suction and pressure side of the test pump. The specification of the differential pressure transmitter is shown in

Table 5.2. The second differential pressure transmitter is also used to measure the differential head of the pump, which is not used for measurement but for the control system of the test rig.

Table 5.1: Absolute pressure transmitter [2, p. 61]

Manufacturer	*Rosemount*
Model/Type	*3051 CA2*
Serial no.	*7079927 / 1197*
Measuring range	p_{abs}*=0-10 bar*
Output signal	*4 - 20 mA*

Table 5.2: Differential pressure transmitter [2, p. 61]

Manufacturer	*Rosemount*
Model/Type	*3051 CD4*
Serial no.	*7886438 04/04*
Measuring range	*Dp=+/-20 bar*
Output signal	*4 - 20 mA*

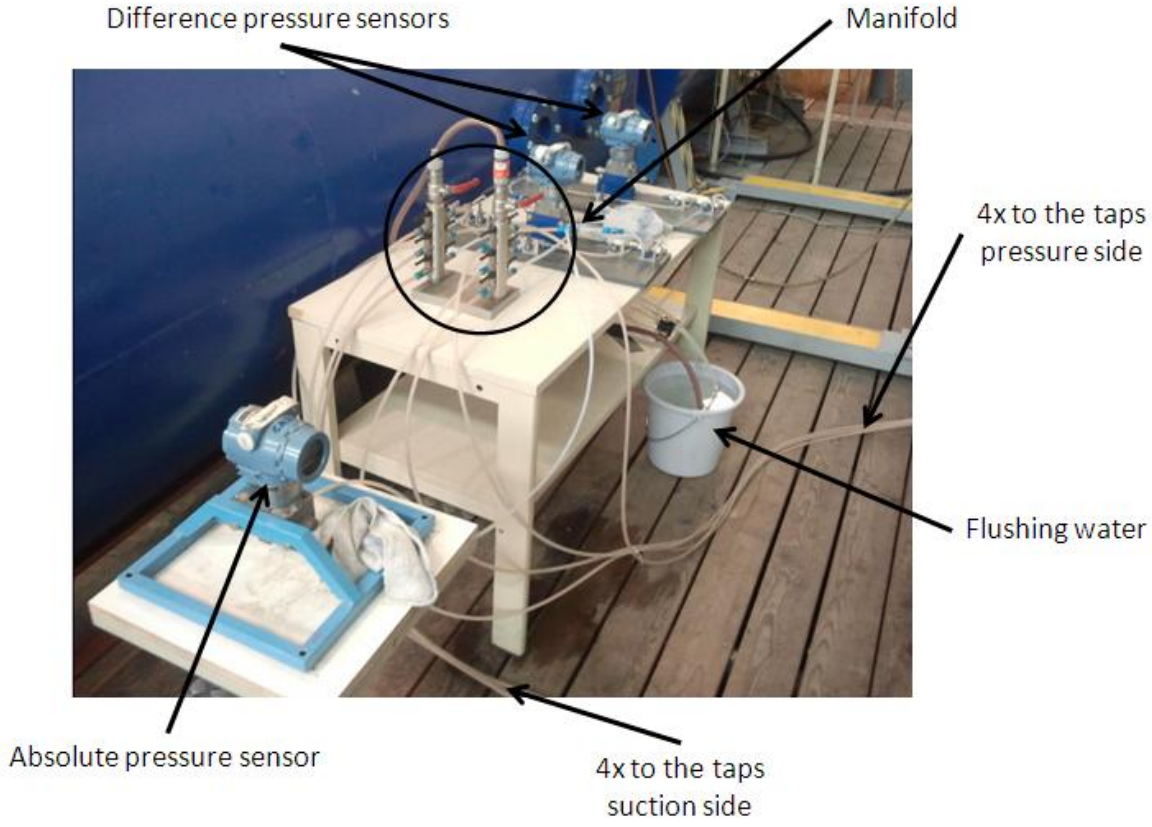

Figure 5.4: Pressure measurement installation

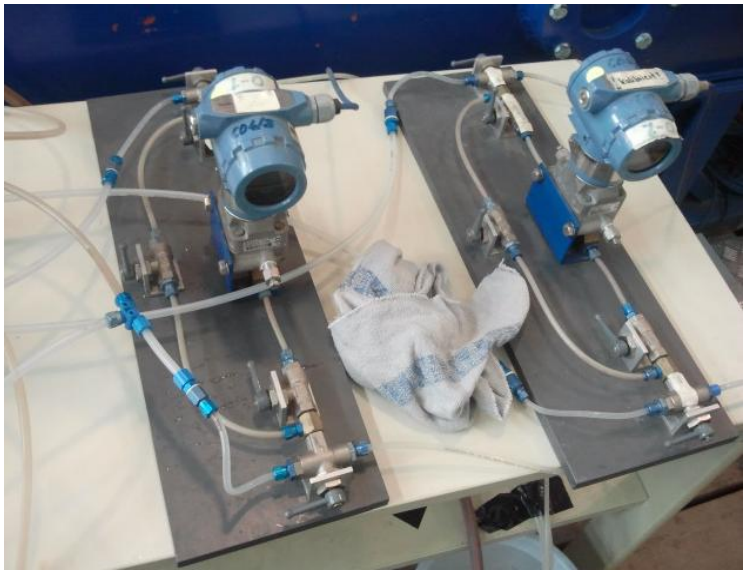

Figure 5.5: Different pressure sensors installed with flushing valves

5.2.2 Torque sensor

For the measurement of the torque and the rotating speed, a HBM T30 FNA/1kNm (Hottinger Baldwin) torque and speed measurement flange is used. This measurement flange is equipped with curved tooth couplings at both sides called “SBG-50 spezial”. These couplings are used to compensate an axial and an angular offset of the pump shaft and the power shaft (engine side). The torque sensor is mounted inside the pump housing and is exposed to the same pressure as in the water tank.

Table 5.3: Torque and speed measurement device [2, p. 62]

Manufacturer	*HBM*
Model/Type	*T30FNA*
Serial no.	*G65993*
Measuring range	*M=+/- 1000 Nm*
Output signal (speed)	*30 impulses p. rev.*
Output signal (torque)	*5-15 kHz*

5.2.3 Temperature sensor

The water temperature is used for the calculation of the density with the “Herbst-Roeger-Methode” and of the vapour pressure. The measurement is realiesed with a P100, which is positioned in the water tank and has the specifications as shown in Table 5.4.

Table 5.4: Temperature sensor [2, p. 62]

Manufacturer	*Conatex*
Accuracy class	*DIN EN 60751 Class B*
Output signal	*4-20 mA*

5.3 Measurement uncertainties

The measurement data registered during different measurements over a long time are used to decide whether the pump meets the requirements or not. In order to be able to reproduce these measurement data, the uncertainty of the measurements applied has to be as low as possible.

The uncertainties of the measurements are divided into two different types, at the one hand random uncertainties and on the other hand the systematic uncertainties. Furthermore, systematic uncertainties consist of known and of unknown uncertainties.

5.3.1 Systematic measurement uncertainty

The systematic measurement uncertainty e_s always leads to deviations to the same direction in reference to the true value. Reasons for a systematic uncertainty are the accuracy class of the measurement equipment, the influence of the measurement object on the device and outer influences. On the one hand there are known uncertainties, which could be compensated by mean of calibration, zero-adjustment, careful measurement of dimensions and so on, and on the other hand there are unknown uncertainties. Unknown systematic uncertainties have to be estimated and included in the result. According to ISO 9906, the permissible relative values are given in reference to the pump performance test acceptance grade, see Table 5.5. [13, p. 17]

Table 5.5: Permissible systematic instrumental uncertainty, e_s [13, p. 18]

Measured quantity	Maximum permissible systematic uncertainty (at guarantee point)	
	Grade 1	Grades 2 and 3
	%	%
Rate of flow	±1,5	±2,5
Differential head	±1,0	±2,5
Outlet head	±1,0	±2,5
Inlet head	±1,0	±2,5
Suction head for NPSH testing	±0,5[a]	±1,0
Driver power input	±1,0	±2,0
Speed of rotation	±0,35	±1,4
Torque	±0,9	±2,0
[a] See Annex J for explanation.		

5.3.2 Random measurement uncertainty

The random measurement uncertainty e_r appears as a scatter of the measurements and could be reduced by a higher number of measurements, assumed that the conditions are unchanged. When the number of measurement data increases, the distribution to the meas-

urements will approximate to a normalised distribution. Hence, the estimation of the random measurement uncertainty could be done by statistical calculations, based on a confidence level. [13, p. 14]

5.3.3 Overall measurement uncertainty

The overall measurement uncertainty could be calculated by a quadratic combination of the systematic and random measurement uncertainty as shown in equation 5.1. The maximum allowed value for the overall measurement uncertainty according to ISO 9906 is shown in Table 5.6. [13, p. 18]

$$f = \sqrt{f_R^{\,2} + f_S^{\,2}} \qquad 5.1$$

Table 5.6: Permissible values of overall uncertainty [13, p. 18]

Quantity	Symbol	Grade 1 %	Grades 2, 3 %
Flow rate	e_Q	±2,0	±3,5
Speed of rotation	e_n	±0,5	±2,0
Torque	e_T	±1,4	±3,0
Pump total head	e_H	±1,5	±3,5
Driver power input	e_{Pgr}	±1,5	±3,5
Pump power input (computed from torque and speed of rotation)	e_P	±1,5	±3,5
Pump power input (computed from driver power and motor efficiency)	e_P	±2,0	±4,0

To minimise the systematic uncertainties known, the measurement devices are calibrated in regular time intervals and zero-adjusted before every usage. The unknown systematic uncertainties are given by the manufacturer of the measurement device. Furthermore, to reduce the random measurement uncertainty, a large amount of measurements have to be read out to calculate a representative mean value. To realise this, every measurement point recorded is the mean value of all measurements which were read out at a defined time Δt with a sampling rate of 1 kHz. For measurements of the characteristic curve of the pump, the measurement time $\Delta t=20$ s leads to a mean value of a sample containing of 20.000 values. For measurements of NPSH, $\Delta t=10$ s because of the very instable operating points of the test pump at a low the system pressure level, which leads to a sample size of 10.000 values.

5.4 Model test error consideration

For the determination of the measurement uncertainty the individual uncertainties of the main parameters characterizing the hydraulic performance are considered. The results of these considerations containing the systematic uncertainties are presented with the following subchapters.

5.4.1 Flowrate

- Calibration of volumetric tank f_a +/- 0.04%
- Error in density of water f_b +/- 0.02%
- Error in time f_c +/- 0.13%
- Calibration result of the inductive flowmeter f_d +/- 0.30%

The overall systematic flowrate uncertainty is to be calculated by summing up the squared individual uncertainties and taking the square root of this sum. This leads to an uncertainty of +/- 0.331% (equation 5.2) for the flowrate measurement which is far below the allowed value of 1.5% stated in the ISO 9906 [13] standard.

$$f_{QS} := \sqrt{f_a^2 + f_b^2 + f_c^2 + f_d^2} = 0.331\,\% \qquad 5.2$$

5.4.2 Net Head

- Rotary piston manometer - Calibration certificate f_a +/- 0.03%
- Calibration result of the pressure transducer f_b +/- 0.10%

The overall systematic head uncertainty is to be calculated by summing up the squared individual uncertainties and taking the square root of this sum. This leads to an uncertainty of +/- 0.104% (equation 5.3) for the net head measurement which is far below the allowed value of 1.0% stated in the ISO 9906 [13] standard.

$$f_{HS} := \sqrt{f_a^2 + f_b^2} = 0.104\,\% \qquad 5.3$$

5.4.3 Torque

- Length of lever arm f_a +/- 0.10%
- Calibration of check weights f_b +/- 0.01%
- Calibration result of the torque measuring flange f_c +/- 0.50%

The overall systematic torque uncertainty is to be calculated by summing up the squared individual uncertainties and taking the square root of this sum. This leads to an uncertainty of +/- 0.51% (equation 5.4) for the torque measurement which is below well the allowed value of 0.9% stated in the ISO 9906 [13] standard.

$$f_{TS} := \sqrt{f_a^2 + f_b^2 + f_c^2} = 0.51\,\% \qquad 5.4$$

5.4.4 Speed

According to the calibration of the speed signal of the torque measuring flange the maximum relative error accounts for f_{nS}=+/-0.05%.

5.4.5 Efficiency

According to the definition of the hydraulic efficiency the systematic uncertainty of the efficiency is composed of the individual errors of flowrate "Q", head "H", torque "T" and speed "n".

$$f_{\eta S} := \sqrt{f_{QS}^2 + f_{HS}^2 + f_{TS}^2 + f_{nS}^2} = 0.619\,\% \qquad 5.5$$

The random uncertainty (based on the determined repeatability) is calculated according to ISO 9906 clause 4.3.3.1[13]. For a number of 20 measurement readings (n = 20, see chapter 5.3.3) the value of the Student's t-distribution accounts for t=2.09. According to the evaluated measurement results the random uncertainty $f_{\eta R}$ accounts for maximum +/-0.15%. Therefore the total uncertainty of the measured efficiency is calculated as shown in equation 5.6.

$$f_{\eta tot} := \sqrt{f_{\eta S}^2 + f_{\eta R}^2} = 0.637\,\% \qquad 5.6$$

The resulting total efficiency uncertainty of 0.637% is far below the allowed value of 2.9% stated in the ISO 9906 [13] standard.

5.5 Hydraulic acceptance

Referring to the requirements shown in Table 1.1, there are requirements with explicitly defined acceptances and some requirements with acceptances according to standard ISO 9906. The acceptance tolerance for the delivery head and the discharge is defined according to ISO 9906-grade 1B, see in Table 5.7.

Table 5.7: Pump test acceptance grades and corresponding tolerances[13, p. 20]

Grade	**1**			**2**		**3**	
$\Delta\tau_Q$	10 %			16 %		18 %	Guarantee requirement
$\Delta\tau_H$	6 %			10 %		14 %	
Acceptance grade	**1U**	**1E**	**1B**	**2B**	**2U**	**3B**	
τ_Q	+10 %	±5 %		±8 %	+16 %	±9 %	Mandatory
τ_H	+6 %	±3 %		±5 %	+10 %	±7 %	
τ_P	+10 %	+4 %		+8 %	+16 %	+9 %	Optional
τ_η	≥0 %		−3 %	−5 %		−7 %	
NOTE $\tau_x(x = Q, H, P, \eta)$ stands for the tolerance of the indicated quantity.							

All relevant hydraulic requirements and acceptance tolerances have been given by the customer see Table 5.8.

Table 5.8: Hydraulic requirements and acceptance tolerances

specifiation	unit	target value	acceptance tolerance	
Specific speed	m³/min, m	280	-10	10
Q_design	m³/h	430	-5%	5%
H @ Q_design	m	34,5	-3%	3%
overall efficiency	%	87%	-1,50%	-
shutt off ratio	%	124%	-4%	4%
NSS @ 70%Q_design	m³/min, m	1400	0%	-
NSS @ 100%Q_design	m³/min, m	1600	0%	-
NSS @ 130%Q_design	m³/min, m	1400	0%	-

These acceptance tolerances are depicted in the diagram which is shown in Figure 5.6. The acceptance of pump flow and head will be obtained, if one of these values or both values are found within the accepted tolerance. Furthermore, the shut-off head must be within the accepted tolerance and the $NPSH_3$ values must be lower than the points defined in Figure 5.6.

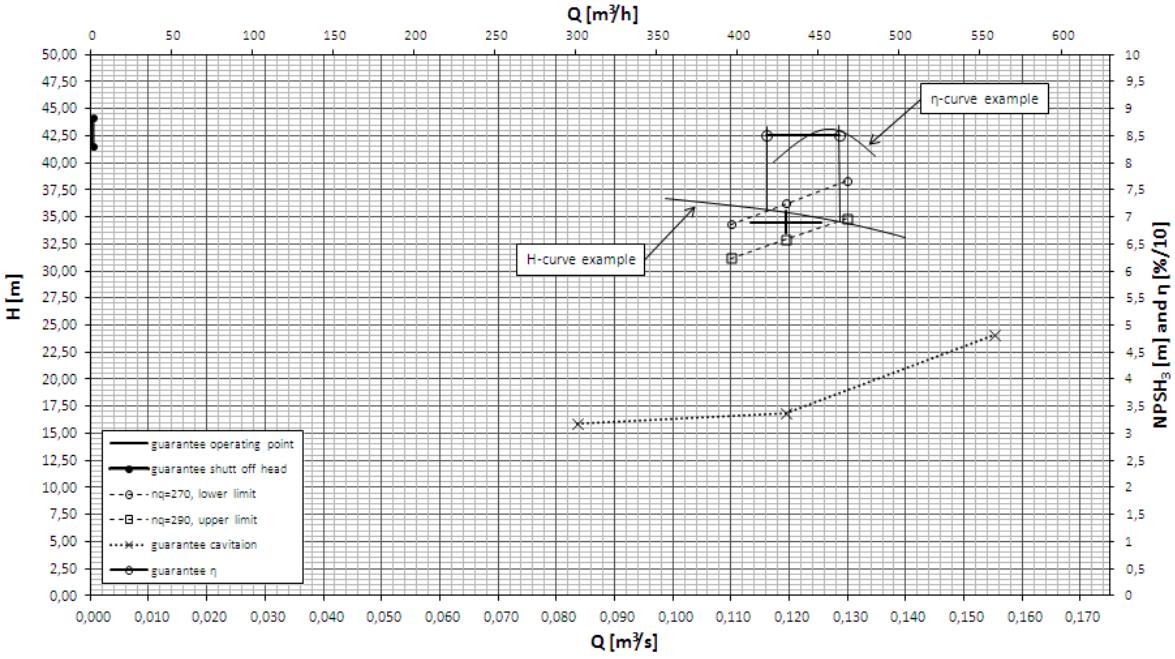

Figure 5.6: Target value and acceptance tolerances

Furthermore, the best overall efficiency must be at least 85% and the range of the flowrate of the best efficiency point is depending on the current characteristic curve and must be within an n_q range of 280+/-10 rpm.

In Figure 5.6 the example head is within the acceptance tolerance of flowrate and head the intersection of the head curve and the lower and upper limit curve give the acceptance range of the best efficiency point. The highest efficiency has to be within this tolerance range and must not be at least 85%. The example in Figure 5.6 is used to show the approach of acceptance control and meets the requirements in the actual case.

5.6 Requirements fulfilment

5.6.1 Measurement data analysis

The measurement points are mean values which are documented with the software LabVIEW by National Instruments. The analysis of the measurement data is already done with this software, according to ISO 9906. The measurement data and the results of the analysis could be exported to Microsoft Excel®, where further evaluations, corrections and comparisons with other measurement results could be realised. Fluctuations with great amplitude have to be taken into account, which is also done in Microsoft Excel® per hand. The permissible amplitude of the fluctuations allowed is shown as a percentage value of the measured quantity in Table 5.9.

Table 5.9: Permissible amplitude of fluctuations [13, p. 16]

Measured quantity	Permissible amplitude of fluctuations		
	Grade 1	Grade 2	Grade 3
	%	%	%
Rate of flow	±2	±3	±6
Differential head	±3	±4	±10
Outlet head	±2	±3	±6
Inlet head	±2	±3	±6
Input power	±2	±3	±6
Speed of rotation	±0,5	±1	±2
Torque	±2	±3	±6
Temperature	0,3 °C	0,3 °C	0,3 °C

If there is an error in the measurement of the pump inlet head, which can occur to the partial flow due to pre-swirl, it should be detected and corrected as recommended in ISO 9906, see Figure 5.7.

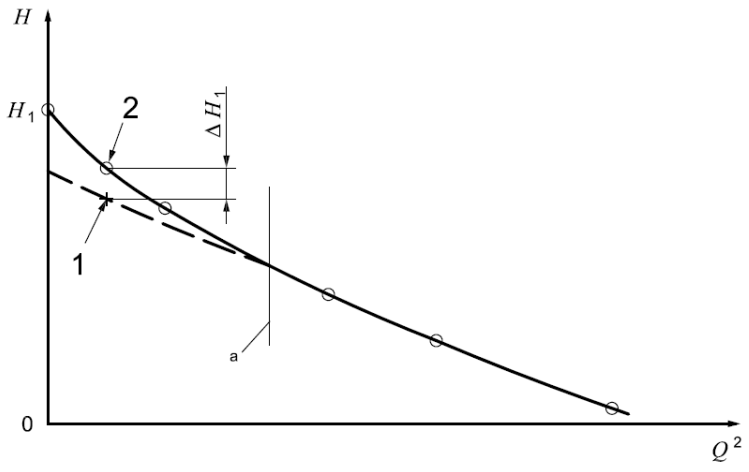

Key

1 real value
2 value of H_1 affected by pre-swirl
a Onset of pre-swirl.

Figure 5.7: Correction of the inlet total head [13, p. 35]

5.6.2 Measurements results

To get an overview on the hydraulic performance of this test pump, with some modified parts, various modifications are performed as shown in the list below:

- Different gap clearances
- Modified hub cap
- Different versions of swirl break
- Balancing holes for axial load compensation

The influence of different gap clearances is shown in Figure 5.8 whereas no significant change of the head curve could be detected. However, with a higher gap clearance the head curve is a little bit lower than with a small gap width.

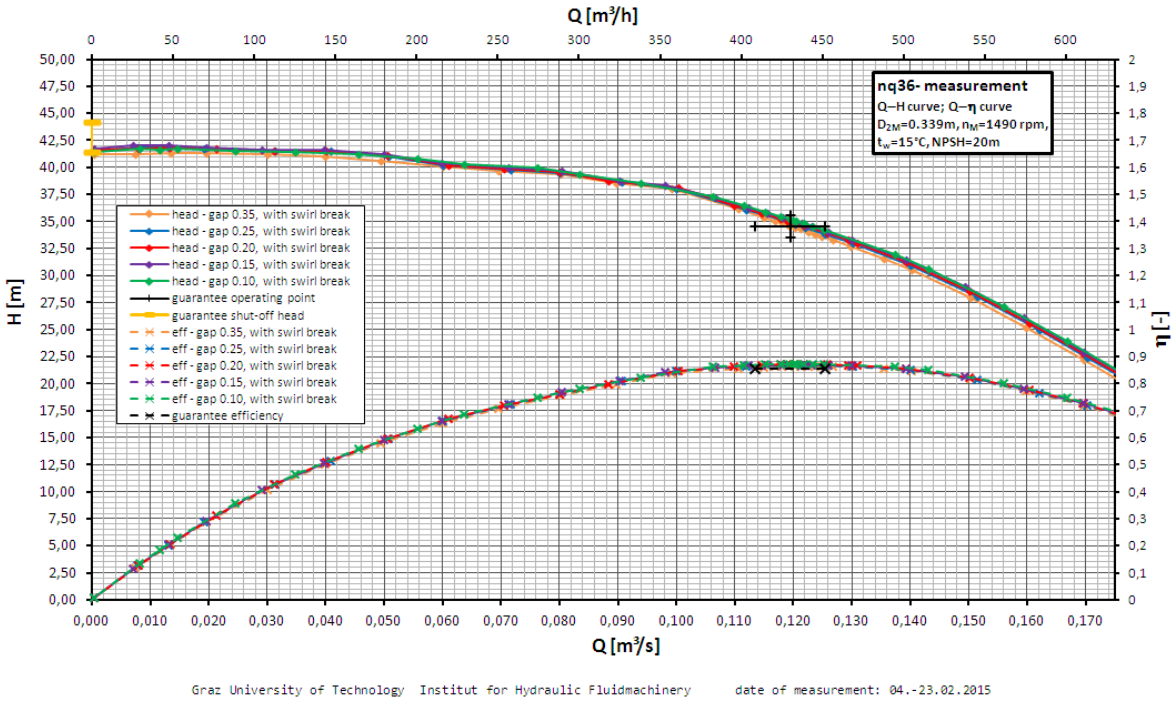

Figure 5.8: Influence of different gap clearances [3]

The modified hub cap is used to simulate the influence on the pump performance caused by the rotating shaft between the stages in multistage configuration (see Figure 5.9). This modification increases the intensity of the pre-swirl and lowers the head curve in part load in case of a higher measured pressure at the suction side. The effect of this pre-swirl is only visible in part load, with a flowrate of more than 40% of the best efficiency point no significant influence could be detected as shown in Figure 5.10.

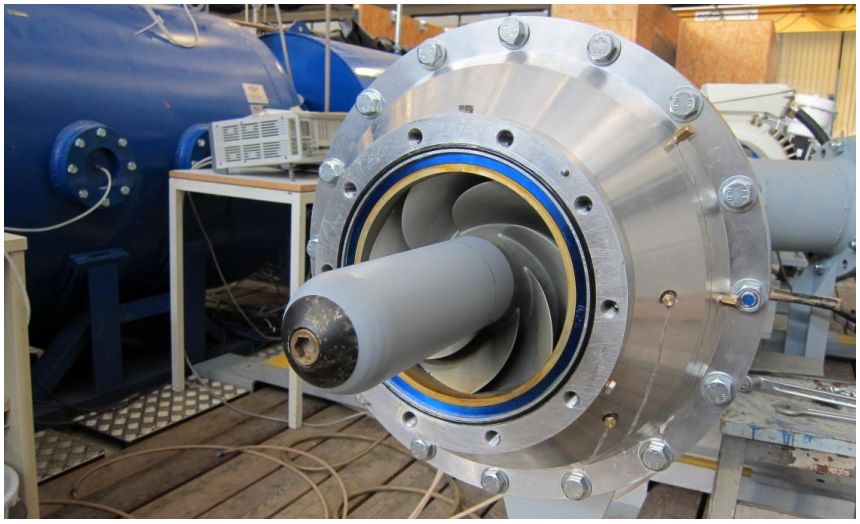

Figure 5.9: long hub cap [3]

With a pre-swirl in the suction pipe at part load, which influences the measured pressure at the suction side, the shut-off head could not be reached. In order to reduce the effect of the pre-swirl, different versions of swirl break configurations were realised and measured. The different configurations are shown in detail in Figure 5.11 and in Appendix C.

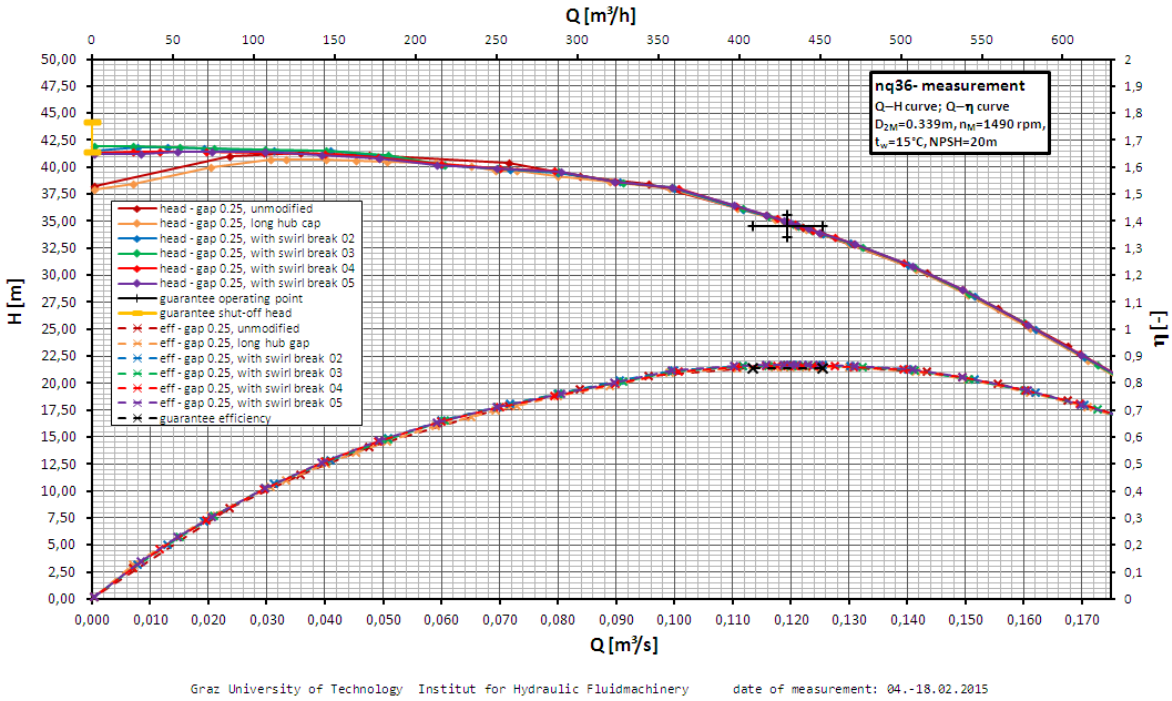

Figure 5.10: Measurement of different swirl break versions and long hub cap [3]

As shown in Figure 5.10, the effects to the head curve in reference to the different swirl break configurations are the same and lead to a higher shut-off head, however small differences between the configurations are visible. The final swirl break version 05, which is used for acceptance measurements, is positioned in front of the pump inlet to enable mounting also in case of a bell mouth.

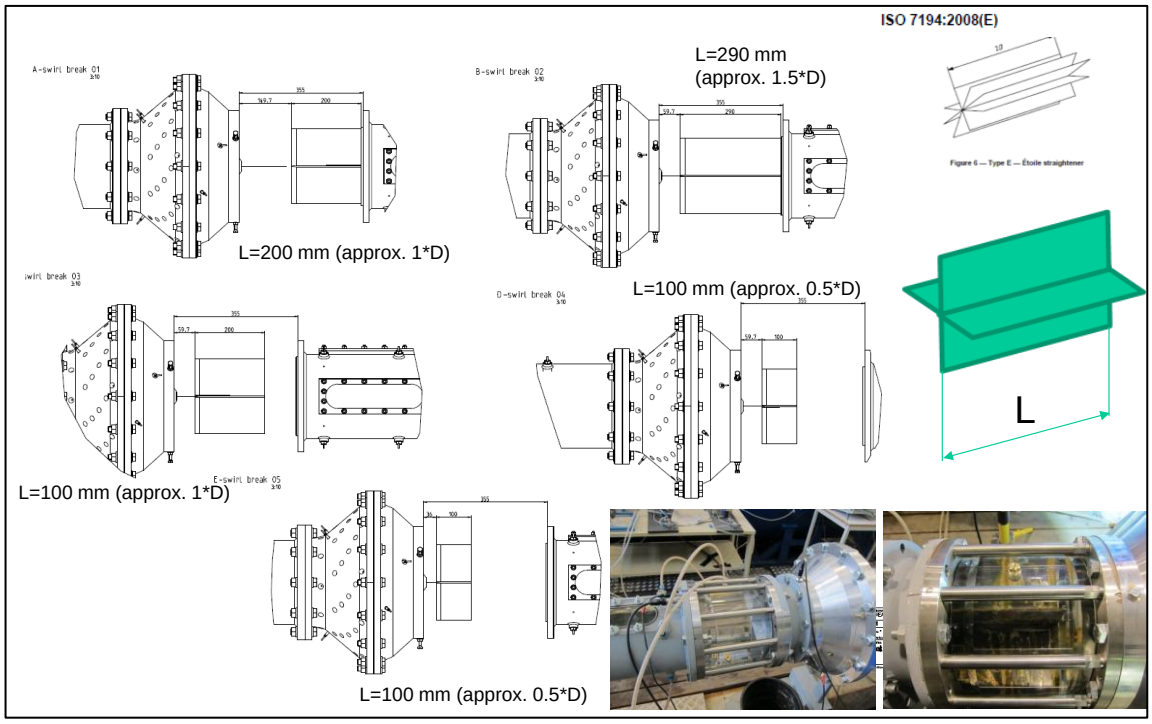

Figure 5.11: Overview of different swirl break configurations

For applications in a multi-stage configuration, axial load compensation is necessary. To realise this in a very simple way, modifications of the impeller and the bearing holder were done after the acceptance measurements. Therefore, balancing holes were realised in the impeller and a gap sealing at the backside of the impeller was installed. The detailed construction is shown in Appendix C, and the measurement results are shown in Figure 5.12.

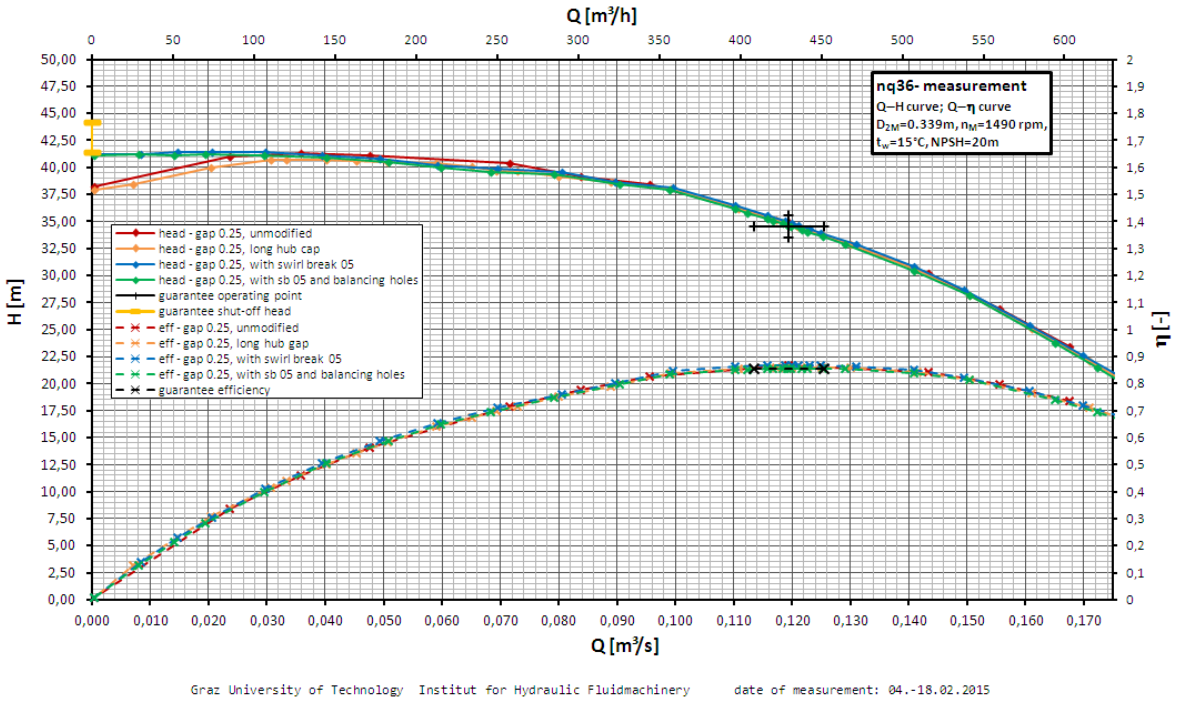

Figure 5.12: Measurement data of final modifications

5.6.3 Measurement acceptance

The measurement results of the final arrangement shown in the diagrams are depicted in different representations. On the one hand, the acceptance tolerances are drawn, and on the other hand the measurements of the pump are given.

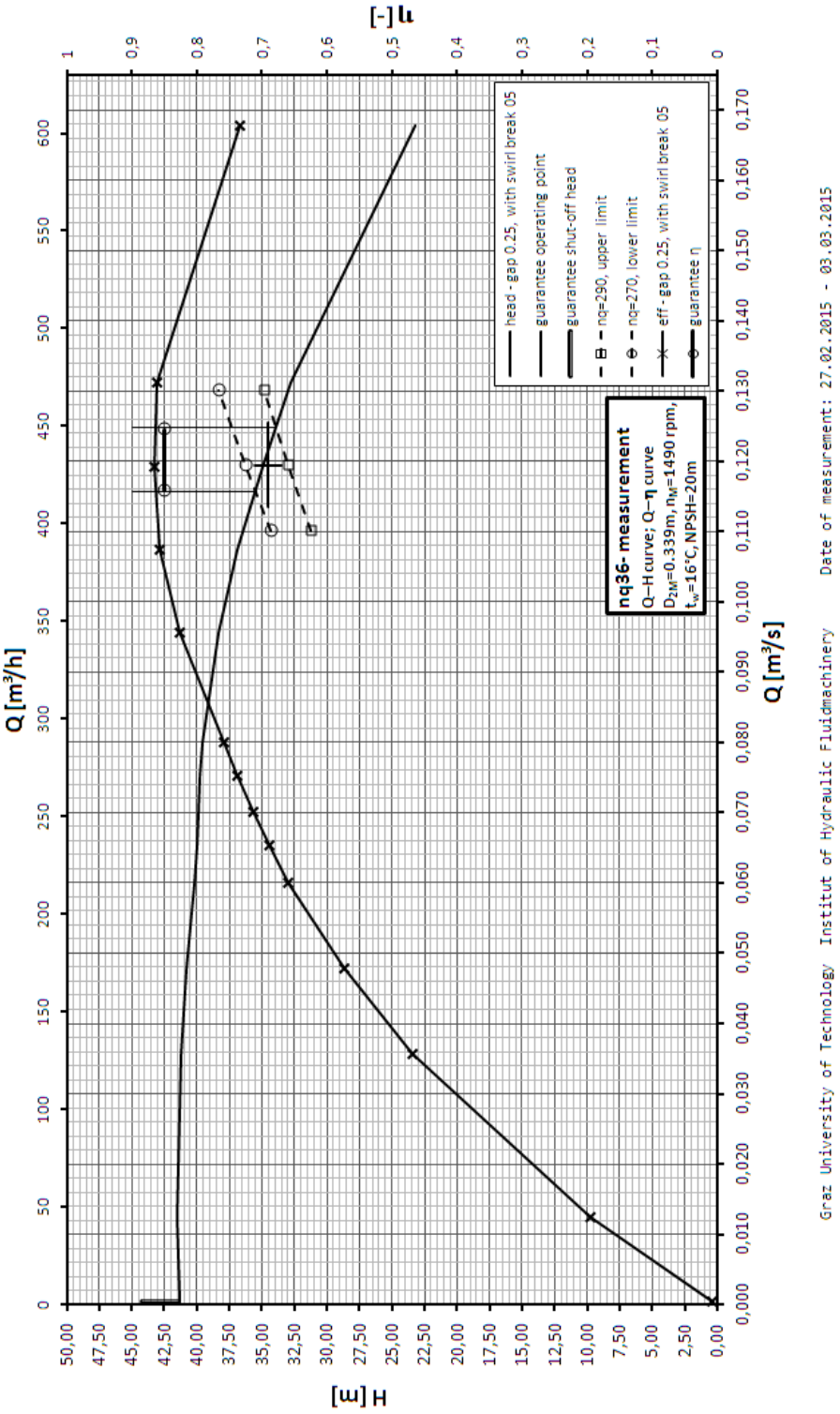

Figure 5.13: Measurements results; Q-H-η

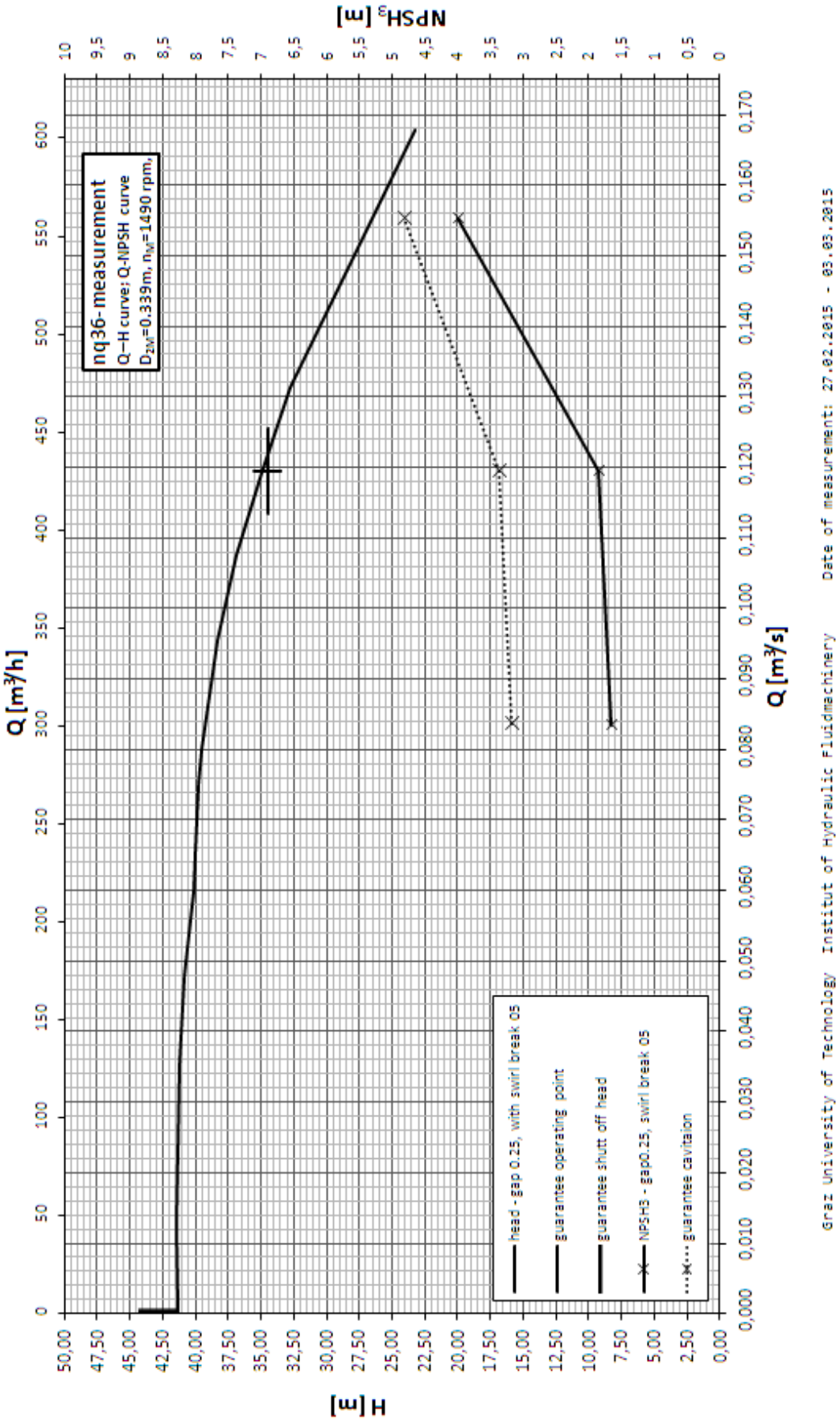

Figure 5.14: Measurements results; Q-H-NPSH$_3$

6 Summary and recommendations

Finally, the hydraulic measurements had been finished without any failure of the test rig. The measurement of the test pump shows, that the requirements of the customer were met. The best efficiency point was met exactly and the $NPSH_3$ values were much lower than claimed, also the shut-off head was within the acceptable tolerance.

Referring to the correlation between CFD results and measurement data makes it visible that a verification of the CFD calculation by means of a test rig is necessary, as a CFD simulation is not able to describe the real flow conditions satisfactorily.

It would also be useful to do further research work with different axial load compensation methods, because in later applications, this pump will be used in multi-stage arrangements and in equal cases it is necessary to minimise the axial load of the impeller.

This type of pump will be used in multi-stage configurations with a long power train for applications in deep reservoirs. The long pump shaft influences the rotor dynamical behaviour of the pump and could lead to low natural frequencies. This fact may lead to low lifetimes of the bearing units of this kind of long pump shaft. In order to avoid the problem, it takes a lot of engineering work based on vibration measurements, which was also done on the test rig in Graz.

It also has to be mentioned that it was quite useful to gather the project team with members who have various professional skills, as it was done in this case. The project team consisted of a project leader, one person that did the CFD calculations, another one that was responsible for manufacturing, one that realised the construction and one member with experiences in measurements.

This Master`s Thesis documents the development process of a test rig and can be used as a technical support for future constructions with applications similar to this one.

List of figures

List of tables

References

[1] J. Handl, Aufbau eines Axialpumpenprüfstandes, Institut für Hydraulische Strömungsmaschinen TU Graz: Graz, 2009.

[2] J. Hopfgartner, Construction of a test rig of a mixed flow pump, Masterarbeit, Institut für Hydraulische Strömungsmaschinen TU Graz: Graz, 2013.

[3] S. Höller-Litzlhammer, H. Benigni and H. Jaberg, Fixed-Type Impeller Semi-Axial Pump, Hydraulic Design, HFM - Institute of Fluidmachinery: Graz, 22.10.2014.

[4] J. F. Gülich, Kreiselpumpen, 3. Auflage, Springer-Verlag: Berlin-Heidelberg, 2010.

[5] KSB-Aktiengestellschaft, Selection Centrifugal Pumps, KSB Aktiengesellschaft, Communications (V5): Frankenthal / Germany, 2005.

[6] Standard API 610, Centrifugal Pumps for Petroleum, Petrochemical and Natural Gas Industries, 11th edition; Sep. 2010;.

[7] Standard IEC 60 193, Hydraulic turbines, storage pumps, and pump-turbines-model acceptance tests, 2. edition, 1999.

[8] H. Petermann, Strömungsmaschinen, 7. Auflage, Springer-Verlag: Heidelberg, 2005.

[9] VDI, VDI-Wärmeatlas, 10. Auflage, Springer-Verlag: Berlin-Heidelberg, 2006.

[10] Sulzer Pumps, SJT / SJM / SJP, Large Vertical Pumps, Sulzer Pumpen: www.sulzer.com, Abfrage 22.01.2015.

[11] Simrit GmbH & Co. KG, Technical Manual, Simrit GmbH & Co. KG: Freudenberg, 2007.

[12] P. Köhler, Pro/ENGINEER-Praktikum,4. Auflage, Vieweg Verlag: Wiesbaden, 2006.

[13] Standard EN ISO 9906, Kreiselpumpen - Hydraulische Abnahmeprüfung Klassen 1 und 2, Ausgabe: 2002-07-01.

[14] Schäffler, Product cataloque:, www.medias.ina.de, Abfrage 25.04.2015.

[15] B. Künne, Maschinenteile 2, Auflage 9, B.G. Teubner: Wiesbaden, 2004.

[16] W. Matek, D. Muhs, H. Wittel, M. Becker and D. Jannasch, Roloff/Matek, Maschinenelemente, Auflage 15, Vieweg Verlag: Braunschweig/Wiesbaden, 2001.

[17] W. Matek, D. Muhs, H. Wittel, M. Becker and D. Jannasch, Roloff/Matek,

Maschinenelemente - Tabellen, Ausgabe 15, Vieweg: Braunschweig/Wiesbaden, 2001.

[18] Sulzer Pumpen, Kreiselpumpen Handbuch, 4. Auflage, Vukan-Verlag: Essen, 1997.

[19] Institut für Maschinenelemente und Entwicklungsm., Formelsammlung, Graz, 2010.

[20] KSB Aktiengesellschaft, Kreiselpumpenlexikon spezifische Saugzahl, www.ksb.com, Abfrage 11.04.2015.

[21] A. T. Troskolański and S. Łazarkiewicz, Kreiselpumpen - Berechnung und Konstruktion, Birkhäuser Verlag: Warschau, 1976.

[22] Standard ISO 13709, Centrifugal Pumps for Petroleum, Petrochemical and Natural Gas Industries, Ausgabe: 2010 (2009 identisch).

[23] H. Haberhauer and F. Bodenstein, Maschinenelemente - Gestalten, Berechnung, Anwendung, 13. aktualisierte Auflage, Springer-Verlag: Berlin Heidelberg, 2004.

[24] Schäffer Group Industries, Technische Grundlagen, Deutschland, 2006.

Appendix

A Calculations

B Datasheets

B.1 Datasheet of the slide ring sealing

B.2 Datasheets of the radial shaft ring sealings

B.3 Datasheet of the jaw clutch

B.4 Datasheets of the bearings

C Drawings

C.1 Drawings of the test rig assembly and assembly order

C.2 Drawings of the subassemblies

C.3 Drawings of the single parts

C.4 Drawings of the modifications